**Response to Reviewers: tc-2020-25 by Kelly Hogan et al. "Revealing the former bed of Thwaites Glacier using sea-floor bathymetry"**

The comments of the two reviewers and the short comment are listed below with our responses below *in blue italics*.

**tc-2020-25-RC1: Matteo Spagnolo**

**General comments:**

1. The main conclusions that emerge from the discussion, and in particular the idea of soft and hard bedrock highs and their implication to ice dynamics, are very important and yet there is little mention to them in the abstract and no mention at all in the title. I would therefore recommend incorporating this and other highlighted points in the abstract and consider an alternative, more result-focused, title.

*We have rewritten the Abstract and Title to highlight the main conclusions of the work rather than list the work done. This also addresses comment for Line 429 to include numbers on cross-sectional areas in the Abstract (we have now included these numbers) and for Line 507 asking for the variable composition of pinning points to be alluded to in the title.*

2. Evidence of glacial erosion on the flat-topped highs does not necessarily implies that the flat top morphology is due to erosion. It could be simply related to the presence of harder horizontal layers in a sedimentary rock. Nonetheless, the role of a more or less thick blanket of glacial sediment that could be eroded and its importance for a potential feedback mechanism remains valid.

*We have taken this comment about erosion by an ice shelf on board, also noted in the short comment, and made the following additions to the text to consider the various possibilities for the flat-topped morphology of the highs. We have toned down and further explained our interpretation of the flat tops; we have also added a short paragraph to "Section 3.3: Bathymetric highs and ridges" to explore the alternate explanations namely, that the morphology is inherited from previous subglacial erosion or that rugged bedrock features were mantled by some amount of glacigenic sediment that levelled this topography. The paragraph reads:*

*"We note, however, that alternative explanations are possible for this morphology, namely that the flat tops are an inherited feature produced by erosion down to horizontal bedrock strata or that rugged bedrock highs, which are typical of the inner Amundsen Sea shelf (cf. Nitsche et al., 2013), were mantled by some thickness of glacigenic material that levelled the topography below. The former is relatively easy to discount accepting that the inner shelf of the ASE is composed of crystallite basement with seismic-reflection profiles showing that northward-dipping sedimentary strata only occur on the middle and outer shelf (cf. Graham et al., 2009; Gohl et al., 2013). In this setting close to the current TG*

*grounding zone, it is perhaps easier to conceive of the latter explanation that rugged bedrock features were mantled by glacigenic material delivered to the area when the grounding zone was located on or near the highs, and then flattened by some degree of glacial compaction and/or erosion as it was overtopped by TG and the subsequent Thwaites Ice Shelf. This is consistent with our suggestion for the formation of these flat tops as we cannot tell from our data either what sediment thickness occurs on the highs or how much erosion by took place, and we acknowledge that amount of ice-shelf erosion may have been low only skimming unconsolidated material from the surface of the highs. The presence of GZW and glacial lineations on the highs, and sub-bottom profiler data (Fig. S4), confirms that at least some thickness of unconsolidated material occurs on the highs but seismic-reflection profiles would be required to fully capture the internal structure of these features."*

*Despite the comments, we are happy to agree with R1 that the potential feedback mechanism or erosion from the tops of the highs remains valid! We have added some clarifying text to Section 6.2"Implications from sea-floor morphology" to make the feedback mechanism clearer to the reader, naming the erodible highs as "soft" and the crystalline/bedrock highs as "hard" (the latter is the same as the original text) and we have explained the relative timing of this feedback mechanism with the text below. We also now referred to the concept of soft/hard pinning points in the Abstract.*

3. Generally speaking, there are a number of sentences that area bit vague, and I have highlighted places where the authors should make an effort, if possible, to quantify mentioned differences, similarities, significant implications for, etc. This is especially important in terms of CDW. How much the refined topography of this new bathymetry redraws the estimates of CDW incursion towards Thwaites grounding zone?

*We have addressed individual sentences in the specific comments listed below. Regarding the significance for CDW inflow, although we appreciate this comment, and agree that it would be great to assess to significance of the new bathymetry on the inflow of CDW, to do this robustly is the subject of an oceanographic study and probably beyond the scope of this paper. To fully quantify the implications for CDW influx requires an ocean circulation model (e.g. Nakayama et al, 2019) that implements the high-resolution bathymetry data and is calibrated by CTD data in the troughs (non-existent yet!). Nevertheless, we have tried to make a first pass attempt at quantifying the change in heat flux for the two cross sections over T2, i.e. the one from the older gravity-derived bathymetry and for our new MBES dataset. These "first-pass estimates" use data from oceanographic studies to provide temperature and flow velocities through the troughs, thus allowing us to estimate heat fluxes. This is now documented in Supp. Info. section "Oceanic heat flux calculations", Table S2, and is discussed in Section 6.1. We have also added information on critical sill depths, and channel widths at these sill depths, along sea-floor troughs T2-T4 that may act as conduits for CDW to the Thwaites GZ in Section 3.2 and new Fig. S3 to show the long profiles/sills and channel widths. This suggestion about critical sill depths was also made during discussions with our oceanographer colleague (now co-author Anna Walhin) and hopefully our additions provide useful information for future oceanographic studies.*

4. The spectral analysis description (as the entire manuscript), is interesting and very well written but comes across as rather technical, and a departure from the rest of the manuscript. I recommend the authors to look into ways of making it more accessible to the wider glaciology community, perhaps by moving some its technicality to the supplementary materials and/or by taking greater advantage of an illustrative example. On the other hand, I had the impression that some of the key parameters used in the analyse are not fully explained, but this could all go into the supplementary material.

*We appreciate this comment (which is also in line with comments made by R2) and we have now attempted to better integrate the spectral analysis work into the manuscript. We prefer not to move material from this section to the Supplementary Materials because the derivation of power spectra and its relationship to basal drag is a key component of this work that broadens its appeal to glaciologists and "over-ice" geophysicists alike. It is also important to lead the reader through the derivation so that the results can be linked to specific parts (behaviour of some parameters) in the derivation. Thus, we have made the following changes to address this comment:*

- *We have added a new paragraph in the Introduction that introduces the use of MBES datasets for both glacial landform mapping and its potential for bed roughness analyses.*
- *We have separated out the methods and results sections of the spectral analysis sections (new Sections 5.1 and 5.2) to lead the reader through the process more clearly and provided more text to explain the most important parameters, what the periodograms represent, and how our results link to other studies of subglacial roughness.*

**Specific comments in tc-2020-25-RC1-supplement.pdf:**

*We have addressed each of the comments in the PDF document supplied by Reviewer 1. If we agreed with the comments we have accepted the change this is noted only briefly. Important comments requiring a significant change and comments that we refute are listed here with our full response below.*

Line 48-49: I would order these aspect with a better logic. In facts, I would have mentioned increased ice shelf calving/disintegration of ice shelves first which then induce reduced buttressing, increased upstream ice flow and grounding zone retreat.

*We have reordered the text as suggested by R1.*

Line 78: [Re TGT has periodically advanced and calved] over which period of time?

*We have added the timescale of the Thwaites Glacier Tongue advance and calving (multi-decadal).*

Line 122: this [sounding density] is pretty amazing but it would be more informative if you would provide a resolution range based on the water depth range you had in the area, and perhaps the

average or median value as well. Otherwise this mentioned high resolution is at odd with the choice of a 50m gridded DEM.

*We now also provide sounding densities (on the sea floor) based on the maximum depth range of our working area (~1200 m) to illustrate the range in spacings, as well as examples of sounding densities for some of the older MBES systems used to acquire the data in the final grid (see Table 1). We have added the following sentences to "2: Geophysical Methods" to explain the choice of 50 m grid cell size:*
*"Note that the sounding spacing achievable by each MBES system varies considerably depending on the system setup with older systems generally attaining lower spatial resolution. For example, at 1200 m water depth and a 60° beam angle, the Kongsberg EM120 MBES would achieve an across-track sounding spacing of only 22 m, and the Seabeam 2112 MBES only 35 m. Together, these two systems were responsible for acquiring 5 cruises worth of data in the area (Table 1)."*
*"Ultimately, and to accommodate the different resolutions of the original datasets, the bathymetric sounding data were gridded in MB-System using a Gaussian weighted mean filter algorithm to produce an isometric 50-m digital elevation model (DEM) for the sea floor on the southern ASE shelf."*

Line 146: what dictated the choice of the location of these profiles [additional profiles for spectral analysis]?

*We have now added the following description of why the bed profiles were chosen to the spectral analysis methods section (new Section 4.1):*
*"Profiles were selected based on their location along the central glacier trunk, and their quality in terms of continuity and along-track resolution. The profiles from the Dotson-Getz Trough, offshore from the Getz A Ice Shelf (Fig. S2b), were selected as representative of a sedimentary palaeo-ice stream bed characterised by mega-scale glacial lineations (MSGL) (Graham et al., 2009; Spagnolo et al., 2014). These were extracted from a MBES dataset fully described by Larter et al. (2009) and Graham et al. (2009)."*

Line 198: [Dimensions of the lineations are ] very much like MSGL. What is their spacing? Or do you recognise these as erosional or depositional?

*We have added the spacing between lineations (crest-crest 200-500 m). We do not have a good feel for whether these features are erosional or depositional; their dimensions are consistent with mapped MSGL or glacial lineations (e.g. Spagnolo et al., 2017) and we think it would be difficult to discern from our relatively small patch of lineations to determine whether they are erosional or depositional features – this is also in line with the findings of Spagnolo et al. that this is difficult to determine and may be a combination of processes! Ultra-high resolution data from the AUV missions flown on NBP19-02 (to be worked up and published) may shed more light on this.*

Line 230: [troughs…have been variously modified by ice] and perhaps water as well? or can you exclude this entirely?

*We have added modification by subglacial water flow as a possibility here.*

Line 231: [Re channel widths] measured how? over how many profiles etc.?
*The methodologies for deriving trough and channel metrics are given in Kirkham et al. (2019) which is referenced in the Geophysical methods section (2.1); however, we have added the total number of cross sections analysed here for information. We also add a line to the methods section pointing the reader to Fig. 2 of Kirkham et al. which very clearly describes how the channel metrics are measured in graphical form.*

Lines 257-259: I would like to see a brief discussion on this specific, and rather interesting point. As I think this might help with their overall interpretation.
*We have added several sentences to discuss the different heights of the flat-topped highs, notably the similar heights of features in Pine Island Bay and in front of Thwaites Glacier, and that highs with different heights along one flowline would be of interest for distinguishing between pre-existing topography and ice dynamics (assuming that the bedrock composition is the same, which is thought to be the case for the inner Amundsen Sea).*

Line 264: Despite evidence of glacial erosion, you cannot be sure that the highs flattened top was produced by the erosion of the moving ice necessarily. For instance, they could simply be the expression of selective erosion around bedrock horizontal structures, as we see in many (generally non glaciated) onshore structures. A further possibility is that the highs top is depositional, mantled by a considerable amount of glacial deposit which leveled a more rugged, underneath topography. I would like you to consider this possibility and discuss it, if you haven't done already.
*This comment is linked to general comment 2 – please see full response to that above.*

Line 266: If I recall correctly, Damon David observed flat topped ridges below the current Pine Island ice shelf, although perhaps they are of different size. It is all in his 2017 paper
*The flat-topped mounds surveyed by Autosub AUV under Pine Island Ice Shelf are much smaller in scale and interpreted as glaciotectonic rafts of sedimentary material and so are not directly comparable to the flat highs that we see here. Still, we thank the reviewer for pointing us toward a possible analogous feature!*

Line 293: [glacigenic sediment was transported] by what?
*We have qualified transport of material down-slope was by gravity-driven processes (although we cannot be more specific than this based on our morphological data alone).*

Line 307: did you consider doing this for different orientations, as in Spagnolo et al., to quantify basal drag relative to ice flow direction?
*We did do power spectra and basal drag analyses for 6 across-flow lines as well as along-flow lines (see Figs. S5a, b). This is discussed in (new) Section 5.2 and we have added a sentence about across-flow vs*

*along-flow roughnesses for the MSGL area. One future study that we have already considered is spectral analyses of roughness for, say 8, orientations around the compass (like a Rose diagram) on a grid of the bathymetry data to assess the anisotropy (or not) of bed roughnesses. This, however, is beyond the scope of this current work, we just need to get a student or post-doc to do it now!*

Section 4.2: This section is interesting and well exposed but extremely technical and a big jump from the previous, largely descriptive, part of the paper. Part of the technicality is intrinsic, and also it is clear that one needs to read Schoof paper to fully appreciate this section. However, I wonder if a further, better effort could be made to keep the non-expert reader better engaged with this section. Perhaps the most technical aspects could be moved into the supplementary and an easier-to-grasp/simplified explanation be maintained here. Or else, could the use of an example, which is already partly incorporated here, be further exploited, to show what each (component of the) equation means in practice?

*We fully address this in our response to general comment 4 above (see new Sections 5.1 and 5.2).*

Line 407: This is kind of obvious to most of us, but for the wider audience I wonder if you should have stressed this important point earlier on as well, when you described landforms that are clear evidence of grounded ice.

*We have added a statement at the end of Section 3.1 (Glacial landforms) that the mapped area represents the former bed of TG.*

Line 418: Could you specify by how much [gravity-derived bathy underestimates seafloor depths], on average?

*We have added average numbers for the differences between the new MBES gridded bathymetry and gravity-derived bathy from Millan et al. and IBCSO, 119 m and 65 m, respectively.*

Line 431-433: Could you quantify [the significance of underestimating CDW volumes by underpredicting trough depths], rather than generically saying that it is significant?

*We have addressed this fully in our response to general comment 3 above.*

Line 469: Is this to say that TG was less dynamic than its neighbors? I would say this more explicitly, if so.

*This is not what really what we are saying. All the evidence to available date (i.e. before any ITGC dates come through) points towards a similar retreat history for Thwaites Glacier to that of Pine Island Glacier and is nicely collated and summarised by Larter et al. (2014). The more recent history (last century or so) has only been speculated about, and should be illuminated by ITGC, but it has been hypothesised that Thwaites ice shelf unpinned from the highs in front of it 55-150 years ago (Tinto and Bell, 2011), which is similar to the unpinning of PIG ice shelf from a submarine ridge ~30 years ago. We have added the following sentence to the text to clarify this:*

*"This retreat history is in line with what we know about ice-sheet retreat more generally in the Amundsen Sea, where rapid grounding-zone retreat occurred from 15 to10 ka to reach near modern limits (Hillenbrand et al., 2013; Larter et al., 2014); however, more marine dates and terrestrial thinning histories will certainly provide more clarity."*

Line 483-485: "Our interpretation of a proportion of unconsolidated sedimentary substrate, and thus low density material, on the H2 and H3 highs may explain why bathymetries derived from gravity over-estimate the height of some of these features (Figs. 8a, b)." Could you explain why?
*Although we believe that the confusion here was caused by an error in the text - if we consider Figs 8a, b and d the heights of the highs are sometimes underestimated but not OVER ESTIMATED – we have elected to remove this sentence. We have discussed this with our airborne geophysicist co-author who noted that the gravity inversion actually did a good job of predicting the heights of H2 and H3 as the free air anomaly goes down as you move west along the highs. Thus, we have removed that sentence and added a linking sentence about the interpretation of sediment on the highs as an explanation for their flat-topped morphology:*
*"All of the landform evidence we present here, supported by cores and acoustic sub-bottom profiles, suggest that the tops, fronts and sides of the H2 and H3 highs are mantled by some thickness of sediment, probably over a bedrock core. Seismic-reflection profiles would be needed to determine the internal structure of these features and sediment thicknesses."*

Line 507: This is such an important outcome and I think you should hint at it somewhere in the title
*We have changed the title to: "Revealing the former bed of Thwaites Glacier using sea-floor bathymetry: implications for warm-water routing and bed controls on ice flow and buttressing"*

Line 514: but how different would the topography need to be in order to obtain considerably different roughnesses? Would, for example, all ice stream bedrock beds (no MSGL) have a comparable roughness?
*This is definitely an interesting question. It was certainly a little surprising that all of our bed profiles (onshore and offshore, along-flow and across-flow, MBES and radar) had similar roughness properties. In a future study it would be interesting to compare our results with the findings of, for example, Jordan et al. (2017) who looked at the roughness of bedrock terrains in N Greenland and determined bedrock bed roughnesses with differing power law scaling behaviour.*

Line 527-528: This is also very interesting and makes me wonder if there are specific conditions/thresholds above which an ice stream is able to ignore topography and below which is forced to follow it. It would be great if we were able to quantify these.
*We agree with the reviewer that it would be great if we could quantify how "big" the topography needs to be before it steers the ice or, conversely, how thick the ice needs to be to ignore the topography and/or when cavitation occurs. It is certainly intuitively that thicker ice would be less sensitive to being*

*steered by large-scale bed topography (e.g. O Cofaigh et al., 2010). It may be that numerical modelling as part of ITGC, and perhaps over this offshore terrain, will provide new insights on this.*

Line 545: I do not quite see the need to stress this aspect. I would expect bed types to be the same, whether onshore or offshore. Or perhaps I am missing the point..?
*We take this point that offshore vs onshore is not the issue so we have replaced "in onshore areas" with "beneath the modern glacier".*

Line 565-566: I think this sentence is overselling. Could you distinguish between grain sizes from high res bathymetry?
*We have modified the language in this sentence to the below to not oversell our findings and to avoid repetition:*
*"These analyses add to our understanding of across-flow contributions to basal drag or hydraulic potential (e.g. Muto et al., 2019a), and allow us to consider the spatial variability of bed types (e.g. sedimentary vs. hard beds), particularly where sea-floor sediments are cored for ground-truthing."*

**References:**

Jordan et al. (2017): Self-affine subglacial roughness: consequences for radar scattering and basal water discrimination in northern Greenland. The Cryosphere, 11, 1247–1264, 2017. doi:10.5194/tc-11-1247-2017

O Cofaigh et al. (2010): Large-scale reorganization and sedimentation of terrestrial ice streams during late Wisconsinan Laurentide Ice Sheet deglaciation. GSA Bulletin (2010) 122 (5-6): 743–756.
https://doi.org/10.1130/B26476.1

**Comments by tc-2020-25-RC2: Martin Jakobsson**

Line 29: ", suggesting a positive feedback mechanism." Standalone in the abstract, it is difficult to understand what kind of positive feedback this refers to? Can it be a positive feedback for ice-shelf grounding that the ridge is flattened by the ice shelf when it grounds? I am afraid I do not get this.
*We have rewritten the Abstract (as per R1 general comment 1.) and clarified what the potential feedback mechanism is. The relevant text is: "Spatial variations in the morphology of topographic highs, known to be former pinning points for TG and its floating ice shelf, indicate differences in bed composition that are supported by landform evidence. We discuss links to ice dynamics for an overriding ice mass including a potential positive feedback mechanism where erosion of "soft" erodible highs may lead to ice-shelf ungrounding even with little or no ice thinning."*

Line 38: "...without these data calculations, of the capacity of bathymetric troughs,..." insert comma after calculations.
*This text has been rewritten (see above).*

Line 58: "Obtaining direct sea-floor measurements..." perhaps consider "Geophysical mapping at marine...."
*We have adjusted the text as suggested.*

Line 61: Consider moving Fig 1 ref to the end of the sentence since Pine Island Glacier is also shown on the figure.
*Adjusted as suggested.*

Line 71: "...ice sheet instability", change to "...ice-sheet instability"
*Adjusted as suggested.*

Line 73: Consider avoiding the term "collapse", perhaps "retreat" is more appropriate here.
*Adjusted as suggested.*

Line 86: "...hydrographic data", consider using "oceanographic data" to avoid confusion, as hydrographic data also is used for seafloor bathymetry.
*Adjusted as suggested.*

2. Geophysical datasets: Consider changing this heading to the classical "Methods", since it is not only the geophysical datasets that are described. Perhaps also some C2 parts of how the roughness analysis would fit here, such as what kind of tools were used, Matlab or?
*We acknowledge these comments on the structure of the paper. However, we feel that the two parts of the paper should remain separate (bathymetry and spectral analyses) mostly to help lead the reader through the spectral analyses section (also a comment by R1), which would be harder to follow if separated into Methods/Results/Discussion in the traditional way. We suggest a compromise structure where the paper retains the two parts but that each parts has its own Methods and Results section, with the Discussion bringing both components together. Therefore, the proposed revised structure is:*
*1. Introduction*
*2. Methods I: Multibeam echosounder datasets (MBES)*
*3. Results I: A new bathymetric compliation for the inner Amundsen Sea Embayment shelf*
*3.1 Glacial Landforms*
*3.2 Troughs and channel metrics*
*3.3 Bathymetric highs and ridges*
*4. Methods II: Bed roughness and basal drag*

*4.1 Spectral analysis of bed roughness*
*4.2 Relating bed topography to basal drag*
*5 Results II: Assessing roughness and drag contributions for palaeo- and modern glacier beds*
*5.1 Bed roughnesses*
*5.2 Basal drag contributions*
*6 Discussion*
*6.1 Implications from the new bathymetric compilation*
*6.2 Implications from sea-floor morphology*
*6.3 Implications from the new bed roughness data*
*7 Conclusion*

Line 115: Information on the navigation/motion-system is missing
*We have added information on navigation and vessel motion system (Seapath 330) used alongside the MBES during cruise NBP19-02.*

Line 128-129: Consider using the acronyms CTD and XBT since they are standard across several disciplines.
*We have added the acronyms at this point in the methods to make it accessible to those from other disciplines.*

Line 138: Add version number also for QPS Fledermaus, and earlier for MB System, to be systematic with that version number is written for ArcGIS.
*We have added the version number of Fledermaus.*

3. New Bathymetric compilation….: This is where the results begin, consider making all of this under a heading called "Results and Interpretation".
*See the above comment proposing a new structure. IN the revised structure, this section would become Results I.*

Line 174: The pinning point on H2 is seen in Fig 3a, as a the former grounding line, but consider putting some arrow or other indicator so it is readily seen when looking for it after reading the text.
*We have labelled this on Fig 3b ad Fig 4 also.*

Line 194: The semi-circular moats – crescentic scours are not in the legend of the Figures, nor pointed out. While I see them, I think readers not dealing with seafloor morphology should be guided.
*We have revised Figure 3b to show the mapped crescentic scours and we have provided a close-up view in the new Fig S1d which shows type examples of the main landforms discussed in the text. We have also now referred to this new supplementary figure in the text in Section 3.1.*

3.2 Trough and channel metrics. The description of the troughs and channels is good, but I do lack a bit on the oceanographic perspective on how they can act as present routes for the CDW flow towards the glaciers. There is a last sentence about potential pathway for CWS, but more information could be added, for example if there are critical sills along the troughs. If this could be expanded, it would help the oceanographic community to readily make use of the results.

*We have added a paragraph in 3.2 about along-trough pathways, critical sill depths, and channel widths at the sills (shown in new Fig. S5). The paragraph reads: "Long profiles from the T2-T4 troughs (Fig. S5) identify sill depths along the pathways of the troughs that may act as important constrictions for ocean circulation, in particular if they impede CDW inflow towards the Thwaites grounding zone (cf. De Rydt et al., 2014). T2 has a smooth long profile with a prominent sill at 710 m depth at about 107°3'W, 75°3.6'S whereas T3 has a rugged profile with three bathymetric sills in its northern (ice distal) part with depths of 750-760 m, and several other sills further south (ice proximal) around 780 m water depth. The bathymetry around T4, east of the EIS, is generally deeper (>1000 m) than most of T2 and T3, so the main constriction on this trough seems to be between the NE-SW trending sea floor ridge in Pine Island Bay (Fig. 2a). At this location, around 105°24.4'W, 74°35.4'S, there is a sill at 780 m depth. Channel widths at these locations are 5000 m for the T3 sills and 2500 m for the T4 sill; widths were measured at 500 m depth as this is taken to be a reasonable top-CDW depth for the area (based on oceanographic measurements; B. Queste, pers. comm.). The bathymetry of the highs around T2 is all >500 m depth meaning that CDW could effectively "flood" over this topography rather than be constrained to the trough; however, if it was topographically routed (cf. Nakayama et al., 2019) through T2 then the channel width at the sill is 4700 m (at 640 m water depth)."*

Line 279: "In addition, their long-profiles have negative slopes (i.e., deepen consistently down the flank of the highs)..." I find it very hard to envision what this means, and how I can see this in the imagery? What else can a gully do that deepen down the flank? I miss something here.

*This sentence was added at the request of a non-geomorphologist to explain the form of gullies. Having added a type example of gullies in Fig. S1f to aid the reader, and referred to this in the text describing the gullies, we have removed this sentence.*

4.1 Spectral analysis of bed roughness. This section presents an interesting approach to analyse the sea-floor topography. It is technical, but important if one like to follow exactly what has been done. I would even encourage that some additional bits and pieces are added in order to make it even easier to follow the approach (see below). Perhaps consider a flow chart that illustrate the approach?

*We take this point on board, it is similar to a comment also made by R1. In the revised version we have provided more linking text to help guide the reader through the analysis –see response to R1 general comment 2.*

Line 304: The applied theoretical expression for form drag is referenced to Schoof (2002), I would

recommend that the expression is shown in the paper and referenced. It would help the reader that really likes to follow the approach.

*Although we acknowledge this comment, it is difficult to simply insert the Schoof equation because he uses non-dimensional quantities whereas we use dimensional quantities because we want to relate our parameters to physical quantities e.g. length scales. We have rewritten the spectral analyses sections further explaining the relationship to Schoof (2002) as well as many of the important parameters which hopefully should aid readers particularly interested in the approach.*

Line 307-308: This repeats the sentence above, line 303-304.

*Now that we have moved the methods to its own section (5.1) this repetition is avoided.*

Line 308: I cannot find which of the bed elevation profiles shown in Fig. S1 that is shown? It only says, "a profile", but not which one.

*We have added the profile name and specific part of Fig S1 to clarify this (e.g. profile 6 in Fig. S1a).*

Line 310: Which tools are used to implement the Welch method? Was it Matlab, or? I think this could be shortly described in the Methods previously.

*Yes, Matlab R2017a; this is now fully described in the new section 5.1 (bed roughness methods).*

Line 316: "in the vertical..:" why not say "random offset of the depth value for each..:",

*We have altered the text as suggested.*

Line 317: The figure reference SF4 is presumably S4? I note that also within the Supplementary Information, the figure references are made to SF...instead of only S....

*We have corrected these all to e.g. S4 as per TCD formatting.*

Figure S4 (*now Fig. S7*): My first interest was to compare the plots for profile 7 with any of the others. First, I thought that that profile 7 was missing from Supplementary figure S4, but it was there although not placed in the order of the numbered profiles 1-n, it is shown in panel p. Perhaps consider placing it in the order, and perhaps showing a comparison between profile 7 across the MSGLs with any of the other profiles in the main article since it will visualize what spectral analyses really show?

*We have placed the profiles in order in Fig S7 and also in Fig 7 as requested and we direct the reader to Fig 7 in the main text which shows profile 7 alongside along-flow profiles from the Thwaites MBES dataset.*

**Comments in tc-2020-25-SC1-supplement:**

Lines 185-218: I appreciate the thorough description of landforms here, but often found it hard to link the text to the figures (and differentiate landforms) the way the authors did. I understand that looking at these things is interpretive, and at times as much an art as a science, but I think it would be helpful if the authors put forth an image for a type example for each of the described features. Crag-and-tails, glacial lineations, grooves, gulleys, channels, troughs, grounding-zone wedges, slide scars, crescentic scours; linking them to the figures is often very challenging, and figuring why one elongate feature is called a groove and one a lineation in these data is often difficult to do. When I was faced with my own data from swath radar under Thwaites, trying to differentiate features, I really wished I had a clearer articulation in the literature of how others defined features in their data from morphology alone.

*We appreciate that the interpretation of glacial landforms (here submarine) is not in every reader's skillset and we want this paper to be accessible to a wide readership. As such, we have made a new Supplementary Figure (new Fig. S3) to give type examples of the main glacial landforms discussed in the text and noted in this short comment. We have used examples from the Amundsen Sea Embayment, and from this dataset wherever possible, to make them as relevant as possible for this paper.*

*Beyond this, we strongly recommend that readers interested in glacial landforms consult the "Atlas of Submarine Glacial Landforms: Modern, Quaternary and Ancient", Geol. Soc. Memoir 46, edited by J.A. Dowdeswell et al. which has numerous type examples of glacial landforms from the marine realm.*

Lines 195-197: These moats are gorgeous, and really interesting to think about. In the reviews of our swath radar paper at Thwaites (Holschuh et al., 2020), we were challenged on the interpretation that they must be carved by water, and have spent a fair amount of time since thinking about that problem. There are reasons to believe that ice might be the primary actor here. Is there a reason you only mention meltwater and till slurries, when Graham and Hogan list "meltwater erosion, erosion by a saturated till slurry, or the direct action of mobile basal ice"?

*Agreed! This was an oversight on our part and we have now added mobile basal ice to the text. Unfortunately, we do not have room to go into a detailed discussion of how these features form, however, we think about this often too and are interested in doing more on this topic. One question that we come back to is why these features are observed in some areas and not others, and particularly in areas where you might expect less basal melt? We have also noted differences in moat morphology (e.g. the absence of a downstream obstacle) that are hard to explain. These are definitely topics for future research.*

Lines 477-480: What specifically indicates that flat-topped surfaces are erosional? Given that tablelands have been described in many places under Antarctica (as far back as Drewry 1975), I think more evidence might be required to call them planed-off. In general, features that act as ice rises are thought to have been areas of uniquely low erosion rates (Matsuoka et al., 2015). The fact that they

interrupt deep glacial troughs seem to imply that those features are in fact more resistant than their surroundings. I would just like more (or clearer) evidence before arguing there is some new, unique positive feedback here, distinct from existing discussion of erosion / ice-flow feedbacks (e.g., Kessler et al, 2008).

*We have addressed a similar comment about the origin of the flat tops from R1, and discounted the flat tops as hard sedimentary surfaces based on seismic-reflection data for the inner Amundsen Sea shelf. We have also added new text to both the descriptions of this morphology and its interpretation in Section 3.3 and its implications for ice dynamics in Section 6.2 to explain that our suggestion is not of a large amount of erosion occurring rather that some glacial sediment was deposited on the highs when they were at the GZ and then the motion of TGT over them may have promoted slope failures and skimmed sediment from their tops. We also discuss that for the duration of observations (55 years) the TGT has moved quickly over the area of sea floor highs (i.e. THwaites ice shelf has not formed an ice rise) acknowledging that these sites are considered to have low erosion rates. Hopefully, our expanded discussion of build up of sediment at the GZ, and then its potential for failure/erosion but the subsequent ice shelf is clearer than our original text. This is certainly distinct from erosion/ice-flow feedbacks of grounded-ice flow with arguably higher erosion rates in areas of thicker ice (e.g. Kessler et al., 2008) as we are discussing the motion of an ice shelf over relatively recent GZ sediments. However, we also state clearly that we do not know if this mechanism has occurred at THwaites, only that it is* ***possible*** *(as R1 also states!).*

Lines 493-495: This was a problem we were having comparing swath radar data with the terrestrial record – sediment in-fill of crescentic features was making it hard to evaluate their true depths in the paleo record. Definitely interesting to see the same challenges here!

*Agreed! The crescentic scours are arguably a bigger problem than the troughs, seismic-reflection or acoustic methods can at least tell us whether there is sediment infill in the troughs but the small-scale of the crescentic scours means that they are not well imaged by our shipborne methods. Coring attempts in a moat around a drumlin in Marguerite Trough (see Kilfeather et al. 2011; GSA Bulletin 123) did not really hit the sediment in the moat; AUV studies over these features (including sub-bottom profiling, maybe as part of ITGC-TARSAN…) would definitely help see what is in them!*

Line 509: Again, it seems unlikely that (after all of Antarctica's growth and retreat cycles) we might catch a very transient pinning point now. Doesn't it seem more parsimonious that there is no such thing as a particularly weak pinning point? Either that, or the authors should expand on the idea that erosion of pinning points requires ungrounding (maybe higher velocities in ice shelves/ice rises, as opposed to fully grounded ice are required to erode the underlying pinning point, or slump events are a required precursor, and so this feedback is unique to ice rises as opposed to the general erosion/ice flow feedback already described in the literature).

*We are not sure that we agree with this comment. In response to comments from R1 we have added text to expand on the idea of an erodible pinning point in this setting and we think that this may help*

*address this comment also. At Thwaites, we know that the GZ was on/near the highs probably for a long time flushing all that sediment down between the highs, into the fans, when it is possible that rather a lot of glacigenic sediment built up at the GZ on the highs (we have a GZW there). At some point, the GZ retreated and there was a transition to an ice shelf, would this not keep bulldozing sediment from the tops of the highs esp if the ice shelf accelerated? Wouldn't the GZ sediments provide a perfect chance to make a soft pinning point? Failures on the highs, which could have occurred as the GZ retreated off these features, would only promote instability of grounding on the high as material would be moved downslope rapidly in discrete events. Hopefully, our new text clarifies that it is the sequence of events at Thwaites (GZ on the highs, build up of sediment, retreat of GZ, rapid flow of Thwaites Ice Shelf over the high) that opens up the possibility of this mechanism occurring. Thus, we now highlight that higher ice shelf velocities would be required and that at Thwaites we have no evidence of this in the observational record (e.g. TGT has continued to move rapidly over the highs for the past 55 years). We also stress that this is only a possibility, not that it definitely happened. Of interest may be that we acquired new seismic reflection profiles from Pine Island Bay this year that indicates variable composition of seafloor highs in the area.*

Line 532-533, 537-539, and 544-545: Without seismic data or rock cores, I do not think you have the data required to validate Muto et al.'s work (although I do think it has interesting implications for your data set). Muto was looking at features within a region of the Thwaites bed that, if interpreted morphologically, would have been assumed to be uniformly hard bedded. Below, you can see a figure from our swath radar paper (Holschuh et al., 2020), that shows that the bed looks like in the vicinity of Muto et al.'s seismic line:

You can see the upstream region, characterized by crag-and-tails and MSGL, is uniformly weak in the seismic data. It is in the downstream half of the Thwaites grid that is described in detail by the authors, showing that (in a region that might be interpreted as uniformly hard by the morphology alone), the lee and stoss sides of bed features show variable bed properties. I think the only way to actually validate the Muto et al. study is to look in more places with coincident high-resolution morphological data and acoustic property or rock property measurements, it is not possible to validate or contradict their results with morphological data alone.

*The reviewer is right that we are not looking explicitly at an area thought to be uniformly hard bedded as in Muto et al (2019 a, b). However, when we consider the length scales of our crag and tails on H3 in particular (<5 km) they are more in line with the "hard bedded terrain" of Muto et al. (2019) than the large crag and tails further upstream (>12km) and we think the comparison is still reasonable. However, we acknowledge that without coring/seismic profiles we cannot validate Muto's work and we have changed the emphasis of our wording so as not to say that we are validating Muto et al.'s work but that our results are consistent with their findings. Thus, we replace ""We note that these features exhibit the same correlation …" put "We interpret morphological characteristics of these features as being consistent with the correlation of morphology with bed type that has been described from on-ice seismic reflection profiles for TG (Muto et al., 2019a, b), although we recognize that high-resolution*

*seismic reflection data would be required to confirm this". We also slightly change the emphasis of this section to point out the similarity between the crag and tails in Holschuh et al (2020) and under the Rutford Ice Stream as the most comparable terrains to our data.*

Line 563-564: I have always been jealous of how nice multibeam data look – you are right that conventional radar sounding and seismic sounding can't compare. But swath radar data are finally giving sea-floor observations competition! I know you mention the substance of the Holschuh et al., 2020 paper below, but some of the predecessors deserve mention here. (Paden et al., 2010; Jezek et al., 2011).
*We have added these references in Section 6.2 when introducing swath radar (but before talking about swath radar at Thwaites where we refer to the Holschuh paper.*

Line 566-567: Again, I'm not sure you have the data required to do more than assume variability in bed type.
*We take this on board (see above comment to 532-533) and have changed the wording from "These analyses … and allow us to constrain the spatial variability of bed types" to "These analyses … and, in combination with high-resolution seismic data and ground-truth from sediment cores, have the potential to constrain the spatial variability of bed types".*

Line 591-594: I worry that there is something that I missed– do you have direct observation of substrate type from acoustics or coring? If so, that needs to be described in more detail, because I really think Muto et al., 2019 cannot be validated without them.
*In the case of the MSGL terrain analysed we do have direct observations of substrate type from sub-bottom profiles. The profiles show that the MSGL are sedimentary are included as a supplementary figure in Larter et al. (2009) and, additionally, high-resolution seismic profiles over the area are included in Graham et al. (2009).*

Lingering Questions:
Because we are interested in moats generally, we noticed a commonality between your data and our swath radar data at Thwaites. Moats on the leading edge of bedforms often meet exactly at the center of a downstream mot, at the head of a new bedform. I find this to be a really curious pattern – any thoughts on why this might be the case?
*This is definitely an interesting/exciting observation! Could one possibility be that whatever process/material that causes the erosion of the moat (ice/water/slurry), which then extends around the sides of the obstacle (as the moat continues there) would be the focus for erosion should another obstacle on the bed be met? We have started work to assess the morphological variation in crescentic scours (and their "obstacles") which may shed more light on how common this pattern really is. I have not, however, noticed this exact pattern before… We would certainly be very happy to continue this discussion offline and compare notes on the moats!*

As one last note – due to the highlands you've pointed out (H1/H2/H3), the main trough and pathway for CDW to route in toward the ice-sheet terminus is actually to the true west of the modern Thwaites shelf. Do you have any thoughts on what implications that has for Thwaites retreat? It looks as though there are available high-spots for shelf regrounding to the west, but perhaps the Thwaites tongue was never resilient enough, given its closer proximity to this CDW pathway? I think some more discussion of the oceanographic implications of these data could be a really useful addition.

*This is a really interesting point that I think will be discussed in detail in both future THOR-ITGC papers that look at the retreat history for Thwaites and possibly by the oceanographers looking at circulation here. It may be that as ice retreated across the shelf that the large Thwaites Trough "funnelled" warmer water to access at Thwaites GZ promoting retreat there. The chronological constraints on retreat that will come out from the THOR project should illuminate when this occurred and whether it was coincident with retreat at PIG. Pine Island Bay is a wide and generally deep embayment that may have simply been flooded with warmer water during retreat. In the modern setting, a paper with our oceanographic colleagues shows CDW accessing the Thwaites cavity from east of the EIS so it may be that this branch of inflow became more important over time, as ice stepped back. We look forward to tackling these questions in future papers that use this bathymetry as their backdrop!*

**References:**

Graham, A. G. C., Larter, R. D., Gohl, K., Hillenbrand, C.-D., Smith, J. A., and Kuhn, G.: Bedform signature of a West Antarctic palaeo-ice stream reveals a multi-temporal record of flow and substrate control, Quaternary Science Reviews, 28, 2774-2793, 2009.

Kilfeather, A. A., et al. (2011): Ice-stream retreat and ice-shelf history in Marguerite Trough, Antarctic Peninsula: Sedimentological and foraminiferal signatures. *Geological Society of America Bulletin* 2011;123;997-1015. doi: 10.1130/B30282.1.

Larter, R. D., Graham, A. G. C., Gohl, K., Kuhn, G., Hillenbrand, C.-D., Smith, J. A., Deen, T. J., Livermore, R. A., and Schenke, H.-W.: Subglacial bedforms reveal complex basal regime in a zone of paleo–ice stream convergence, Amundsen Sea embayment, West Antarctica, Geology, 37, 411-414, 2009.

Additional unsolicited changes:

1. *We have altered the nomenclature of our troughs to match another paper that will be submitted imminently that uses these same bathymetric data to assess CDW circulation in front of Thwaites Glacier (Wahlin et al., In Prep.). Thus, the main sea floor trough in front of TG is named Thwaites Trough and the small troughs interrupting the high have been renamed here from west to east T1-T4: (see revised Figs. 2 and 8).*
2. *We have gone through the MS and replaced "grounding line" with "grounding zone" for consistency.*
3. *We have added one co-author (Anna Wahlin) who has helped us to do some calculations on oceanic heat fluxes through the sea floor troughs; this is fully described in the revised Supplementary Information.*
4. *We have gone through the text, figures and supplementary information and corrected small errors and typos discovered during the response to review process.*

# Revealing the former bed of Thwaites Glacier using sea-floor bathymetry: implications for warm-water routing and bed controls on ice flow and buttressingbuttressing~~Revealing the former bed of Thwaites Glacier using sea-floor bathymetry~~

Kelly A. Hogan[1], Robert D. Larter[1], Alastair G. C. Graham[2], Robert Arthern[1], James D. Kirkham[1,3], Rebecca Totten Minzoni[4], Tom A. Jordan[1], Rachel Clark[5], Victoria Fitzgerald[4]~~Fitzgerald[4]~~, Anna K. Wåhlin[6], John B. Anderson[7]~~Anderson[6]~~, Claus-Dieter Hillenbrand[1], Frank O. Nitsche[8]~~Nitsche[7]~~, Lauren Simkins[9]~~Simkins[8]~~, James A. Smith[1], Karsten Gohl[10]~~Gohl[9]~~, Jan Erik Arndt[10]~~Arndt[9]~~, Jongkuk Hong[11]~~Hong[10]~~, Julia Wellner[6]~~Wellner[5]~~

[1] British Antarctic Survey, Natural Environment Research Council, High Cross, Madingley Road, Cambridge, CB3 0ET, UK
[2] College of Marine Science, University of South Florida, Saint Petersburg, FL 33701, USA
[3] Scott Polar Research Institute, University of Cambridge, Lensfield Road, Cambridge, CB2 1ER, UK
[4] Department of Geological Sciences, University of Alabama, Tuscaloosa, AL 35487, USA
[5] Department of Earth and Atmospheric Sciences, University of Houston, Houston, TX 77204, USA
[6] Department of Marine Sciences, University of Gothenburg, 40530 Göteborg, Sweden
~~[5] Department of Earth and Atmospheric Sciences, University of Houston, Houston, TX 77204, USA~~
~~7~~6 Department of Earth Science, Rice University, Houston, TX 77005, USA
~~8~~7 Lamont-Doherty Earth Observatory, Columbia University, Palisades, New York, USA
~~9~~8 Department of Environmental Sciences, University of Virginia, Charlottesville, VA 22904, USA
~~10~~9 Alfred Wegener Institute Helmholtz-Centre for Polar and Marine Research, 27568 Bremerhaven, Germany
~~11~~10 Korea Polar Research Institute (KOPRI), Incheon 21990, Republic of Korea

*Correspondence to*: Kelly A. Hogan (kelgan@bas.ac.uk)

**Abstract.** The geometry of the sea floor immediately beyond Antarctica's marine-terminating glaciers is a fundamental control on warm-water routing but it also describes former topographic pinning points that have been important for ice-shelf buttressing. Unfortunately, this information is often lacking due to the inaccessibility of these areas for survey leading to modelled or interpolated bathymetries being used as boundary conditions in numerical modelling simulations. At Thwaites Glacier (TG) this critical data gap was addressed in 2019 during the first cruise of the *International Thwaites Glacier Collaboration* (*ITGC*) project. We present more than 2000 km$^2$ of new multibeam echo-sounder data (MBES) acquired in exceptional sea-ice conditions immediately offshore TG, and we update existing bathymetric compilations. The cross-sectional areasdepths of sea-floor troughs are under-predicted by up to 40% where MBES arewere missing, or are not resolved at all, suggesting that calculations of trough capacity, and thus oceanic heat flux, may be significantly underestimated. Spatial variations in the morphology of topographic highs, known to be former pinning points for the floating ice shelf of TG, indicate differences in bed composition that are supported by landform evidence. We discuss links to ice dynamics for an overriding ice mass including a potential positive feedback mechanism where erosion of "soft" erodible highs may lead to ice-shelf ungrounding even with little or no ice thinning. Analyses of bed roughnesses and basal drag contributions show that the sea-

floor bathymetry in front of TG is an analogue for extant bed areas. Ice flow over the sea-floor troughs and ridges would have been affected by similarly high basal drag to that acting at the grounding zone today. We conclude that more can certainly be gleaned from these 3D bathymetric datasets regarding the likely spatial variability of bed roughness and bed composition types underneath TG. This work also addresses the requirements of recent numerical ice-sheet and ocean modelling studies that have recognised the need for accurate and high-resolution bathymetry to determine warm-water routing to the grounding zone and, ultimately, for predicting glacier retreat behaviour. ~~The geometry of the sea-floor beyond Thwaites Glacier (TG) is a major control on the routing of warm ocean waters towards the ice stream's grounding zone, which has led to increased mass loss through sub-ice-shelf melting and resulting accelerated ice flow. Nearshore topographic highs act as pinning points for the Thwaites Ice Shelf and potentially provide barriers to warm water incursions. To date, few vessels have been able to access this area due to persistent sea-ice and iceberg cover. This critical data gap was addressed in 2019 during the first cruise of the *International Thwaites Glacier Collaboration* (*ITGC*) project, with more than 2000 km² of new multibeam echo-sounder data (MBES) were acquired offshore TG. Here, these data along with legacy MBES datasets are compiled to produce a set of standalone bathymetric grids for the inner Amundsen Sea shelf beyond both Pine Island and Thwaites glaciers. At TG, the bathymetry is dominated by a >1200 m deep, structurally-controlled trough and discontinuous ridge, on which the Eastern Ice Shelf is pinned. The geometry and composition of the ridge varies spatially with some parts having distinctive flat-topped morphologies produced as their tops were planed off by erosion at the base of the seaward-moving Thwaites Ice Shelf, suggesting a positive feedback mechanism for ice-shelf ungrounding. Knowing that this offshore area is a former bed for TG, we applied a novel spectral approach to investigate bed roughness and find that derived power spectra can be approximated using an inverse-square law, a result that is consistent with spectra for bed profiles from the modern TG. Using existing ice-flow theory, we also make a first assessment of the form drag (basal drag contribution) for ice flow over this topography. Ice flowing over the sea-floor troughs and ridges would have been affected by similarly high basal drag to that acting in the grounding zone today. We show that the sea-floor bathymetry is an analogue for extant bed areas of TG and that more can be gleaned from these 3D bathymetric datasets regarding the likely spatial variability of bed roughness and bed composition types underneath TG. Comparisons with existing regional bathymetric compilations for the area show that high-frequency (finer than 5 km) bathymetric variability beyond Antarctic ice shelves can only be resolved by observations such as MBES and that without these data calculations of the capacity of bathymetric troughs, and thus oceanic heat flux, may be significantly underestimated. This work meets the requirements of recent numerical ice-sheet and ocean modelling studies that have recognised the need for accurate and high-resolution bathymetry to determine warm water routing to the grounding zone and, ultimately, for predicting glacier retreat behaviour.~~

## 1 Introduction

Knowledge of Antarctica's coastal bathymetry is essential when considering ocean circulation and recent dynamic changes at the ice-sheet margin. Sea-floor bathymetry influences ice-ocean interactions in two ways. First, deep (> 500 m water depth)

bathymetric troughs and channels provide access routes for warm, salty Circumpolar Deep Water (CDW: ~ 0.5-1.5 °C, located below ~300-500 m water depth; Jacobs et al., 1996, 2013) to present-day grounding zones. The inflow of CDW increases basal melting and ice-shelf thinning (Jacobs et al., 1996; Rignot et al., 2013) leading to ice-shelf disintegration, reduced buttressing, ~~grounding-zone retreat, reduced ice-shelf buttressing and ultimately~~ the acceleration of the ice shelves and grounded ice upstream, and ultimately grounding-zone retreat (Schoof, 2007; Joughin et al., 2010; Favier et al., 2014; De Rydt & Gudmundsson, 2016). This effect is particularly significant for ice resting on reverse-slope beds (i.e. retrograde, when the bed slopes down towards the interior of the continent) where grounding-zone retreat may initiate marine ice~~-~~sheet instability, a positive feedback that could lead to runaway retreat (Weertman, 1974; Schoof, 2007). Secondly, bathymetric highs can slow ice retreat by acting either as pinning points for floating ice or as "sticky spots" at the grounding zone itself, and by partially blocking warm water access to modern grounding zones (e.g. De Rydt et al., 2014). An ice shelf pinned on a bathymetric high is subject to increased buttressing, and a topographic high at the grounding zone similarly contributes to basal drag that restricts ice flow. Both have the potential to act as stabilising influences (Alley et al., 2007; Parizek & Walker, 2010).

Geophysical ~~Obtaining direct sea-floor measurements~~Geophysical mapping ~~-~~at marine-terminating ice-sheet margins is often difficult due to more or less persistent floating ice cover in the form of icebergs, ice tongues, ice shelves and sea ice. This is certainly the case at Thwaites Glacier (TG), West Antarctica, which is one of the two dominant fast-flowing glaciers draining into the eastern Amundsen Sea Embayment (ASE~~) (Fig. 1)~~; the other being Pine Island Glacier (PIG; Fig. 1). Together, Thwaites and Pine Island glaciers were responsible for >30 % of the annual ice discharge from the West Antarctic Ice Sheet (WAIS) between 2009 and 2017 (compared with 25 % for 1979-1989; Rignot et al., 2019), and TG and adjacent smaller glaciers ~~alone~~ accounted for ca. 50-55% of the annual net mass ~~balance~~ loss from the WAIS ~~between~~ since 1992 ~~and 2017~~ (Shepherd et al., 2019; Smith et al., 2020). Recent observations and mass balance calculations show that TG is experiencing some of the highest rates of flow acceleration (Mouginot et al., 2014), discharge (Rignot et al., 2019), thinning (McMillan et al., 2014; Milillo et al., 2019; Shepherd et al., 2019), and grounding-~~line~~ zone retreat (Rignot et al., 2014; Milillo et al., 2019) across the entire ice sheet. For example, over the past ~~three~~ four decades net mass loss from TG is calculated to have increased from ~~12±1~~ 4.6 Gt yr$^{-1}$ during the period 1979~~1992-1997~~79-1989 to ~~76±6~~ 34.9 Gt yr$^{-1}$ from 2009~~2009~~12 to 2017 (~~2017~~6 ~~(Shepherd~~ Rignot et al., 2019). Its configuration, on a reverse-bed slope with direct connectivity to the deep WAIS interior (Holt et al., 2006), and its wide marine-terminating ice front (>120 km) with only small, unconfined frontal ice shelves, implies that TG is particularly susceptible to retreat via marine ~~ice~~ ice-sheet instability (Weertman, 1974; Hughes, 1981; Schoof, 2007; Vaughan & Arthern, 2007~~; Schoof, 2012~~). Furthermore, a significant retreat in this system could lead to a much wider WAIS ~~collapse~~ retreat and the future behaviour of this glacier system is now in the spotlight (e.g. Joughin et al., 2014; Scambos et al., 2017).

At present, the eastern and central parts of TG are fronted by two protruding floating ice masses, the Eastern Ice Shelf (EIS) and the Thwaites Glacier Tongue (TGT), which extend for 40-50 km beyond the grounding zone, to the west of which a 20-km wide mélange of icebergs and sea-ice exists (Fig. 2). For simplicity, we shall refer to these floating ice masses collectively as the Thwaites Ice Shelf (Fig. 2a; cf. Heywood et al., 2016). The TGT extends from the fastest-flowing region of TG (Fig.

2a) and has, on multi-decadal timescales, ~~periodically~~ advanced ~~to extend~~ up to 130 km from the grounding line before the majority of the floating tongue has calved (MacGregor et al., 2012). As a result, the inner shelf beyond this area has been rendered inaccessible by remnants of the TGT as they have drifted north-northwest, including the very large B-10 and B-22A icebergs that remained grounded on the shelf for decades after they had calved before ~~1972~~ 1965 and in 2002, respectively (Fig. 1) (Ferrigno et al., 1993; Rabus et al., 2003; MacGregor et al., 2012). In contrast, the EIS remains pinned on a sea-floor high that restricts its flow (Rignot et al., 2001; Tinto and Bell, 2011; Jordan et al., 2020) and induces shear between the EIS and TGT. Satellite imagery confirms that since 2006 increased crevassing and fracturing has weakened the shear zone between the EIS and TGT (Kim et al., 2015), with the two ice shelves remaining connected until 2010 (MacGregor et al., 2012). Due to its inaccessibility, few marine observations have been made on the inner shelf in front of TG (Jacobs et al., 2012). The existing ~~hydrographic~~ oceanographic data, along with more comprehensive results from Pine Island Bay, confirm the presence of CDW in the deep troughs east and north of the EIS (Dutrieux et al., 2014; Jenkins et al., 2016) and identify these troughs as potential pathways for warm water to the TG grounding zone (Fig. 2a; Milillo et al., 2019).

Regional bathymetric compilations for the ASE shelf use multibeam echo-sounder ~~data~~ (MBES) data where available in offshore regions (Nitsche et al., 2007, 2013; Arndt et al., 2013) ~~and~~ with gravity inversions and a limited amount of echo-sounding data from autonomous underwater vehicles for sub-ice shelf cavities (Jenkins et al., 2010; Tinto and Bell, 2011; Millan et al., 2017; Jordan et al., 2020)~~.~~). These datasets have identified glacially-modified depressions on the continental shelf that act as conduits for CDW transport towards present-day ocean-terminating glacier margins in the ASE (Fig. 1) (e.g. Nitsche et al., 2007; Walker et al., 2007; Jacobs et al., 2012; Nakayama et al., 2013). Landward of the MBES data coverage that existed prior to this study, gravity inversions had indicated the presence of an NE~~east-west~~NE-SW trending ridge on which the EIS is pinned (Rignot, 2001; Tinto & Bell, 2011; Millan et al., 2017). Millan et al. (2017) reported that the ridge is interrupted by at least three channels with water depths between 600 and 1000 m, interpreted to be potential CDW pathways towards the grounding zone.

Considering the use of sea-floor bathymetry at higher spatial scales (than regional compilations), the analysis and interpretation of submarine glacial landforms revealed by MBES datasets provides important information on the dynamics and configuration of former glaciers and ice sheets. On the inner ASE shelf, for example, the bed of an expanded PIG has revealed the past flow direction of a large ice stream that extended more than 400 km to the continental shelf break (Evans, et al., 2006; Graham et al., 2010; Jakobsson et al., 2012), as well as evidence for extensive erosion by subglacial water during past glaciations (Nitsche et al., 2013; Kirkham et al., 2019). These offshore areas also contain well-preserved information on the form and composition of the former ice-sheet bed that may, by analogy, shed light on basal conditions under the modern ice sheet (e.g. Clark et al., 2003; Ó Cofaigh et al., 2005). The roughness of an ice-sheet bed, or its variation in the vertical over a certain horizontal distance, is a primary control on basal drag and therefore ice-flow velocity, and can be analysed for past ice-sheet beds from MBES datasets (offshore) or from satellite-derived DEMs (onshore) (e.g. Falcini et al., 2018). Even small (metre-scale) obstacles on the bed have been shown, theoretically, to exert critical basal drag on an overlying ice mass (e.g. Nye, 1970; Schoof, 2002). The great value in analysing MBES datasets for this purpose lies in their higher resolution and even 2-

dimensional spatial coverage when compared with ~~airborne~~ radar or seismic-reflection data acquired in over-ice studies (Spagnolo et al., 2017).. Previous roughness analyses (from contemporary ice-sheet beds) have associated fast-flowing ice with smoother beds (e.g. Siegert et al., 2004; Rippin et al., 2011); however, recent papers acknowledge that the picture is likely to be much more complex than this with observations of fast flow occurring over even hard, rough beds, including at TG (Schroeder et al., 2014), and acknowledging that processes acting at a variety of spatial scales (including erosion and deposition) will affect spatially-varying bed conditions and roughnesses (Jordan et al., 2017; Falcini et al., 2018).

Here, we present the first direct observations of sea-floor bathymetry adjacent to Thwaites Ice Shelf acquired as part of the first *International Thwaites Glacier Collaboration* (*ITGC*) cruise on RV/IB *Nathaniel B. Palmer* in January–March 2019 (cruise NBP19-02). In the first part of the paper, we use these data to investigate the character (bed geometry and substrate composition) of topographic highs as former grounding zones and ice-shelf pinning points, and to better resolve sea-floor troughs as potential modified CDW ~~(CDW)~~ pathways to the modern Thwaites grounding zone. In the second part of the paper, we investigate the roughness characteristics of this palaeo-glacier bed as a potential analogue for the current bed of TG and~~use a spectral approach to~~and we relate flow-line roughness to the drag contribution of~~for an~~of an overriding ice mass. We compare bed roughnesses and basal drag contributions from ~~using~~ bathymetric profiles from the inner ASE shelf to~~, and~~ bed profiles from upstream areas of PIG~~Pine Island and Thwaites glaciers~~PIG and TG, as well as to a "smooth" palaeo-ice stream bed offshore the nearby Getz A Ice Shelf. To reflect these two components of the paper~~, (1)~~ we describe: (1) the observational (geophysical) datasets used and interpret the new bathymetric dataset, which is also provided as a publically-available standalone grid; and (2) ~~we describe~~ the spectral approach and how we use it to quantitatively examine the roughness and basal drag contributions from former and modern TG beds. We use sea-floor landform evidence to describe both the flow of an expanded TG over the area as well as the spatial variability in bed composition over a series of topographic highs that once acted as both the grounding zone for TG and as pinning points for its ice shelf. We demonstrate that the offshore area just seaward of Thwaites Ice Shelf is an appropriate analogue for the modern grounding zone of TG, both in terms of its bed characteristics and in the effect of its rugged bed topography on ice flow by calculating drag contribution for different scales of roughness. Finally, wew~~We~~ highlight the importance of high-resolution MBES observational data for constraining gravity inversions and regional bathymetry compilations, which are essential boundary conditions for predictive numerical modelling experiments, and for accurately calculating the flux of warm water to the grounding zone.

## 2 Methods~~Geophysical datasets~~Methods I: Multibeam echosounder datasets (MBES)

### ~~2.1 Multibeam echosounder datasets (MBES)~~

During *ITGC* cruise NBP19-02, the marine areas in front of TG were unusually clear of sea-ice and icebergs providing a unique opportunity for bathymetric data acquisition at the margin of Thwaites Ice Shelf (Larter et al., 2020). MBES data were~~w~~ere~~as~~ acquired using a hull-mounted 1° x 1° Kongsberg EM122 echo sounder with 288 across-track beams and an operational

frequency in the range 11.25-12.75 kHz. Navigation and vessel motion information, used to correctly locate depth measurements in real-time, were taken from the ship's Seapath 330, a combined GPS and motion reference unit. The MBES was configured with "High Density Equidistant" beam spacing meaning that more than one sounding can be produced per beam (up to 432) effectively increasing across-track resolution, and in "Dual Ping" mode which ensures equal across- and along-track sounding spacing. As an example, in 600 m water depth with a 60° beam angle (typical conditions and settings on NBP19-02), this results in a sounding spacing on the sea floor of ~5-7 m; in 1200 m water depth (near maximum survey depths during NBP19-02) this sounding spacing would effectively double to 10-14 m. Here, in addition to this new dataset, we have compiled all available MBES data in the area from UK, US, German, Swedish and Korean expeditions (Table 1; Fig. 2) to produce gridded bathymetric data products. Note that the sounding spacing achievable by each MBES system varies considerably depending on the system setup with older systems generally attaining lower spatial resolution. For example, at 1200 m water depth and a 60° beam angle, the Kongsberg EM120 MBES would achieve an across-track sounding spacing of only 22 m, and the Seabeam 2112 MBES only 35 m. Together, these two systems were responsible for acquiring 5 cruises worth of data in the area (Table 1).

For NBP19-02, data processing was performed on board using MB-System (Caress and Chayes, 1996; Caress et al., 2019) in order to apply optimal sound velocity profiles (SVPs) to each data file and to remove erroneous soundings. Ray tracing and sea-floor depths were calculated using SVPs generated from conductivity-temperature-depth (CTD) and expendable bathythermograph (XBT) casts made during NBP19-02 (Larter et al., 2020). Most of the other bathymetry datasets were also initially ping-edited during each respective cruise; however, minor additional cleaning was performed in MB-System and QPS Fledermaus (Mayer et al., 2000) after the datasets were collated when clear outliers could be easily identified. Ultimately, and to accommodate the different resolutions of the original datasets, the bathymetric sounding data were gridded in MB-System using a Gaussian weighted mean filter algorithm to produce an isometric 50-m digital elevation model (DEM) for the sea floor on the southern ASE shelf. A degree of interpolation was applied to the final grids in data gaps only, filling areas six cell widths away from cells with real soundings, i.e. for a 50-m grid interpolation will fill cells up to 300 m away from a cell with real soundings. A lower resolution DEM (500-m grid cells) was produced for studies that typically use coarser bathymetric information. Together, the 50-m and 500-m DEMs are presented as a standalone regional mid-resolution bathymetric dataset. In addition, in order to examine the nature of specific sea-floor features (e.g. ice-shelf pinning points), higher-resolution grids (30-m grid cells) were produced where sounding densities allowed (e.g. Fig. 4). Final grids were visualised and analysed in QPS Fledermaus 7.8.6 and ArcGIS 10.6. Sea-floor trough and channel metrics (including widths, depths, symmetry, form ratio, u-/v-shape characterisation) were derived using the methods described in Kirkham et al. (2019);;; the reader is referred to Figure 2 of Kirkham et al. (2019) for a graphical depiction of the channel metrics measured.

Commented [HKA1]: Add DOI

~~**2.2 Bed profiles for investigating bed roughness and basal drag**~~

~~The gridded bathymetric datasets that we have produced represent the former bed of an expanded TG. Palaeo-flow lines across this former bed were picked manually by tracing lines parallel to subglacial landforms taken to indicate palaeo-ice flow~~

~~directions (e.g. Fig. 3b). We also perform this exercise for bed profiles from three additional areas for comparison with the Thwaites offshore area (Figs. S1, S2): (i) modern along-flow bed profiles for Thwaites Glacier and (ii) Pine Island Glacier, and (iii) an area of "smooth" bed topography on the middle continental shelf in the Dotson-Getz palaeo-ice stream trough, offshore from the Getz A Ice Shelf, representing a sedimentary palaeo-ice stream bed characterised by mega-scale glacial lineations (MSGL) (Graham et al., 2009; Spagnolo et al., 2014). Onshore bed profiles were extracted from the AGASEA (Holt et al., 2006) and Operation IceBridge (Cochran & Bell, 2010, updated 2014) datasets for Thwaites and Pine Island glacier beds, respectively; the profile from the Dotson-Getz Trough was extracted from an MBES dataset fully described by Larter et al. (2009) and Graham et al. (2009).~~

## 3 Results I: A newn~~New~~ bathymetric compilation for the inner Amundsen Sea Embayment shelf

Our bathymetric compilation includes more than 2000 km$^2$ of new MBES data between the EIS and the TGT and west of the TGT that provides near-continuous bathymetric coverage for ~40 km north of the present day ice-shelf margin (Figs. 2, 3). Data gaps remain in the western part of the area in front of the ice mélange, east of Crosson Ice Shelf, as icebergs and bergy bits released from the ice mélange persistently covered this region during NBP19-02. In addition, perennial fast ice and huge icebergs, such as the 80-km long and 45-km wide iceberg B-22A, that calved periodically from the TGT and then moved slowly north- and northwest, thereby episodically running aground, have generally prevented survey between TGT and Crosson Ice Shelf (see area with B-22A outlines on Fig. 1).

The sea-floor bathymetry offshore Thwaites Ice Shelf is dominated by an elongate depression oriented NNE-SSW (Thwaites Trough~~1~~) and a series of topographic highs (H1-H3) along its southern margin (Fig. 3a). The depression is characterized by water depths of 1100-1250 m, which is 200 to 400 m deeper than the sea floor on its flanks; it typically has a relatively flat or gently-inclined floor (Figs. 3a, c). Although the depression appears to be continuous for at least 75 km, and connects with areas of deep (>1300 m) sea floor directly north of the EIS and in Pine Island Trough further east (Fig. 2a), its width varies significantly along its length and the flanks are discontinuous in form. As a result, we do not define this feature as a "channel", which implies incision by water flow, but rather as a small trough. The topographic highs that make up the southern flank of the trough (H1-H3) decrease in height (above the surrounding sea floor) from NNE~~east to west~~NNE to SSW and appear to form a broad (>15 km) but discontinuous ridge, also oriented NNE-SSW. The large, discontinuous ridge is the extension of a bedrock ridge in Pine Island Trough to the east that has the same orientation (Figs. 2, 3a; Nitsche et al., 2013). The most prominent high (H1) occurs immediately north of the EIS with a shallowest recorded water depth of just 82 m and extends at least 40 km in a north-south direction. The northern part of the EIS is pinned, about 45 km downstream of the grounding zone (Rignot et al., 2001; Tinto and Bell, 2011; MacGregor et al., 2012), on the southern part of this high, forming an ice rumple in the EIS (Matsuoka et al., 2015). The shallowest water depths on the two highs H2 and H3 (from NNE to SSW) are 362 m and 611 m, respectively. Indeed, ~~remote-sensing data had identified~~ a pinning point for TGT on H2 has been identified from remote-sensing data (Rignot et al., 2011) but the TGT must have fully retreated from that point prior to NBP19-02. North of

the trough and ridge (north of 74°30' S) is an area of rugged morphology characterised by shallow ~~sea~~ sea-floor ridges and deep basins (>1400 m); this area merges with similar terrain in Pine Island Trough described by Nitsche et al. (2013) as their "area 2" (Fig. 2). East of the EIS, the eastern flank of H1 is just exposed but the bathymetry is dominated by a deep (1000-1200 m), rugged area of sea floor, bounded on its eastern edge by a bedrock high in Pine Island Bay that continues southeastwards towards the grounding zonezone~~line~~ (Fig. 2a). The deepest part of this area appears to form a poorly-defined bathymetric trough oriented NNE-SSW (T4; Fig. 3a); oceanographic measurements and models confirm that this deep acts as a pathway for CDW towards grounding lines in western Pine Island Bay (Fig. 2a) (Dutrieux et al., 2014; Nakayama et al., 2019).

### 3.1 Glacial landforms

The large-scale morphology of the sea floor offshore Thwaites Ice Shelf is overprinted by linear features oriented sub-parallel to the trough and ridge. Streamlined subglacial landforms occur in areas where bedrock crops out at the sea floor, on either topographic highs or interrupting the smooth trough floor or rugged basin floors (Figs. 3a, b). These features are identified as crag-and-tails by their tapering form and are 750-4000 m long, 200-2000 m wide and 25-250 m high (Figs. 3, 4, S1a), and their morphological similarity to crag-and-tails from other deglaciated terrains (e.g. Dowdeswell et al., 2016; Maclean et al., 2016; Nitsche et al., 2016). The wider southern ends of the crag-and-tails are rugged and have significant relief, suggesting bedrock composition, whereas the northern ends are smooth and elongate, ~~suggesting~~ indicative of a sedimentary composition. These landforms are produced subglacially as glacier ice flows across bedrock obstacles producing the characteristic morphology through erosion and deposition (Benn & Evans, 2010; Nitsche et al., 2016). The tapering of these features north-northeastward indicates palaeo-ice flow of TG in this direction towards Pine Island Trough (Fig. 3b); east of the EIS the orientation of these landforms varies from N-S to NW-SE depicting flow around the H1 high (Fig. 3b). Curved or semi-circular moats - crescentic scours (Lowe and Anderson, 2003; Graham et al., 2009; Graham and Hogan, 2016) - occur around the southern (upstream) sides of some crag-and-tails (Figs. 3b, 4a, S1d) and are suggestive of erosion by meltwater ~~(~~or, alternatively, a till slurry or mobile basal ice,~~)~~ upstream of bedrock obstacles (cf. Graham & Hogan, 2016). On the H2 and H3 highs, subtle elongate ridges separated by linear grooves also occur (Fig. 3a). These glacial lineations have parallel sides, lack a pronounced and wider end, and are 1000-2500 m long, 100-200 m wide and 2-10 m high; their crest-to-crest spacing is typically 200-500 m (e.g. Fig. S1b). These features, which were produced subglacially, have relatively short elongation ratios (<10:1) and are oriented parallel to crag-and-tails also on the tops of the highs but are slightly oblique to crag-and-tails in the trough (Fig. 3). A distinct but discontinuous scarp is mapped on the top of the H2 high, upstream from its frontal edge (Figs. 3, 4b, 4d). The scarp has a curved planform and a steep (3-4°) northern and gentle (0.5°) southern slope; glacial lineations occur on the gentle back-slope of this feature which extends for about 15 km in a SW-NE direction. The asymmetric geometry and lineated back-slope of this landform identify it as a grounding-zone wedge (GZW; Fig. S1c) (Alley et al., 1989; Larter and Vanneste, 1995; Dowdeswell & Fugelli 2012; Jakobsson et al., 2012), i.e. a wedge of sedimentary material that built up at the grounding ~~line~~ zone when it was stable for a time on the H2 high. This feature is interrupted, however, by a ~40 m deep groove

or small channel with bedrock ridges visible on either side suggesting that the sedimentary wedge is not thick enough to fully bury the underlying topography, i.e. it is only tens of metres thick. Discrete 6-10 m deep linear to curvilinear furrows~~furrow~~ with small berms (4-6 m) were mapped ~~and~~ on H3 and north of the GZW front scarp (Figs. 4a, b); these are interpreted as iceberg ploughmarks.

Sea-floor highs in the area are also variously gouged and streamlined, resulting in a pattern of grooves and bedrock ridges (Fig. S1e).~~.~~ Grooves on the H1-H3 ridges occur on their southern (upstream) parts and exhibit a range of orientations that probably relate to the structure of the underlying bedrock exploited by glacial erosion. The grooves are typically <20 m deep, <200 m wide and <6000 m long. The surfaces of sea-floor highs north of the H1-H3 ridge have a more streamlined appearance resulting from shallow, semi-parallel shallow grooves that are preferentially aligned with the crag-and-tails (Figs. 2, 3). Streamlined bedrock highs of thist~~This~~ type are~~of streamlined bedrock highs is~~are typical of inner-shelf morphologies around Antarctica (e.g. Wellner et al., 2006; Livingstone et al., 2013) including in the adjacent eastern part of Pine Island Bay (Nitsche et al., 2013). Taken together, the orientations of the streamlined subglacial landforms (crag-and-tails, glacial lineations, bedrock grooves/ridges) define the former ice-flow directions of an expanded TG (depicted by ~~red~~ white arrows in Fig. 3b) confirming that this area is the former bed for grounded glacier ice.

### 3.2 Trough and channel metrics

Multiple bathymetric troughs and bedrock channels were mapped and analysed in the area beyond Thwaites Ice Shelf as part of this study (Fig. 3a). Troughs and channels in the adjacent ~~eastern~~ part of Pine Island Bay have been described comprehensively by Nitsche et al. (2013) and Kirkham et al. (2019). The larger troughs in our study area, which have also been identified on gravity-derived regional bathymetry maps (Millan et al., 2017; Jordan et al., 2020),~~.),~~ are considered important as potential pathways for the transport of CDW towards the grounding zone of TG and warrant full description here. We distinguish these comparatively larger troughs, based on their size, connectivity and variable flank form (as described above), from the channels which are notably smaller in scale (Fig. S2~~S23~~) ~~with~~ have continuous, parallel sided-flanks, undulating thalwegs, and incise into rugged sea-floor areas interpreted as bedrock (e.g. Fig. S1e). It is widely accepted that channels of the latter type were eroded by pressurised subglacial water flow (Lowe and Anderson, 2003; Nitsche et al., 2013; Kirkham et al., 2019), whereas the troughs likely relate, at least in part, to underlying geological structures such as ~~mafic~~ dykes and tectonic deformations (cf. Gohl et al., 2013) that have been variously modified by ice, as well as possibly by subglacial water flow.

Cross-sectional analyses of the troughs (n = 166) reveal their large scale, with average widths, depths and cross-sectional areas being 2090 m, 90 m and 144 000 m$^2$, respectively (Fig. S2~~S23~~). The troughs are typically 10-30 times as wide as they are deep, although we note that there is a significant size difference between the main NE-SW trough (Thwaites Trough~~1~~) and the remaining troughs (Figs. 3a,S2,~~; Fig. S23~~). By comparison, the bedrock channels (n = 822) are on average 520 m wide, 50 m deep with a cross-sectional area of 18 000 m$^2$. The channels are generally 5-10 times wider than they are deep. The derived *b values*, which characterise cross-sectional shape (Pattyn and Van Huele, 1998), suggest that the bedrock channels are between

v- and u-shaped, whereas the larger troughs have no dominant cross-section shape (Fig. S2~~S2~~3). In general, the trough floors are flat or inclined in cross-profiles (Fig. 3c), and are gently undulating in along-trough profiles.

The main Thwaites Trough~~T1 trough~~ is oriented NE-~~NNE-SS~~W, which is oblique to the northerly palaeo ice-flow directions immediately in front of Thwaites Ice Shelf (Fig. 3b). This indicates that, at the time that the subglacial landforms were produced, ice was thick enough not to be fully steered by even major elements of the bed topography. The two southernmost troughs that we have analysed (T2 and T3 on Fig. 3a) are oriented perpendicular to Thwaites Trough~~I~~ (i.e. NNW-SSE), and the troughs north and east of the EIS are generally aligned with palaeo-ice flow directions (Figs. 2, 3a). Note that the T1 trough is not well covered by our MBES dataset and is not discussed in detail here. The T2 and T3 troughs, whose floors have water depths of 800-900 m, separate the H1-H3 bathymetric highs and are of interest as potential pathways for CDW to the TG grounding zone~~line~~zone. Long profiles from the T2-T4 troughs (Fig. S3) identify sill depths along the pathways of the troughs that may act as important ~~constrictions~~ pinch points for ocean circulation, in particular if they impede CDW inflow towards the Thwaites grounding zone (cf. De Rydt et al., 2014). T2 has a smooth long profile with a prominent sill at 710 m depth at about 107°3'W, 75°3.6'S whereas T3 has a rugged profile with three bathymetric sills in its northern (ice distal) part with depths of 750-760 m, and several other sills further south (ice proximal) around 780 m water depth (Fig. S3a). The bathymetry around T4, east of the EIS, is generally deeper (>1000 m) than most of T2 and T3, so the main constriction on this trough seems to be between the NE-SW trending sea floor ridge in Pine Island Bay (Fig. 2a). At this location, around 105°24.4'W, 74°35.4'S, there is a sill at 880 m depth (Fig. S3d). Channel widths at these locations are 5000 m for the T3 sills and 2500 m for the T4 sill (although this is note the only interruption in the ridge in Pine Island BayPIB). Widths were measured at 500 m depth as this is taken to be a reasonable top-CDW depth for the area (based on oceanographic measurements; B. Queste, *pers. comm.*). The bathymetry of the highs west of T2 is >500 m depth meaning that CDW could effectively "flood" over this topography rather than be constrained to the trough; however, if it was topographically routed (cf. Nakayama et al., 2019) through T2 then the channel width at the sill is 4700 m (at 640 m water depth).

### 3.3 Bathymetric highs and ridges

Owing to the importance of sea-floor highs in front of the Thwaites Ice Shelf as barriers to CDW inflow, and as former ice shelf/sheet pinning points, we examine the morphology of the discontinuous NNE-SSW trending ridge in detail (Fig. 4). The ridge comprises the H1-H3 highs separated by the two troughs described above (T2 and T3; Fig. 3a). The width of the ridge varies significantly, from 6 km in the SW of the study area to at least 40 km over H1, although we acknowledge that data coverage is limited. In places, the bathymetric highs are strikingly flat-topped. These planar features are accentuated in maps of the first derivative of bathymetry, slope, which reveals both low slopes (<2°) (Figs. 4c, d), and low roughness over H2, H3 and the western part of H1. The continuation of the ridge further north into Pine Island Trough has a similar surface expression but is generally narrower (Fig. 3a). These areas with low surface slopes are atypical when compared with other bathymetric highs in the area, which have rugged surface morphologies characterised by bedrock grooves and channels (Figs. 2, 4d) (Nitsche et al., 2013; Arndt et al., 2018; Kirkham et al., 2019). Instead, the low slope values are similar to those derived for

the base of the troughs in front of Thwaites Ice Shelf (Fig. 4a) and the sediment-filled basins just seaward of the Pine Island Ice Shelf front (Nitsche et al., 2013; Kuhn et al., 2017). At least ~~three~~ two distinct levels of flat-topped surfaces occur at 400 m~~, 570 m~~ and ~~620~~ 640 m water depth (Fig. 5). We ~~interpret~~ suggest that this morphology was~~as being~~was generated as~~during a prolonged period of overriding~~as the highs were overridden and eroded by a formerly expanded TG and Thwaites Ice Shelf (with the necessary ice thickness to reach the depth of the flat-topped surfaces). A value of ~400-500 m is similar to ice-shelf thicknesses for Thwaites Ice Shelf today (Griggs and Bamber, 2011; Jordan et al., 2020) and a prevalence of flat-topped highs at this depth may, therefore, support recent modification of the ~~features~~ sea-floor highs at TG ~~in line with mapped grounding lines on the highs~~. In contrast, the deeper flat top of H3 (640 m depth) was probably formed at an earlier stage, as was the flat top of the high in Pine Island Trough, as that area is known to have been ice-free (sheet and shelf) for at least the last 10 kyrs (e.g Kirshner et al., 2012; Hillenbrand et al., 2013). The interpretation or erosion or planing off by an ice shelf is supported by the occurrence of ~~Support for this comes from the orientation of~~ glacial lineations on the tops of the highs (Fig. 3b), which are in line with modern ice-velocity vectors (Mouginot et al., 2019) but oblique to the orientation of crag-and-tails in the troughs thus indicating a change in flow direction from grounded ice flow to ice-shelf flow over the high. A similar interpretation was made for the lineated surface of a former pinning point of the Pine Island Ice Shelf (PIIS) that has been recently exposed by ice-shelf calving events (Arndt et al., 2018), although that feature was not planed off to form a flat-topped high but rather has a stepped and rugged surface morphology albeit with some gently-sloping parts (see their Fig. S3). We note, however, that alternative explanations are possible for this morphology, namely that the flat tops are an inherited feature produced by erosion down to horizontal bedrock strata or that rugged bedrock highs, which are typical of the inner Amundsen Sea shelf (cf. Nitsche et al., 2013), were mantled by some thickness of glacigenic material that levelled the topography below. The former is relatively easy to discount accepting that the inner shelf of the ASE is composed of crystallite basement with seismic-reflection profiles showing that northward-dipping sedimentary strata only occur on the middle and outer shelf (cf. Graham et al., 2009; Gohl et al., 2013). In this setting close to the current TG grounding zone, it is perhaps easier to conceive of the latter explanation that rugged bedrock features were mantled by glacigenic material delivered to the area when the grounding zone was located on or near the highs, and then flattened by some degree of glacial compaction and/or erosion as it was overtopped by TG and the subsequent Thwaites Ice Shelf. This is consistent with our suggestion for the formation of these flat tops as we cannot tell from our data either what sediment thickness occurs on the highs or how much erosion took place, and we acknowledge that the amount of ice-shelf erosion may have been small, only "skimming" unconsolidated material from the surface of the highs. The presence of GZWs and glacial lineations on the highs, and sub-bottom profiler data (Fig. S4), confirms that at least some thickness of unconsolidated material occurs on the highs but seismic-reflection profiles would be required to fully capture the internal structure of these features.

No matter the exact formation mechanism, thet~~The~~ flat-topped morphology of the highs in our study area is striking and notably rare for sea-floor highs around Antarctica. We~~However, we do~~We ~~identify~~ note a similar but less pronounced terrain over some highs along the same structural ridge in ~~eastern~~ Pine Island Bay, i.e. east of the EIS (Fig. 5b), and a solitary ~~veryplaned off~~very flat-topped high, with comparable dimensions to those offshore TG, is visible <5 km north of the Getz-A Ice Shelf

(Fig. 5c). Outwith these rare examples, the best analogy for this morphology probably comes from a set of "iceberg terraces" on terminal moraines at the mouth of a Svalbard fjord, which display remarkably flat-topped surfaces at several bathymetric levels. These are interpreted to have formed as tabular, flat-based icebergs over-topped and eroded morainal sediments (Noormets et al., 2016). It should be noted, however, that sediments of this morainal bank complex probably consist of unconsolidated material that has not been overridden (or compacted) by grounded ice, meaning that they are likely more erodible than ~~the~~ basement highs in front of Thwaites Ice Shelf. Nevertheless, the flat-topped morophology is suggestive of a sedimentary cap on the pinning points at TG, and the fact that similar features exist in Pine Island Bay and beyond the Getz-A Ice Shelf may indicate ~~a wider variability in~~that pinning point composition with such sedimentary caps are widespread on the inner shelf in the Amundsen Sea.

New geomorphic information is also revealed by the flanks of the highs (Figs. 4a, b). The northern (ice distal) flank of the H2 and H3 highs are characterised by subtle down-slope trending gullies that transition into a smooth but inclined sea floor in the troughs at a distinct break of slope. In addition, there are a few, discrete semi-circular indentations in the scarp between the surface of the highs and their flanks (Fig. 4a). The gullies have simple non-branching geometries, small dimensions (widths 150-700 m, depths 5-50 m, lengths <2 km), and typically define broad u-shapes in cross-section, although some v-shaped forms are present. In addition, their ~~l form is consistent with other Antarctic submarine gully systems (long profiles have negative slopes (i.e.g.,, deepen consistently down the flank of the highs) and their form is consistent with other Antarctic submarine gully systems (e.g.~~ Fig. S1f; Gales et al., 2013; Post et al, 2019). Thus, we interpret the gullies as the result of the down-slope mass movement of material from the tops and sides of the H2 and H3 highs via gravitational processes into the small sediment fans at the base of the slope (Fig. 4a). The semi-circular indentations may be the headwalls of small slide scars (cf. Noormets et al., 2009; Gales et al., 2013). One 6 km by 2.6 km segment of the H3 high is somewhat detached from other parts of the ridge and appears particularly fragmented on its flanks (Fig. 4a). About 1500 m south of this, on the main H3 high, is a distinct break in slope with the same planform shape as the back of the detached segment that we refer to as a "block" (bl in Figs. 4a, c). Similarly, 2 km west of this block is another somewhat isolated 3 km by 1.8 km block of H3 that is incised by gullies on its northern front and lacks lineations on its surface (Fig. 4a). We consider several interpretations for these features.. ~~:~~ First, it is possible that they are detached ~~slide~~ blocks of the H3 high that had been displaced down-slope over a short distance (black arrows in Figs. 4a, c), remaining largely intact, but subsequently affected by some gravitational collapse of their flanks. Slide "megablocks" with similar dimensions (or larger), non-crystalline compositions, and degraded flanks are known from, for example, the Hinlopen Slide scar on the northern Barents Sea margin (Vanneste et al., 2006; Hogan et al., 2013). The second possibility is that the blocks are small bedrock highs that have been variously mantled by and surrounded by glacigenic sediment, either deposited subglacially on their surfaces or as it was transported down-slope by gravity-driven processes (towards the sediment fans) from the H3 high (see blue arrows on Fig. 4a). If the latter case is true, then the pronounced semi-circular indentation on the eastern block (labelled in Fig. 4a) may be an erosional scour mark formed by the persistent motion~~bottom water motion~~ of water, as is evidenced by the small channel on the eastern side of the block (white arrows in Fig. 4c).

## 4 Methods II: Bed roughness and basal drag

### 4.1 Spectral analysis of bed roughness

The idea that the drag experienced by a glacier can be analysed by treating the basal roughness as a superposition of sine waves of different wavelengths (λ) has a long history in glaciology (e.g. Nye, 1970; Kamb, 1970; Hubbard et al., 2000). In these approaches, Fourier methods are used to find the drag contributed by roughness that falls within some range of wavelengths (or band of spatial frequencies). More recently, a similar approach has treated the longer wavelength undulations that can affect flow near the upper surface of the ice (Schoof, 2002). Knowledge about the power spectrum of the basal roughness is an essential input to all of these studies.

The high-resolution bathymetric grid that we have produced (Fig. 2) represents the former beds of expanded TG and PIG. As such, it contains information about bed geometry and roughness that can be used to investigate the behaviour of glacier ice over this terrain, specifically how roughness due to bedrock topography and subglacial landforms at various wavelengths, λ, might generate "form drag" within the ice (Schoof, 2002). As an example, Figure 6a shows a bed elevation profile from Pine Island Bay (profile 6 in Fig. S5a) sampled at 25-m intervals along a flow line. To analyse the variance of roughness at each wavelength scale we computed the power spectrum of the bathymetric topography (e.g. Fig. 6b). It is conventional to plot the power spectrum as a function of spatial frequency, defined as $f = \lambda^{-1}$, rather than wavelength. This function, $P(f)$, referred to as the periodogram, shows how the variance of roughness is distributed among different frequency intervals. Thus, the variance attributable to roughness within any frequency interval is the integral of the periodogram over that interval. Figure 6b shows the one-sided periodogram $P(f_n)$, evaluated at equally-spaced frequencies $f_n = n/a$, where $a$ is the length of a moving window. The periodogram was obtained in Matlab~~n~~ R2017~~20~~aMatlan R2020a using Welch's method (Welch, 1967), with a window of length $a$ =6.4 km, and 50% overlap between consecutive windows along the bed profile. Within each 6.4 km window we removed a linear trend from the bed profile and applied a Hamming window before computing the one-sided power spectrum using the absolute-square of the Fast Fourier Transform, appropriately scaled. We then averaged spectra from the multiple windows along the bed profile to provide results for the flow line as a whole.

Periodograms were computed for a total of fourteen palaeo- and modern flow lines for TG and the Dotson-Getz palaeo-ice stream (locations in Figs. S5, S6). For TG and PIG, six palaeo-flow lines were picked manually across the bathymetric grid by tracing lines parallel to subglacial landforms that indicate palaeo-ice flow directions (e.g. Fig. 3b profiles 1-6, Fig. S5a). We performed calculations for bed profiles from four additional areas for comparison: (i) modern along-flow bed profiles for TG (profiles 8-9, Fig. S6a); (ii) modern bed profiles for PIG (profiles 10-11, Fig. S6b); (iii) an area of "smooth" bed topography on the middle continental shelf in the Dotson-Getz palaeo-ice stream trough (profile 7, Fig. S5b); and (iv) six across-flow profiles from the bathymetric datasets (profiles a-f, Figs. S5a. S5b). Onshore bed profiles were extracted from the AGASEA (Holt et al., 2006) and Operation IceBridge (OIB; Cochran & Bell, 2010, updated 2014) airborne radar datasets for TG and PIG beds, respectively. Profiles were selected based on their location, along the central glacier trunk, and their quality in terms of continuity and fewer outliers. The profiles from the Dotson-Getz Trough, offshore from the Getz A Ice Shelf (Fig. S6b),

were selected as representative of a sedimentary palaeo-ice stream bed characterised by mega-scale glacial lineations (MSGL) (Graham et al., 2009; Spagnolo et al., 2014). These were extracted from a MBES dataset fully described by Larter et al. (2009) and Graham et al. (2009).

The power spectrum of natural terrain is often approximated as a power law in frequency (e.g. Jordan et al. 2017). The results of our spectral analysis (Figs. 6 and 7) show that a good approximation can be obtained using an inverse-square power law,

$$P = Af^{-2}, \quad \text{(eqn. 1)}$$

where the constant $A$ has units of length. This is the periodogram expected for a 'Brown-noise' or 'random-walk' elevation profile, as produced by taking an uncorrelated random step in the vertical direction for each unit step in the horizontal.

For Brown noise, the parameter $A$ represents the roughness variance per unit length of profile. If we consider a section of profile having length $l$, and restrict our definition of roughness to all wavelengths $\lambda \leq l$, we expect this roughness to have variance obtained by integrating the periodogram $P$ over frequencies $f > l^{-1}$. For the Brown-noise periodogram (equation 1), this integration provides,

$$\sigma^2 = Al. \quad \text{(eqn. 2)}$$

Thus, for Brown noise, the variance grows in proportion to the section length considered, and the r.m.s. roughness $\sigma = \sqrt{Al}$ grows with the square root of the section length (e.g. Jordan et al. 2017). If we take a longer section of profile, we expect to see larger r.m.s. roughness within it. This makes it clear that, at least for Brown noise, the roughness can only be characterised by its r.m.s. value if reference is also made to the length scale under consideration. Next, we examine the consequences of roughness for the drag that resists the sliding of a glacier. We pay particular attention to the case when the periodogram follows an inverse-square law (eqn. 1) that is appropriate for a Brown-noise power spectrum.

### 4.2 Relating bed topography to basal drag

In this section, we will use the power spectra of the high-resolution bathymetry, together with a theoretical expression for form drag (Schoof, 2002, equation 67), to assess how roughness at different scales affects the drag that opposes glacier sliding. This allows us to consider the contribution that the observed sea-floor bathymetric roughness at short wavelengths would make to form drag when covered by flowing ice.

The theory of ice flow over an undulating bed (Schoof, 2002) provides an approximate expression for the form drag $\tau_f$, expressed as a basal shear stress that acts to resist sliding. Here, we use dimensional quantities rather than the non-dimensional quantities (as used by Schoof (2002)). In our notation, Schoof's (2002, equation 67) expression for form drag becomes,

$$\tau = \beta U \quad \text{(eqn. 3)}$$

In this expression, $\beta$ is the drag coefficient and $U$ is the speed of ice flow averaged over some horizontal length scale significantly larger than the ice thickness. Here, we choose this length as $a = 6.4$ km, the window length used in our spectral analysis. According to Schoof (2002), the drag coefficient $\beta = \sum_{n=1}^{\infty} \beta_n$ is the sum of contributions, $\beta_n$. Each contribution $\beta_n$ is caused by roughness that falls within a frequency band of width $1/a$ centred at frequency, $f_n = n/a$. The spatial wavenumbers corresponding to these frequencies are defined as $k_n = 2\pi f_n$.

Schoof (2002) provides an expression for the drag contributed by roughness within each frequency band. In our notation, this translates to:

$$\beta_n = 4\beta^*(k_n/k^*)^3 F(k_n/k^*)\left(\left|\hat{h}_n\right|^2/H^2\right) \quad \text{(eqn. 4)}$$

In this expression, $\hat{h}_n$ is the Fourier component of the bed roughness at spatial frequency, $f_n$. We estimate $\left|\hat{h}_n\right|^2 = \frac{1}{2}P_n a^{-1}$, as appropriate for the Fourier series defined by Schoof (2002). The one-sided periodogram $P_n$ can either be obtained directly from the bathymetric observations as described above (Sect. 4.1), or by fitting the inverse-square power law described by equation 1 to those periodograms (see Figs. 6 and 7 for examples). The scaling constants are $\beta^* = \eta/H$ and $k^* = 1/H$, where viscosity $\eta$ and thickness $H$ are representative values averaged over the length scale $a$ (Schoof, 2002).

We consider two limiting cases for the function $F$:

$$F_1(k_n/k^*) = \frac{\sinh^2(k_n/k^*) - (k_n/k^*)^2}{(k_n/k^*) + \cosh(k_n/k^*)\sinh(k_n/k^*)}, \quad \text{(eqn. 5)}$$

$$F_2(k_n/k^*) = \frac{(k_n/k^*) + \sinh(k_n/k^*)\cosh(k_n/k^*)}{\sinh^2(k_n/k^*)}. \quad \text{(eqn. 6)}$$

These are derived by Schoof (2002) as his equations 65 and 66 for small and large bed roughness, respectively. We use dimensional quantities, so $k_n/k^*, \hat{h}_n/H$ and $F(k_n/k^*)$ in our notation equate respectively to non-dimensional quantities $k_n$, $\nu\hat{h}_n$ and $f(k_n)$ in Schoof (2002). For sufficiently small wavelengths $k_n \gg k^*$ the functions $F_1(k_n/k^*)$ $F_2(k_n/k^*)$ both tend to unity. In this case, the contribution to form drag becomes insensitive to ice thickness and to the choice of function used (Schoof, 2002).

If the bed follows a Brown-noise power spectrum, we can use the inverse-square law $P_n = A f_n^{-2}$. Under those circumstances, the drag contribution $\beta_n$ will grow approximately linearly with frequency at sufficiently high wavenumbers $k_n \gg k^*$:

$\beta_n = 16\eta\pi^3 A a^{-1} f_n$. (eqn. 7)

For the Brown-noise power spectrum, the amplitude of roughness decreases at shorter wavelengths. Nevertheless, equation 7 shows that those short-wavelength scales will still be more effective at causing form drag than the longer wavelengths, despite their smaller amplitude. This is because the factor $(k_n/k^*)^3$ increases faster than the inverse-square law decreases.

As a consequence of the linear increase in the drag contribution with frequency, the total drag would become unbounded, and the sliding would stop, unless the bed of the glacier departs from the Brown-noise assumption and becomes smooth at scales smaller than some wavelength (Nye, 1970). This wavelength, $\lambda_N$, provides an upper bound to the spatial frequencies that cause drag. $f_N = \lambda_N^{-1} = N/a$. Under this assumption, the total drag can be approximated by truncating the sum:

$\beta = \sum_{n=1}^{N} \beta_n = 16\eta\pi^3 A a^{-2} \sum_{n=1}^{N} n = 8\eta\pi^3 A a^{-2} N(N+1)$. (eqn. 8)

When $\lambda_N \ll a$, so that $N \gg 1$, this gives the approximation:

$\beta = 8\eta\pi^3 A \lambda_N^{-2}$. (eqn. 9)

Therefore, if the Brown-noise inverse-square law power spectra applies down to the finest wavelength $\lambda_N$, the drag will be determined by that scale, along with the viscosity $\eta$, and the coefficient of the power law $A$ that can be recovered from the periodogram.

It is common in sliding theories to define the slip length, $L = \eta/\beta$. The slip length $L$ is an important quantity that allows us to make a distinction between two regimes of ice flow. When the slip length is much larger than the ice thickness $H$, the drag is too small to induce significant shearing within the ice column and the ice can be considered to slide over the base as a 'plug flow' having uniform velocity with depth. This is the situation modelled for slippery-based ice streams by MacAyeal (1989). By contrast, when the slip length is much smaller than the ice thickness, the drag is able to induce a substantial amount of shearing through the ice column, so the flow velocity varies significantly with depth.

Using equation 9, we obtain the following expression for the slip length under the assumption of a Brown-noise power spectrum, truncated at some frequency $f_N = \lambda_N^{-1}$.

$L = \lambda_N^2/(8\pi^3 A)$. (eqn.10)

One consequence of this is that if we wish to infer the amount of form drag using equation 9, or the slip length using equation 10, it is not enough to evaluate the roughness parameter $A$ alone. We must also establish $\lambda_N$, the smallest wavelength that is effective at causing drag.

~~The high-resolution bathymetric grid that we have produced (Fig. 2) represents the former beds of expanded Thwaites and Pine Island glaciers. As such, it contains information about bed geometry and roughness that can be used to investigate the behaviour of glacier ice over this terrain, specifically how roughness at the bed (e.g. bedrock topography and subglacial landforms) might generate "form drag" (Schoof, 2002) within the ice. The bathymetry contains roughness at various wavelengths, λ, each equivalent to a spatial frequency f=1/λ. We use power spectra of the high-resolution bathymetry (Figs. 6, 7), together with a theoretical expression for form drag (Schoof, 2002, equation 67) to recover the drag caused by undulations at each spatial frequency. The theoretical expression applies to flow lines and was applied to palaeo- and modern flow lines for TG and the Dotson-Getz palaeo-ice stream as described in Section 2.2 (locations in Fig. S1).~~

~~To analyse the variance of roughness at each wavelength scale we computed the power spectrum of the bathymetric topography (Figs. 6, 7). As an example, Figure 6a shows a bed elevation profile (location in Fig. S1) sampled at 25-m intervals along a flow line. Figure 6b shows the derived one-sided periodogram $P(f_n)$, evaluated at a set of equally-spaced spatial frequencies $f_n = \lambda_n^{-1} = n/a$, where $a$ is the length of a moving window. The periodogram was obtained using Welch's method (Welch, 1967), with a Hamming window of length $a$ =6.4 km and 50% overlap between consecutive windows along the bed profile.~~

## 5 Results II: Assessing roughness and drag contributions for palaeo and modern glacier beds

### 5.1 Bed roughnesses

The power spectra of selected bathymetric profiles are shown in Figures 6 and 7. Figure 6b shows that the one-sided periodogram $P(f_n)$, computed using the bathymetric profile shown in Figure 6a (location in Fig. S5a), hashas~~The periodogram shows~~ no strong peaks at any particular preferred scales of roughness.~~ (Fig. 6b).~~ Instead, the periodogram decreases continuously as spatial frequency increases. This decrease approximately follows the inverse-square power law appropriate for Brown noise, so that the periodogram can be approximated as $P_n = P(f_n) = Af_n^{-2}$. The red line in Figure 6b shows this power law, with a value $A$ = 0.1 m. The spectra are remarkably consistent across many of the profiles considered (Figs. 7, S7) with the exception of the smoother MSGL area (Figs. S5b). There, the Brown-noise inverse-square law can still provide a good approximation to the periodogram, but the value of $A$ = 0.001 m that is required to provide a good match to the observations is much smaller (Figs. 7, S7p, S7q).

~~Instead, the variance of roughness decreases continuously as spatial frequency increases and the reduction of variance with increasing spatial frequency approximately follows an inverse-square power law so that the periodogram can be approximated as $P_n = P(f_n) = Af_n^{-2}$. This is the power spectrum of a fractal 'Brown-noise' or random-walk elevation profile, as would be produced by adding an uncorrelated random offset in the vertical for each unit-length step taken in the horizontal. The inverse-~~

~~square law provides a good approximation to all power spectra observed (Figs. 7, SF4), so the variance of roughness at any particular frequency scales inversely to the square of that frequency and proportionately to the coefficient, $A$. The red line in Figure 6b corresponds to a value $A$ = 0.1 m and the spectra are remarkably consistent across many of the profiles considered (Figs. 7, SF4) with the exception of the smoother MSGL area that is discussed in section 4.2.~~

The power-law approximation to the power spectrum ~~provides reasonable agreement for multiple flow lines from the offshore bathymetry (Figs. 7, SF4). It~~ also agrees closely to power spectra of profiles of bed elevation from airborne radar flown over TG (Fig. 7e~~7c~~), so the MBES data provides a~~an~~ good analogue to the subglacial undulations that control the sliding of TG~~Thwaites Glacier~~TG today. Despite improvements in the methodology of high-resolution radar surveys of the active subglacial bed (King et al., 2016; Bingham et al., 2017), the MBES provides a more detailed view of the shorter spatial scales than airborne or ground-based radar. Comparisons with previous studies of subglacial roughness are not straightforward because individual studies have used different window lengths to investigate roughness (e.g. Jordan et al., 2017; Falcini et al., 2018). However, for the Brown-noise power spectra in equation 1, we expect the r.m.s. roughness for a section of length $l$ to be $\sigma = \sqrt{Al}$. Most of our spectra are close to the Brown-noise spectra with $A$ = 0.1 m (Figs, 6, 7) and for this value, we would expect window lengths from 80 m to 1000 km to produce r.m.s. roughness estimates in the range 2.8 m to 10 m. These values are similar to those reported previously for glaciated terrain (Jordan et al., 2017; Falcini et al., 2018).

### ~~4.2~~5.2 Basal~~Relating bed topography to basal drag~~Basal drag contributions

~~In this section, we will use a theory of ice flow to assess how the roughness at these different scales will affect the drag that opposes glacier sliding. As demonstrated above, the power-law approximation is appropriate for bed profiles from both the bathymetric data as well as for bed profiles from airborne radar data. This allows us to consider the contribution that the observed sea-floor bathymetric roughness at short wavelengths would make to form drag when covered by flowing ice. The theory of ice flow over an undulating bed (Schoof, 2002) provides an approximate expression for the form drag $\tau$, expressed as a basal shear stress that acts to resist sliding:~~

~~$\tau = \beta U$ (eqn. 1)~~

~~In this expression, $U$ is the speed of ice flow averaged over some horizontal length scale (here, chosen as $a$, the window length, i.e. the longest wavelength considered in the spectral analysis) and $\beta$ is the drag coefficient. According to Schoof (2002), the drag coefficient $\beta = \sum_{n=1}^{\infty} \beta_n$ is the sum of contributions $\beta_n$, each of which is caused by roughness at a different wavelength scale $\lambda_n$. As per the spectral analysis above, these wavelengths correspond to equally-spaced spatial frequencies $f_n = \lambda_n^{-1} = n/a$, and spatial wavenumbers $k_n = 2\pi f_n$.~~

~~Schoof (2002) provides an expression for the drag contributed by each spatial frequency:~~

~~$\beta_n = 4\beta^*(k_n/k^*)^3 F(k_n/k^*)\left|\hat{h}_n/H\right|^2$~~ ~~(eqn. 2)~~

~~In this expression, $\hat{h}_n$ is the Fourier component of the bed roughness at spatial frequency $f_n$. The scaling constants are $\beta^* = \eta/H$ and $k^* = 1/H$, where $\eta$ and $H$ are representative viscosity and thickness, respectively, averaged over the length scale $a$ (Schoof, 2002). We estimate the squared magnitude of the Fourier component of the roughness using the one-sided periodogram, $\left|\hat{h}_n\right|^2 = \frac{1}{2}P_n H^{-2} a^{-1}$. This corresponds to the definition of the roughness Fourier series used by Schoof (2002). We consider two limiting cases for the function $F$:~~

~~$F_1(k_n/k^*) = \frac{\sinh^2(k_n/k^*) - (k_n/k^*)^2}{(k_n/k^*)+\cosh(k_n/k^*)\sinh(k_n/k^*)}$~~ ~~(eqn. 3)~~

~~$F_2(k_n/k^*) = \frac{(k_n/k^*)+\sinh(k_n/k^*)\cosh(k_n/k^*)}{\sinh^2(k_n/k^*)}$~~ ~~(eqn. 4)~~

~~These are derived by Schoof (2002) (equations 65 and 66 for small and large bed roughnesses, respectively). Note that we have used dimensional quantities throughout, so $k_n/k^*$, $\hat{h}_n/H$ and $F(k_n/k^*)$ in our notation are equivalent to non-dimensionalised quantities $k_n$, $v\hat{h}_n$ and $f(k_n)$ respectively in Schoof's notation.~~

~~For the same example bed profile in Figure 6a, values of $\beta_n/\beta^*$ are plotted against spatial frequency $f_n$ in Figure 6c for a representative ice thickness $H = 1$ km. For sufficiently small features, so that $k_n \gg k^*$, the functions $F_1(k_n/k^*)$ $F_2(k_n/k^*)$ both tend to unity. Then the form drag becomes insensitive to ice thickness and to the choice of function used (Schoof, 2002). In those circumstances, we can use $k_n = 2\pi f_n = 2\pi n/a$, with the inverse-square law $P_n = A f_n^{-2} = A a^2 n^{-2}$, to show that the drag contribution $\beta_n$ will grow approximately linearly with frequency according to:~~

~~$\beta_n = 16\eta\pi^2 A a^{-1} f = 16\eta\pi^2 A a^{-2} n$~~ ~~(eqn. 5)~~

~~Even though the amplitude of roughness decreases at shorter wavelengths, our results, combined with the theory, show that those short scales will be more effective at causing form drag. This is because the factor $(k_n/k^*)^3$ increases faster than the inverse square law decreases. The resulting linear dependence is shown as a red line on Figure 6c. As a consequence of the linear increase in the drag contribution with frequency, the total drag would become unbounded, and the sliding would stop, unless the bathymetry becomes smooth at scales smaller than some wavelength $\lambda_N$. This wavelength provides an upper bound to the spatial frequency $f_N = \lambda_N^{-1} = N/a$. Under this assumption, the total drag can be approximated by:~~

~~$\beta = \sum_{n=1}^{N}\beta_n = 16\eta\pi^2 A a^{-2}\sum_{n=1}^{N} n = 8\eta\pi^2 A a^{-2} N(N+1)$~~ ~~(eqn. 6)~~

~~When $\lambda_N \ll a$, so that $N \gg 1$, this gives the approximation:~~

~~$\beta = 8\eta\pi^3 A\lambda_N^{-2}$ (eqn. 7)~~

~~Therefore, if the observed inverse-square law power spectra applies down to the finest length scale $\lambda_N$, the drag will be determined by that scale, along with the viscosity $\eta$, and the coefficient of the power law $A$ recovered from the periodograms.~~

~~**It is common in sliding theories to define the slip length, $L = \eta/\beta$.**~~

For the example bed profile in Figure 6a, values of $\beta_n/\beta^*$ obtained using the periodogram shown in Figure 6b and equation (4) are plotted against spatial frequency $f_n$ in Figure 6c. The linear dependence predicted by equation 7 for the Brown-noise approximation is shown as a red line on Figure 6c. In these plots we used a value $A$ = 0.1 m and a representative ice thickness $H$ = 1 km.

The expression for the basal slip length (equation 10) lets us use the bathymetry to make a ~~This lets us make a~~ dynamical distinction between regions of fast sliding with little internal deformation $L > H$ and regions of slow sliding and shearing flow $L < H$. Using~~For the situation described above~~Using equation 10, the ratio of slip length to ice thickness is $L/H = \lambda_N^2/(8\pi^3 AH)$. For a value of $A$ = 0.1 m and a typical ice thickness scale of $H$ = 1 km, this suggests that features on scales smaller than $\lambda_N$ = 150 m would provide sufficient drag to induce significant vertical shearing within the ice. Since features on this scale are well resolved by the bathymetric profiles (e.g. Figs. 3, 4) and fall within the range of frequencies where the inverse square power law applies, we conclude that the form drag produced by the observed subglacial roughness would have produced significant shearing within the flow of the grounded ice as it retreated over the highs and ridges surveyed by the MBES. This suggests that it is important to include the effects of form drag caused by basal roughness over such terrain, and by extension over the extant parts of TG today.

A distinction must be made for the region of MSGLs on the Dotson-Getz palaeo-ice stream bed (Fig. S1c). Here, the elevation profile is exceptionally smooth. The spectral analysis confirms this (Figs. S7p~~S~~74~~p~~, q), and the coefficient $A$ that best fits the observations is some two orders of magnitude below the more generally applicable value of A = 0.1 m. Repeating the above analysis with $A$ = 0.001 m shows that the power law would have to apply down to horizontal scales smaller than $\lambda_N$ = 15 m. Features on this scale are not well resolved in our bed profiles (e.g. the MBES grids have cell sizes of 50 m). This means that in contrast to the more general case, it remains possible that the MSGL terrain is so smooth that the resulting form drag produced~~produced~~ds little vertical shearing within ~~the~~ ice that flowed~~flowed~~s over it, making the ice dynamics of this area more akin to the flow described for slippery-based ice streams by MacAyeal (1989). This result is consistent with our understanding of how MSGLs form, i.e. via the self-organisation of deforming sediment at the bed under fast-flowing ice (e.g. Spagnolo et al., 2014). We also repeated the analysis in the direction perpendicular to elongated features (Figs. 7d, S7k~~S~~74k~~-~~o, q). There is no evidence that ice flowed in this direction, but the theory can nevertheless compute the contributions to form drag that

would arise in that hypothetical situation. For most of the across-flow lines (Fig. S7S74), the power spectra are similar to the along-flow direction, and the drag contributions at each frequency are similar. This suggests that the drag coefficient over much of the surveyed terrain is not especially sensitive to the flow direction. For the MSGL terrain there does appear to be some indication that drag would be higher for ice flow in the direction perpendicular to elongated features.

## 664 Discussion

### 664.1 Implications from the new bathymetric dataand geomorphological datadata

Our results provide the first observation-based, high-resolution geomorphic characterisation of the coastal bathymetry at TG, a former bed for the glacier. These data allow us to investigate bathymetric controls on ocean circulation towards the modern grounding zone, as well as to identify the locations, water depths and substrate compositions of ice-shelf pinning points and former grounding zones. The dominant bathymetric features, a NNE-SSW trending trough and landward flanking discontinuous ridge (Fig. 2a), represent a subtly different morphologic terrain from highly rugged, basin-dominated areas north and east of the EIS (Fig. 3a) or the moderate-relief areas of lineated terrain with fewer bathymetric highs in eastern Pine Island Bay (Fig. 2a) (Nitsche et al., 2013; Arndt et al., 2018; Kirkham et al., 2019). The continuity and orientation of the trough and ridge relates to the structure of basement rocks on the inner shelf. NNE-SSW to ENE-WSW structural lineaments have been identified by previous aeromagnetic surveys (Gohl, 2012; Gohl et al., 2013), and gravity-derived bathymetries all resolve a broad NNE-SSW ridge coincident with H1-H3, as well as deeper troughs on either side of the ridge (Tinto & Bell, 2011; Millan et al., 2017; Jordan et al., 2020).). Thermochronological analyses of onshore rock samples also infer a NNE-SSW trending tectonic rift structure (Spiegel et al., 2016).

Our results We highlight several key differences between our new dataset andwhen compared withand the most recentavailable regional bathymetric datasets compilations (Fig. 8). Note that we do not compare our MBES grid with the newly published gravity inversion of Jordan et al. (2020) as that study utilised the MBES dataset to constrain the inversion. Outwith that study, fFor the area of new MBES data in front of TG, gravity-derived bathymetry generally underestimates sea-floor depths (average of 119 m; (Figs. 8a, b), whereas the IBCSO bathymetry, which is based on real sea-floor soundings but relies on gravity-inversion elevations and interpolation in this area (Arndt et al., 2013), generally overestimates sea-floor depths (average of 65 m; (Fig. 8c). All of thethese regional datasets we examined fail to capture the higher-frequency topographic variability revealed by the new MBES data (e.g. Fig. 8d). Although sea-floor highs are sometimes >100 m shallower than the regional products predict, this effect is most notable for the troughs, which are in reality 100 to 550 m deeper than gravity-derived bathymetries, and 50 to 250 m deeper than in the IBCSO dataset (Fig. 8d). When we consider cross-sections of three troughs that are potential pathways for CDW to the grounding zone (T2, T3, T4; locations marked by asterisks in Fig. 8a), the depth errors are up to 500 250 m, 400 500 m and 250 400 m from west to east, to west to east. Using a conservative top-CDW depth of 500 m for the TG area (based on hydrographic data acquired during NBP19-02; B. Queste, *pers. comm.*; cf. Nakayama et al., 2013), we calculate the cross-sectional area that CDW occupies in these troughs from our MBES data and from the grid of Millan et al. (2017).

We find that the gravity-derived bathymetry underestimates the cross-sectional areas by 779%-38% for two of the three troughs, and that trough T3~~T~~3~~2~~ between H1 and H2 (Fig. 3a) is not resolved at all on the Millan et al. (2017) grid (Table S1; Fig. S8~~S5~~S8). Taking this one step further, we perform a simple calculation of the oceanic heat flux through T2 for the two cross-sectional areas (Millan et al. (2017); MBES) and utilising oceanographic observations from the ASE for ocean temperatures and flow velocities (see Supplementary Information for methods). The total heat flux through the trough cross section defined by the gravity inversion is ~0.5 TW, and for the MBES cross section it is 1.1-1.3 TW (Table S2). This equates to an underestimation of the heat flux through T2 based on the gravity-derived bathymetry of 55-65%, or more than a doubling in the heat flux through the trough using the deeper bathymetry provided by the MBES grid. To fully quantify the significance of this for the inflow of CDW to the Thwaites ice-shelf cavity and grounding zone requires the use of an ocean circulation model with the MBES as its bathymetry and that is, ideally, calibrated by CTD data within the troughs. ~~This discrepancy would lead to a significant underestimation of the volume of CDW that can be transported through the troughs to the ice-shelf cavity and grounding zone of TG (cf. Walker et al., 2007; Arneborg et al., 2012; Table S1)~~Conversely, the identification (and implementation in models) of critical sill depths along the trough pathways ~~-~~could limit CDW inflow along certain routes. These~~which has~~These findings have implications for the~~ocean circulation~~the numerical modelling of warm-water access to the grounding zone, oceanic heat fluxes, the resultant ice-shelf melting rates~~, warm water access to the grounding zone~~ and, ultimately, projected mass losses from TG and the WAIS. However, our first-pass calculations underline~~The discrepancy underlines~~ the importance of high-resolution observational datasets like MBES for capturing high-amplitude bathymetric variations at short to medium wavelengths (i.e. $\lambda < 10^3$ m~~km~~), particularly in areas close to ice-shelf cavities and the grounding zone.

~~Having produced a~~A new gravity-derived bathymetry model for the Thwaites, Crosson and Dotson-Getz area, constrained by the NBP19-02 MBES data, produced recently by Jordan et al. (2020) has improved resolution compared to previous gravity-derived models as a result of using a 'strapdown' instrument with closer flight line spacing. Despite the improved resolution of their new model, Jordan et al. (2020) concluded~~(*subm.*) similarly also determined~~ that still higher~~high~~-resolution observations are necessary in areas where knowledge of the bed at scales of less than a few kilometres is required. The need for high-resolution bathymetry ~~was~~ has been underscored by recent predictive modelling studies of Antarctic outlet glaciers, which conclude that the shape of the ice-shelf cavity and knowledge of small, kilometre-scale pinning points are both key to improving predictions of ice-sheet retreat and sea-level change (Berger et al., 2016; Favier et al., 2016). Similarly, the latest high-resolution ocean models demonstrate that warm deep water reaches the grounding zone of TG through topographically-constrained pathways, again highlighting the critical need for high-resolution bathymetry in making accurate predictions (Nakayama et al., 2019).

### 6.2 Implications from sea-floor morphology

The geometry and detailed morphology of the H1-H3 ridge also provide insight on ice-shelf pinning points. Historical grounding~~-line~~ zone positions, as mapped from remotely-sensed ice-shelf tidal response, confirm that the Thwaites Ice Shelf

is still pinned on high H1 and was pinned on high H2 as recently as 1992 and 2011 (Rignot et al., 2011). By 2011, the area of grounding on H2 had reduced to <0.5 km$^2$ (Fig. 3a) but the recent configuration and persistence of the TGT suggests that at least some parts of itthe TGTit remain in (ephemeral) contact with the sea floor. Thus, the exposed H1 and H2 sea-floor highs, and by analogy H3, can be studied as current or recent pinning points for the Thwaites Ice Shelf. Glacial lineations and (or) grounding-zone wedges (GZWs) on the surface of H2 and H3, as well as rare iceberg ploughmarks (Fig. 4b), confirm that these pinning points are mantled by some amount of unconsolidated sediment that can be ploughed or moulded by ice. Sub-bottom profiles over the H2 and H3 highs support this as they show either an incredibly smooth sea-floor response, strongly indicative of unconsolidated sediment cover, or up to 10-15 m of unconsolidated sedimentary units (Fig. S4S46); furthermore, coring of the top of H3 recovered several meters of sediment (Larter et al., 2020). Although the upper section of the sediment on H3 is glacimarine, deposited after grounded ice had retreated or lifted-off from the high, the presence of a GZW there and on H2 (Figs. 4b, d) suggests that at least the uppermost part of this high may have been constructed via sedimentation at the grounding zone (cf. Alley et al., 1989; 2007). The potential effects of this grounding-zone sedimentation are two-fold: when the TG grounding zone had retreated onto these highs during the Holocene (i.e., sometimeat some time after before 10.3 cal. ka BP; Hillenbrand et al., 2013), GZW formation could have temporarily slowed further retreat (Alley et al., 2007). Second, continued pinning of an ice shelf on the high and GZW, when most of the grounding line had eventually retreated further landward, would have buttressed the grounded upstream section of TG. The new MBES dataset we present here and the sea sea-floor landforms it reveals, supported by core recovery and sub-bottom profiles, indicate that more sediment is present in this area than is typical of other Amundsen Sea inner shelf environments that experienced rapid ice-sheet retreat, including the adjacent Pine Island Bay and the Dotson-Getz palaeo-ice stream trough (e.g. Larter et al., 2007, 2009; Graham et al., 2009; Nitsche et al., 2013, 2016). This is likely because this area immediately offshore TG represents a location where the grounding zone was positioned for a relatively long period of time in this area immediately offshore TG, and probably because areas so close to the grounding zones of most other large glacier systems have not yet become accessible for shipborne survey. Furthermore, TG has a much larger drainage basin than the Dotson-Getz palaeo-ice stream trough and therefore the potential to erode and deliver a greater flux of basal sediment to its grounding zone. Our only constraints on grounding-zone retreat through this area (during the Holocene) are from the core on the H1 high which shows that grounded ice withdrawal from the northern part of that high by 10.3 cal. ka BP (Hillenbrand et al., 2013) and grounding zones mapped from satellite-era datasets (Rignot et al., 2011). Thus, the TG grounding zone wasmust have beenwas most probably located between H1 and the current grounding zone, potentially on the sea-floor ridges identified here, for thousands of years delivering a significant volume of sediment to the area. This retreat history is in line with what we know about deglaciation more generally in the Amundsen Sea, where rapid grounding-zone retreat occurred from 15 to10 ka to reach near modern limits (Hillenbrand et al., 2013; Larter et al., 2014; Smith et al., 2014); however, more marine dates and terrestrial thinning histories will certainly provide more clarity and chronological constraints for TG.

The submarine landforms observed on and around the sea-floor highs raises the question of the composition of these features. Landforms on the flanks of the pinning points (gullies, slide scars, isolated blocks; Fig. 4) may indicate that these highs consist,

at least in part, of an erodible (soft) material with a probable (hard) bedrock core. In marine settings, slide scars and gullies incise large, pronounced sedimentary scarps like the shelf edge (e.g. Noormets et al., 2009; Gales et al., 2013) or the headwalls of major submarine slides (e.g. Laberg and Vorren, 2000; Vanneste et al., 2006) but do not characterise hard bedrock (crystalline) settings. Further evidence comes from the new observation of ~~planed-off (~~flat-topped (compacted or planed-off) morphology of the H2 and H3 highs confirming that the upper part of these (down to the level of flattening~~planing off~~flattening) consists of a lithology that is apparently erodible by the motion of an ice shelf (based on the orientation of lineations on the highs). Other examples of flat glacial erosion surfaces planed off by ice shelves or flat-based tabular icebergs from the Arctic all document erosion into sedimentary substrates (e.g. Vogt et al., 1994; Jakobsson et al., 2010; Noormets et al., 2016). Small (<100 m high, <5 km wide), flat-topped mounds in the Ross Sea are also thought to consist of unconsolidated volcanogenic deposits rather than crystalline bedrock and, interestingly, GZWs have built up on them, indicating that these features slowed grounding-zone retreat in that area (Lawver et al., 2012; Greenwood et al., 2018). Although we suggest flattening of the highs by the action of Thwaites Ice Shelf we cannot say, from our data, how much erosion may have occurred. It may be that surface sediments were simply skimmed from the tops of the highs and ~~pushed~~ transported towards their seaward flanks, which in conjunction with instabilities relating to ice-shelf grounding (or ungrounding) on the highs, could have promoted slope failures on the fronts and sides of these features (cf. Bellwald et al., 2019). Despite this caveat, all of the landform evidence presented here, supported by cores and acoustic sub-bottom profiles, suggest that the tops, fronts and sides of the H2 and H3 highs are mantled by some thickness of sediment, probably over a bedrock core. Seismic-reflection profiles would be needed to determine the internal structure of these features and sediment thicknesses. ~~Our interpretation of a proportion of unconsolidated sedimentary substrate, and thus low-density material, on the H2 and H3 highs may explain why bathymetries derived from gravity over-estimate the height of some of these features (Figs. 8a, b).~~ In contrast, the morphology of H1 is consistent with it having a crystalline composition. ~~., which is supported by the small differences between the water depths of our MBES dataset and the gravity-derived datasets at the H1 location (see proximal 25 km in profile x-x' of Fig. 8d).~~ This very shallow, rugged feature is cross-cut by bedrock grooves and channels typical of hard rock exposures on the inner Antarctic shelf (Lowe and Anderson, 2002; Livingstone et al., 2013) and, although bathymetric coverage over this high is incomplete, ~~has no~~ it has few planed-off sections and no~~or~~ glacial lineations have yet been identified on its surface (Figs. 3b; S4b). Therefore, it is clear that there is a spatial variability in pinning point morphology and composition at TG, as well as across the wider Amundsen Sea area (Figs. 2, 5). More broadly, wew~~We~~ also note the relative scarcity of bedrock channels or other landforms related to subglacial meltwater flow in the TG MBES dataset with the crescentic scours (H3 only; Fig. 4a) being the exception. As an example, Kirkham et al. (2019) mapped more than 1000 subglacial channels in Pine Island Bay whereas we map only 175 forms here, albeit over a smaller area. It is not clear whether evidence of previous meltwater routing is buried by sediment in the deep troughs, or has been destroyed by ice flow over the highs. Physical-property and geochemical analyses on cores from the area, acquired as part of *ITGC*, should shed light on the frequency and magnitude of meltwater release during the retreat of grounded ice over the sea-floor highs. Schroeder et al. (2013) identified a transition from a distributed channel network with ponded water behind ridges at the modern grounding zone, to a system of concentrated channels downstream. It is possible

that a similar configuration for the basal hydrological system occurred in this area as ice retreated over the offshore highs and that evidence is preserved in the marine sedimentary record.

The~~Given the~~The apparent shaping and fragmentation of the H2 and H3 highs (Figs. 4a, b)~~), this observation~~ highlights ~~a~~another potential feedback mechanism between bed properties (composition and topography) and ~~influencing~~ glacier retreat dynamics. If~~, because i~~If the substrate of a pinning point is soft enough to be moulded by the flow of an ice shelf and to be susceptible to slope failures, it might be eroded over time. Erosion of material from the surface of a pinning point, as it is planed off, in conjunction with retrogressive failures at its seaward flank and possibly larger slide or slump events may act to reduce its surface height, as well as itsits surface area by "eating away" at the frontal/side flanks, until it cannot serve as a pinning point for the ice shelf (and glacier ice upstream) any longer. As long as the ice shelf continues to move over the high, thist~~This~~ process of unpinning would be exacerbated by any increase inin~~d~~ flow velocities (leading to increased erosion) and/or by ice-shelf thinning (leading to ungrounding), due to either flow acceleration or sub-ice shelf melting.~~, (leading to ungrounding).~~ The result, in a setting with "soft" erodible pinning points, is the potential for ~~rapid grounding-zone destabilisation and resulting mass loss, whereby~~ increased ice-flow velocities to accelerate pinning point destruction which, in conjunction with simultaneous ice-shelf thinning in response to sub-ice-shelf melting, ~~then~~ could promote~~promotes~~ ungrounding earlier than would occur on a corresponding "hard", less erodible pinning point. Needless to say, in order for this feedback to occur, an ice shelf would have to continue to flow quickly over the sea-floor high(s) and not form an ice rise, under which erosion rates are considered to be low (e.g. Matsuoka et al., 2015). At TG we note that, at least for the duration of the observational record (~55 years), the fast-flowing part of the glacier, which feeds the TGT (Fig. 2), has continued to move over the H2 and H3 highs periodically extending several tens of kilometres before calving (Ferrigno et al., 1993; Rabus et al., 2003; MacGregor et al., 2012) whereas the ice rumple at the end of the EIS restricts flow over H1, with most ice flow being diverted around the rumple (Rignot et al., 2001). It is perhaps interesting to also consider that upwards of ~~4~~5045 m of relative sea-level fall due to glacio-isostatic uplift is thought to have occurred on the inner Amundsen Sea shelf ~~since the last deglaciation~~during the Holocene (Whitehouse et al., 2012), and that the uplift of any pinning points would naturally counter ungrounding. Therefore, although we can only speculate on the exact mechanisms affecting rates of unpinning, we suggest that the composition of sea-floor pinning points may be an important factor in their ongoing ability to buttress large Antarctic ice shelves.

### 6.334.2 Implications from the new bed roughness data

One major objective of our research is to assess the deglaciated ~~subaqueous~~ submarine terrain offshore from TG as an analogue for the modern bed to gain new insights on TG bed characteristics. The consistency of derived power spectra and drag contributions for bed profiles from the inner ASE shelf and for upstream areas of Pine Island and Thwaites glaciers (Figs. 7, S7) indicates that the roughness properties of the offshore and onshore areas are comparable across all resolvable frequencies. Furthermore, observations confirm that recent grounding-zone retreat affecting TG has occurred over a series of bedrock ridges with the loss of pinning points and formation of new cavities (Tinto & Bell, 2011; Milillo et al., 2019; Jordan et al., 2020).~~).~~

Further upstream, about 100 km from the recent grounding zone, analyses of radar specularity suggest that the modern TG bed is characterised by high roughness attributed to bedrock cropping out at the glacier base (Schroeder et al., 2014). Our data reveal that the bedrock ridges and intervening troughs underlying the modern grounding zone (Holt et al., 2006; Morlighem et al., 2019), with length scales of up to tens of kilometres and amplitudes of up to several hundreds of metres, constitute a morphological terrain similar to the coastal bathymetry (Figs. 2, 3). Further, we demonstrate that this rugged terrain would exert the same strong influence on basal drag for an overriding ice mass (assuming no cavitation) (Figs. 7, S7~~S~~7~~F~~4). This is consistent with results from inverse methods that~~t~~hat~~o~~ determine basal drag for the modern TG bed (Joughin et al.,~~ which derive high basal shear stresses near the grounding zone that may explain the steep surface profile of the glacier (Joughin et al.,~~ 2009; Arthern et al., 2015). We also note that crag-and-tail landforms (which form subglacially) extend down to the floors of the deep troughs (e.g. Fig. 3, 4b). This confirms that, at least at the time when these features formed, ice of an expanded TG was grounded in the troughs as well as on the highs, and probably experienced high basal shear similar to ice at the present-day grounding zone. The orientation of the crag-and-tails also confirms that ice flow was not directed along troughs but rather overrode the existing topography; this finding is consistent with cosmogenic exposure data from Bear Peninsula (Fig. 1) showing that the ice-sheet surface rose above the top of this terrain during the last glacial period (Johnson et al., 2017).

For shorter wavelengths of bed topography, we can consider the form of the individual sea-floor highs over length scales of several kilometres. We interpret the morphological characteristics of these features as being consistent with the correlation of morphology with bed type ~~that has been described~~ known from onshore glacial-geological studies of crag-and-tail type features (e.g. Benn and Evans, 2010), and more recently has been described from on-ice seismic reflection profiles both for TG (Muto et al., 2019a, b; Holschuh et al., 2020) and beneath the Rutford Ice Stream (Fig. 4 in King et al., 2016).~~,~~), ~~although~~ Still, we recognize that high-resolution seismic reflection data over our bathymetric highs would be required to confirm this. ~~We note that these features exhibit the same correlation of morphology with bed type that has been described from on-ice seismic reflection profiles for TG (Muto et al., 2019a, b).~~ Specifically, the correlation is between "hard" beds on the stoss sides of topographic highs, associated with crag-and-tail landforms, and "soft" or sedimentary beds on the lee sides of these features. ~~Although this correlation was based on data from a single along-flow and two across-flow seismic reflection lines in the upstream area of the glacier, the inference is that this correlation can be applied to the bed in downstream and grounding-zone areas (Muto et al., 2019a, b).~~ This pattern is clearly replicated over the H2 and H3 highs, which have rugged upstream ends with crag-and-tail landforms, glacial lineations over their tops, and sedimentary "tails" on their downstream ends (Fig. 4). ~~This landform pattern is also similar to the 3D morphology of a topographic high near the grounding zone of the Rutford Ice Stream that was imaged using a grid of densely-spaced radar lines (Fig. 4 in King et al., 2016).~~ The correlation of bed types with sea-floor highs (and ridges) holds true for several other areas of the inner shelf around West Antarctica, where streamlining of bedrock highs has often produced landforms with sedimentary tails on the lee sides of bedrock obstacles (e.g. Larter et al., 2009, Graham et al., 2009; Livingstone et al., 2013; Nitsche et al., 2013; 2016), although this is not always the case. Thus, the variability in bed types on topographic highs in offshore regions may provide useful constraints on bed type variability ~~beneath~~ the modern glacierglacier~~in onshore areas~~.

Regarding the spectral analysis of roughness and basal drag contributions presented here (Figs. 6, 7, S5~~S~~54), we acknowledge that these only provide an order of magnitude assessment of the contribution to basal drag from the different wavelength scales resolved by the bathymetric DEM (Fig. 2). Analysis beyond the simple 2D-flow line theory used here (see Section 4.2) would be needed to account for 3D-flow effects, and for the nonlinear dependence of ice viscosity on stress (Glen, 1955). Here, we have not specified the physical mechanism controlling $\lambda_N$, the shortest roughness wavelength that influences basal drag. ~~Here, we have not been specific about the physical mechanism that controls the smallest roughness wavelength ($\lambda_N$).~~ Candidate mechanisms that might limit the influence of roughness at small spatial scales include cavitation (Fowler, 1986), fracture and plucking of crystalline or sedimentary rocks, the formation of a weak internal shear zone (Liu et al., 2020), bulldozing of unconsolidated sediment, or regelation flow around small obstacles (Weertman, 1957). More sophisticated theories accounting for the potential of ice to form cavities in the lee of obstacles could be deployed similarly, but the drag contribution would then depend also on water pressure (Fowler, 1986; Schoof, 2005). Process models of subglacial hydrology, phase change, fracture and sediment transport could all be incorporated in to a more elaborate analysis using MBES datasets as input.

It is clear from our results that the increased spatial resolution of the MBES data is critical for capturing the high-frequency bathymetric variability on the inner continental shelf seaward of TG, which is necessary to understand warm water incursions into sub-ice shelf cavities (Figs. 8, S5; Nakayama et al., 2019). The strong correlation of our observations with interpretations of the present bed conditions of TG and, therefore, the robustness of this deglaciated terrain as an analogue for the modern bed, further demonstrates that more information can be gleaned from this type of marine dataset (i.e. near-continuous bathymetry with spatial resolution better than 0.05~~5~~ km).~~)~~ For example, the 3D-nature of MBES (with approximately equal resolution in all directions) means that bathymetric variability could be examined in any direction, not only along survey lines, as ~~is~~ has been the case until recently with all onshore radar or seismic-reflection profiles of extant bed topography, and over a variety of spatial scales. These analyses ~~contribute~~ add to our understanding of across-flow contributions to basal drag or hydraulic potential (e.g. Muto et al., 2019a), and allow us to ~~constrain~~ consider the spatial variability of bed types (e.g. sedimentary vs. hard beds~~), thickness of deformable till, grain size distribution of subglacial sediments),~~ particularly where~~if the~~where sea-floor sediments are also imaged by seismic profiles and/or cored for ground-truthing. Similarly, the application of theories of subglacial processes as discussed above to high-resolution bathymetric datasets will increase our understanding of ice flow over high-frequency bed roughness, particularly if combined with ultra-high resolution (sub-metre resolution) bathymetries from AUV surveys (e.g. Davies et al., 2017; Dowdeswell et al., 2020). Indeed, AUV surveys and (or) a dense grid of seismic soundings (only obtainable from non-crevassed ice shelves) are the only way to determine bed geometry in ice-shelf cavities. New techniques such as swath-radar that can image the present glacier bed in 3D (Paden et al., 2010; Jezek et al., 2011), albeit in narrow swaths, have already been ~~trialled~~ employed on TG (Holschuh et al., 2020~~2019~~2020) and could be used in conjunction with offshore bathymetric data to build a better-informed, more complete and more uniform resolution picture of basal conditions under TG and at its grounding zone.

## 775 Conclusion

New 3D bathymetric data from just offshore Thwaites Glacier reveals that the coastal bathymetry is dominated by a ~65 km-long, ~1200 m-deep trough and discontinuous ridge with water depths of 600 m to <100 m. Spatial variations in the morphology of the ridge segments/highs and available acoustic sub-bottom profiler data suggest differences in substrate composition along the ridge, with the two southernmost highs having a significant "erodible" component at least in their upper parts, which areis presumablyare sedimentary in composition. The geometry (flat tops) and landform evidence (glacial lineations, gullies, sediment fans) indicate that the bathymetric highs were planed off and variously eroded by the action of Thwaites Ice Shelf as it flowed over them, presumably reducing the height of these former pinning points over time. A feedback mechanism during unpinning may have occurred, whereby as the ice shelf started to lose contact with the high and frontal buttressing weakened, the resultant increase in flow velocities exacerbated erosion of the high and facilitated further unpinning of Thwaites Glacier.

We present three lines of evidence that this coastal bathymetry provides a good analogue for the modern grounding zone of Thwaites Glacier. First, on length scales of several tens of km the ridge and trough morphology is consistent with the bed topography of the grounding-zone area based on available DEMs and over-ice geophysical data. Second, our spectral decomposition of roughness and basal drag over this rugged, deglaciated terrain is consistent with similar spectral decompositions, and inversions of basal drag, for profiles from the modern grounding zone area and for areas of the Thwaites bed, where bedrock crops out subglacially (e.g. Schroeder et al., 2014). In contrast, smooth beds, characterised by thick sedimentary substrates and linear glacial landforms, produce distinctly different power spectra and drag contributions. Third, the distribution of landforms and substrate types (unconsolidated sediment vs. bedrock) over the ridge indicates that it displays the same correlation of bed type with topography that has been described for upstream bed areas and inferred for the grounding zone (Muto et al., 2019a, b; Holschuh et al., 2020). As such, further analyses of this deglaciated terrain may provide realistic constraints on across-flow roughness and bed type distribution, and should inform geophysical observations of the modern TG bed that will be acquired as part of *ITGC*.

As discussed above, observational datasets like MBES are required seaward of Antarctic ice shelves in order to capture the high-frequency variability that characterises the bathymetry of nearshore areas. Modelled bathymetry cannot adequately reproduce the km- to sub-km-scale features that are important for accurately calculating inflows of warm ocean water in troughs, and for defining the topographic highs that may act as pinning points for ice shelves and as barriers to warm water incursions.

*Author contributions.* KAH, RDL, RA, TAJ, and AGCG and FON developed the concept of the paper. KAH, RDL, AGCG, RTM, JDK, RC and VF acquired and performed initial processing on the bathymetry data during NBP19-02; JDK performed all channel metric analyses. KG and JEA, and JH provided bathymetric data from German and Korean cruises, respectively. KAH compiled, part-processed and gridded all bathymetric datasets, and wrote the first draft of the paper with substantial

contributions from RA and RDL. RA developed the methodology for, performed spectral analyses and basal drag estimations, and wrote the text for these sections; KAH and TAJ provided the profile data. AW performed the ocean heat flux calculations. All authors contributed to the development of the final paper and data visualisation.

*Competing interests.* The authors declare no competing interests.

*Acknowledgements.* This work is an output of the THwaites Offshore Research (THOR) project and Glacial Habitat of Subglacial Thwaites (GHOST) projects, components of the *International Thwaites Glacier Collaboration* (*ITGC*). Support for this project is from National Science Foundation (NSF: Grant OPP- 1738942) and Natural Environment Research Council (NERC: Grant NE/S006664/1 THOR; Grant NE/S006672/1 GHOST). Logistics were provided by NSF-U.S. Antarctic Program and NERC-British Antarctic Survey. *ITGC* Contribution No. ITGC-011. We thank the NBP19-02 science party, the Edison Chouset Offshore Inc. captain and crew, and the Antarctic Support Contract technical staff aboard the RV/IB *Nathaniel B. Palmer*. This study is part of the Polar Science for Planet Earth Programme of the British Antarctic Survey.

**References**

Alley, R. B., Anandakrishnan, S., Dupont, T. K., Parizek, B. R., and Pollard, D.: Effect of sedimentation on ice-sheet grounding-line stability, Science, 315, 1838-1841, 2007.

Alley, R. B., Blankenship, D. D., Rooney, S. T., and Bentley, C. R.: Sedimentation beneath ice shelves -- the view from ice stream B, Marine Geology, 85, 101-120, 1989.

Arndt, J. E., Larter, R. D., Friedl, P., Gohl, K., Höppner, K., and the Science Team of Expedition, P. S.: Bathymetric controls on calving processes at Pine Island Glacier, The Cryosphere, 12, 2039-2050, 2018.

Arndt, J. E., Schenke, H. W., Jakobsson, M., Nitsche, F. O., Buys, G., Goleby, B., Rebesco, M., Bohoyo, F., Hong, J., Black, J., Greku, R., Udintsev, G., Barrios, F., Reynoso-Peralta, W., Taisei, M., and Wigley, R.: The International Bathymetric Chart of the Southern Ocean (IBCSO) Version 1.0 – A new bathymetric compilation covering circum-Antarctic waters, Geophysical Research Letters, doi: 10.1002/grl.50413, 2013.

Arneborg, L., Wåhlin, A. K., Björk, G., Liljebladh, B., and Orsi, A. H.: Persistent inflow of warm water onto the central Amundsen shelf, Nature Geoscience, 5, 876-880, 2012.

Arthern, R. J., Hindmarsh, R. C. A., and Williams, C. R.: Flow speed within the Antarctic ice sheet and its controls inferred from satellite observations, Journal of Geophysical Research: Earth Surface, 120, 1171-1188, 2015.

Bellwald, B., Hjelstuen, B. O., Sejrup, H. P., Stokowy, T., and Kuvås, J.: Holocene mass movements in west and mid-Norwegian fjords and lakes, Marine Geology, 407, 192-212, 2019.

Benn, D. I. and J. A. Evans (2010). Glaciers & Glaciation, Hodder Education.

Berger, S., Favier, L., Drews, R., Derwael, J.-J., and Pattyn, F.: The control of an uncharted pinning point on the flow of an Antarctic ice shelf, Journal of Glaciology, 62, 37-45, 2016.

Bingham, R. G., Vaughan, D. G., King, E. C., Davies, D., Cornford, S. L., Smith, A. M., Arthern, R. J., Brisbourne, A. M., De Rydt, J., Graham, A. G. C., Spagnolo, M., Marsh, O. J., and Shean, D. E.: Diverse landscapes beneath Pine Island Glacier influence ice flow, Nature Communications, 8, 1618, 2017.

Caress, D. W. and Chayes, D. N.: Improved processing of Hydrosweep DS multibeam data on the R/V Maurice Ewing, Marine Geophysical Researches, 18, 631-650, 1996.

Caress, D. W., Chayes, D. N., and Ferreira, C.: https://www.mbari.org/products/research-software/mb-system/, last access: 02/12/2019 2019.

Clark, C. D., Tulaczyk, S. M., Stokes, C. R., and Canals, M.: A groove-ploughing theory for the production of mega-scale glacial lineations, and implications for ice-stream mechanics, Journal of Glaciology, 49, 240-256, 2003.

Cochran, J. R. and Bell, R. E.: IceBridge Sander AIRGrav L1B Geolocated Free Air Gravity Anomalies, V01.5. National Snow and Ice Data Center, Boulder, Colorado, 2010.

Davies, D., Bingham, R. G., Graham, A. G. C., Spagnolo, M., Dutrieux, P., Vaughan, D. G., Jenkins, A., and Nitsche, F. O.: High-resolution sub-ice-shelf seafloor records of twentieth century ungrounding and retreat of Pine Island Glacier, West Antarctica, Journal of Geophysical Research: Earth Surface, 122, 1698-1714, 2017.

De Rydt, J. and Gudmundsson, G. H.: Coupled ice shelf-ocean modeling and complex grounding line retreat from a seabed ridge, Journal of Geophysical Research: Earth Surface, 121, 865-880, 2016.

De Rydt, J., Holland, P. R., Dutrieux, P., and Jenkins, A.: Geometric and oceanographic controls on melting beneath Pine Island Glacier, Journal of Geophysical Research: Oceans, 119, 2420–2438, 2014.

Dowdeswell, J. A., Batchelor, C. L., Montelli, A., Ottesen, D., Christie, F. D. W., Dowdeswell, E. K., and Evans, J.: Delicate seafloor landforms reveal past Antarctic grounding-line retreat of kilometers per year, Science, 368, 1020, 2020.

Dowdeswell, E. K., Todd, B. J., and Dowdeswell, J. A.: Crag-and-tail features: convergent ice flow through Eclipse Sound, Baffin Island, Arctic Canada, Geological Society, London, Memoirs, 46, 55, 2016.

Dowdeswell, J. A. and Fugelli, E. M. G.: The seismic architecture and geometry of grounding-zone wedges formed at the marine margins of past ice sheets, Geological Society of America Bulletin, 124, 1750-1761, 2012.

Dutrieux, P., Vaughan, D. G., Corr, H. F. J., Jenkins, A., Holland, P. R., Joughin, I., and Fleming, A. H.: Pine Island glacier ice shelf melt distributed at kilometre scales, The Cryosphere, 7, 1543-1555, 2013.

Evans, J., Dowdeswell, J. A., Ó Cofaigh, C., Benham, T. J., and Anderson, J. B.: Extent and dynamics of the West Antarctic Ice Sheet on the outer continental shelf of Pine Island Bay during the last glaciation, Marine Geology, 230, 53-72, 2006.

Falcini, F. M., Rippin, D. M., Krabbendam, M., and Selby, K. A.: Quantifying bed roughness beneath contemporary and palaeo-ice streams, Journal of Glaciology, 64, 822-834, 2018.

Favier, L., Durand, G., Cornford, S. L., Gudmundsson, G. H., Gagliardini, O., Gillet-Chaulet, F., Zwinger, T., Payne, A. J., and Le Brocq, A. M.: Retreat of Pine Island Glacier controlled by marine ice-sheet instability, Nature Climate Change, 4, 117-121, 2014.

Favier, L., Pattyn, F., Berger, S., and Drews, R.: Dynamic influence of pinning points on marine ice-sheet stability: a numerical study in Dronning Maud Land, East Antarctica, The Cryosphere, 10, 2623-2635, 2016.

Ferrigno, J. G., Lucchitta, B. K., Mullins, K. F., Allison, A. L., Allen, R. J., and Gould, W. G.: Velocity measurements and changes in position of Thwaites Glacier/iceberg tongue from aerial photography, Landsat images and NOAA AVHRR data, Annals of Glaciology, 17, 239-244, 1993.

Fowler, A. C. and Nye, J. F.: A sliding law for glaciers of constant viscosity in the presence of subglacial cavitation, Proceedings of the Royal Society of London. A. Mathematical and Physical Sciences, 407, 147-170, 1986.

Gales, J. A., Larter, R. D., Mitchell, N. C., and Dowdeswell, J. A.: Geomorphic signature of Antarctic submarine gullies: Implications for continental slope processes, Marine Geology, 337, 112-124, 2013.

Glen, J. W. and Perutz, M. F.: The creep of polycrystalline ice, Proceedings of the Royal Society of London. Series A. Mathematical and Physical Sciences, 228, 519-538, 1955.

Gohl, K.: The Expedition of the Research Vessel "Polarstern" to the Amundsen Sea, Antarctica, in 2010 (ANT-XXVI/3), Berichte zur Polar- und Meeresforschung 617, 169 pp, 2010.

Gohl, K.: The Expedition PS104 of the Research Vessel POLARSTERN to the Amundsen Sea in 2017, Berichte zur Polar- und Meeresforschung 712, 100 pp, https://doi.org/10.2312/BzPM_0712_2017, 2017.

Gohl, K.: Basement control on past ice sheet dynamics in the Amundsen Sea Embayment, West Antarctica, Palaeogeography, Palaeoclimatology, Palaeoecology, 335-336, 35-41, 2012.

Gohl, K., Denk, A., Eagles, G., and Wobbe, F.: Deciphering tectonic phases of the Amundsen Sea Embayment shelf, West Antarctica, from a magnetic anomaly grid, Tectonophysics, 585, 113-123, 2013.

Graham, A. G. C. and Hogan, K. A.: Crescentic scours on palaeo-ice stream beds, Geological Society, London, Memoirs, 46, 221, 2016.

Graham, A. G. C., Larter, R. D., Gohl, K., Hillenbrand, C.-D., Smith, J. A., and Kuhn, G.: Bedform signature of a West Antarctic palaeo-ice stream reveals a multi-temporal record of flow and substrate control, Quaternary Science Reviews, 28, 2774-2793, 2009.

Greenwood, S. L., Simkins, L. M., Halberstadt, A. R. W., Prothro, L. O., and Anderson, J. B.: Holocene reconfiguration and readvance of the East Antarctic Ice Sheet, Nature Communications, 9, 3176, 2018.

Ha, H. K., Wåhlin, A. K., Kim, T. W., Lee, S. H., Lee, J. H., Lee, H. J., Hong, C. S., Arneborg, L., Björk, G., and Kalén, O.: Circulation and Modification of Warm Deep Water on the Central Amundsen Shelf, Journal of Physical Oceanography, 44, 1493-1501, 2014.

Heywood, K. J., Biddle, L. C., Boehme, L., Dutrieux, P., Fedak, M., Jenkins, A., Jones, R. W., Kaiser, J., Mallett, H., Garabato, A. C. N., Renfrew, I. A., Stevens, D. P., and Webber, B. G. M.: Between the Devil and the Deep Blue Sea THE ROLE OF

THE AMUNDSEN SEA CONTINENTAL SHELF IN EXCHANGES BETWEEN OCEAN AND ICE SHELVES, Oceanography, 29, 118-129, 2016.

Hillenbrand, C.-D., Kuhn, G., Smith, J. A., Gohl, K., Graham, A. G. C., Larter, R. D., Klages, J. P., Downey, R., Moreton, S. G., Forwick, M., and Vaughan, D. G.: Grounding-line retreat of the West Antarctic Ice Sheet from inner Pine Island Bay, Geology, 41, 35-38, 2013.

Hogan, K. A., Dowdeswell, J. A., and Mienert, J.: New insights into slide processes and seafloor geology revealed by side-scan imagery of the massive Hinlopen Slide, Arctic Ocean margin, Geo-Marine Letters, 33, 325-343, 2013.

Holschuh, N., Christianson, K., Paden, J., Alley, R. B., and Anandakrishnan, S.: Linking postglacial landscapes to~~and subglacial processes through~~to glacier dynamics using swath radar imaging at Thwaites Glacier, ~~West~~ Antarctica, ~~Madison, WI, USA, 12-17 June 2019.~~Geology, 48, 268-272, 2020.

Hubbard, B., Siegert, M. J., and McCarroll, D.: Spectral roughness of glaciated bedrock geomorphic surfaces: Implications for glacier sliding, Journal of Geophysical Research: Solid Earth, 105, 21295-21303, 2000.

Holt, J. W., Blankenship, D. D., Morse, D. L., Young, D. A., Peters, M. E., Kempf, S. D., Richter, T. G., Vaughan, D. G., and Corr, H. F. J.: New boundary conditions for the West Antarctic Ice Sheet: Subglacial topography of the Thwaites and Smith glacier catchments, Geophys. Res. Lett., 33, L09502, 2006.

Hughes, T. J.: The weak underbelly of the West Antarctic ice sheet, Journal of Glaciology, 27, 518-525, 1981.

Jacobs, S., Giulivi, C., Dutrieux, P., Rignot, E., Nitsche, F., and Mouginot, J.: Getz Ice Shelf melting response to changes in ocean forcing, Journal of Geophysical Research: Oceans, 118, 4152-4168, 2013.

Jacobs, S., Jenkins, A., Hellmer, H., Giulivi, C., Nitsche, F., Huber, B., and Guerrero, R.: THE AMUNDSEN SEA AND THE ANTARCTIC ICE SHEET, Oceanography, 25, 154-163, 2012.

Jacobs, S. S., Hellmer, H. H., and Jenkins, A.: Antarctic Ice Sheet melting in the southeast Pacific, Geophysical Research Letters, 23, 957-960, 1996.

Jakobsson, M., Anderson, J. B., Nitsche, F. O., Gyllencreutz, R., Kirshner, A. E., Kirchner, N., O'Regan, M., Mohammad, R., and Eriksson, B.: Ice sheet retreat dynamics inferred from glacial morphology of the central Pine Island Bay Trough, West Antarctica, Quaternary Science Reviews, 38, 1-10, 2012.

Jakobsson, M., Nilsson, J., O'Regan, M., Backman, J., Löwemark, L., Dowdeswell, J. A., Mayer, L., Polyak, L., Colleoni, F., Anderson, L., Björk, G., Darby, D., Eriksson, B., Hanslik, D., Hell, B., Marcussen, C., Sellén, E., and Wallin, Å.: An Arctic Ocean ice shelf during MIS 6 constrained by new geophysical and geological data, Quaternary Science Reviews, 29, 3505-3517, 2010.

Jenkins, A., Dutrieux, P., Jacobs, S. S., McPhail, S. D., Perrett, J. R., Webb, A. T., and White, D.: Observations beneath Pine Island Glacier in West Antarctica and implications for its retreat, Nature Geoscience, 3, 468-472, 2010.

Jenkins, A., Dutrieux, P., Jacobs, S., Steig, E. J., Gudmundsson, G. H., Smith, J., and Heywood, K. J.: Decadal Ocean Forcing and Antarctic Ice Sheet Response LESSONS FROM THE AMUNDSEN SEA, Oceanography, 29, 106-117, 2016.

Jezek, K., Wu, X., Gogineni, P., Rodríguez, E., Freeman, A., Rodriguez-Morales, F., and Clark, C.D.: Radar images of the bed of the Greenland Ice Sheet, Geophysical Research Letters, 38, 1-5, https://doi .org/10.1029/2010GL045519, 2011.

Johnson, J. S., Smith, J. A., Schaefer, J. M., Young, N. E., Goehring, B. M., Hillenbrand, C.-D., Lamp, J. L., Finkel, R. C., and Gohl, K.: The last glaciation of Bear Peninsula, central Amundsen Sea Embayment of Antarctica: Constraints on timing and duration revealed by in situ cosmogenic 14C and 10Be dating, Quaternary Science Reviews, 178, 77-88, 2017.

Jordan, T. A., Porter, D., Tinto, K., Millan, R., Muto, A., Hogan, K., Larter, R. D., Graham, A. G. C., and Paden, J. D.: New gravity-derived bathymetry for the Thwaites, Crosson and Dotson ice shelves revealing two ice shelf populations, The Cryosphere Discuss., 2020, 1-20, 2020.

Jordan, T. M., Cooper, M. A., Schoreder, D. M., Williams, C. N., Paden, J. D., Siegert, M. J., and Bamber, J. L.: Self-affine subglacial roughness: consequences for radar scattering and basal water discrimination in northern Greenland, The Cryosphere, 11, 1247-1264, 2017.

Joughin, I., Smith, B. E., and Holland, D. M.: Sensitivity of 21st century sea level to ocean-induced thinning of Pine Island Glacier, Antarctica, Geophysical Research Letters, 37, 2010.

Joughin, I., Smith, B. E., and Medley, B.: Marine Ice Sheet Collapse Potentially Under Way for the Thwaites Glacier Basin, West Antarctica, Science, 344, 735, 2014.

Kamb, B.: Sliding motion of glaciers: theory and observation, Reviews of Geophysics and Space Physics, 8, 673-728, 1970.

Kim, J.-W., Kim, D.-j., Kim, S. H., Ha, H. K., and Lee, S. H.: Disintegration and acceleration of Thwaites Ice Shelf on the Amundsen Sea revealed from remote sensing measurements, GIScience & Remote Sensing, 52, 498-509, 2015.

King, E. C., Pritchard, H. D., and Smith, A. M.: Subglacial landforms beneath Rutford Ice Stream, Antarctica: detailed bed topography from ice-penetrating radar, Earth Syst. Sci. Data, 8, 151-158, 2016.

Kirkham, J. D., Hogan, K. A., Larter, R. D., Arnold, N. S., Nitsche, F. O., Golledge, N. R., and Dowdeswell, J. A.: Past water flow beneath Pine Island and Thwaites glaciers, West Antarctica, The Cryosphere, 13, 1959-1981, 2019.

Kirshner, A., Anderson, J.B., Jakobsson, M., O'Regan, M., Majewski, W., and Nitsche, F.: Post-LGM deglaciation in Pine island Bay, west Antarctica. Quaternary Science Reviews, 38, 11-26, 2012.

Kuhn, G., Hillenbrand, C.-D., Kasten, S., Smith, J. A., Nitsche, F. O., Frederichs, T., Wiers, S., Ehrmann, W., Klages, J. P., and Mogollón, J. M.: Evidence for a palaeo-subglacial lake on the Antarctic continental shelf, Nature Communications, 8, 15591, 2017.

Larter, R. D., Graham, A. G. C., Gohl, K., Kuhn, G., Hillenbrand, C.-D., Smith, J. A., Deen, T. J., Livermore, R. A., and Schenke, H.-W.: Subglacial bedforms reveal complex basal regime in a zone of paleo–ice stream convergence, Amundsen Sea embayment, West Antarctica, Geology, 37, 411-414, 2009.

Larter, R. D., Anderson, J. B., Graham, A. G. C., Gohl, K., Hillenbrand, C-. D., Jakobsson, M., Johnson, J. S., Kuhn, G., Nitsche, F. O., Smith, J. A., Witus, A. E., Bentley, M. J., Dowdeswell, J. A., Ehrmann, W., Klages, J. P., Lindow, J., O Cofaigh, C., and Spiegel, C.: Reconstruction of changes in the Amundsen Sea ad Bellingshausen Sea sector of the West Antarctic Ice Sheet since the Last Glacial Maximum, Quaternary Science Reviews, 100, 55-86, 2014.

Larter, R. D., Queste, B. Y., Boehme, L., Braddock, S., Wåhlin, A. K., Graham, A. G. C., Hogan, K. A., Totten Minzoni, R., Barham, M., Bortolotto de'Oliveira, G., Clark, R., Fitzgerald, V., Karam, S., Kirkham, J. D., Mazur, A., Sheehan, P., Spoth, M., Stedt, P., Welzenbach, L. Zheng, Y., Andersson, J., Rolandsson, J., Beeler, C., Goodell, J., Rush, and Snow, T.: CRUISE REPORT RV/IB Nathaniel B. Palmer Cruise NBP19-02, January-March 2019: First research cruise of the International Thwaites Glacier Collaboration, ~~2020.~~ http://get.rvdata.us/cruise/NBP1902/doc/NBP1902_report_final.pdf, 2020.

Larter, R. D. and Vanneste, L. E.: Relict subglacial deltas on the Antarctic Peninsula outer shelf, Geology, 23, 33-36, 1995.

Livingstone, S. J., Cofaigh, C. Ó., Stokes, C. R., Hillenbrand, C.-D., Vieli, A., and Jamieson, S. S. R.: Glacial geomorphology of Marguerite Bay Palaeo-Ice stream, western Antarctic Peninsula, Journal of Maps, 9, 558-572, 2013.

Liu, E. W., Räss, L., Suckale, J., Herman, F., and Podladchikov, Y.: Spontaneous Formation of Internal Shear Zone in Ice Flowing over a Topographically Variable Bed, EGU General Assembly 2020, Online, 4–8 May 2020, EGU2020-12602, https://doi.org/10.5194/egusphere-egu2020-12602, 2020.

Lowe, A. L. and Anderson, J. B.: Evidence for abundant subglacial meltwater beneath the paleo-ice sheet in Pine Island Bay, Antarctica, Journal of Glaciology, 49, 125-138, 2003.

Lowe, A. L. and Anderson, J. B.: Reconstruction of the West Antarctic ice sheet in Pine Island Bay during the Last Glacial Maximum and its subsequent retreat history, Quaternary Science Reviews, 21, 1879-1897, 2002.

MacAyeal, D. R.: Large-scale ice flow over a viscous basal sediment: Theory and application to ice stream B, Antarctica, Journal of Geophysical Research: Solid Earth, 94, 4071-4087, 1989.

MacLean, B., Blasco, S., Bennett, R., Hughes Clarke, J. E., and Patton, E.: Crag-and-tail features, Amundsen Gulf, Canadian Arctic Archipelago, Geological Society, London, Memoirs, 46, 53, 2016.

MacGregor, J. A., Catania, G. A., Markowski, M. S., and Andrews, A. G.: Widespread rifting and retreat of ice-shelf margins in the eastern Amundsen Sea Embayment between 1972 and 2011, Journal of Glaciology, 58, 458-466, 2012.

Matsuoka, K., Hindmarsh, R. C. A., Moholdt, G., Bentley, M. J., Pritchard, H. D., Brown, J., Conway, H., Drews, R., Durand., G., Goldberg, D., Hattermann, T., Kingslake, J., Lenaerts, J. T. M., Martín, C., Mulvaney, R., Nicholss, K. W., Pattyn, F., Ross, N., Scambos, T., and Whitehouse, P. L.: Antarctic ice rises and rumples: Their properties and significance for ice-sheet dynamics and evolution, Earth Science Reviews, 150, 724-745, 2015.

Mayer, L. A., Paton, M., Gee, L., Gardner, S. V., and Ware, C.: Interactive 3-D visualization: a tool for seafloor navigation, exploration and engineering, 11-14 Sept. 2000 2000, 913-919 vol.912.

McMillan, M., Shepherd, A., Sundal, A., Briggs, K., Muir, A., Ridout, A., Hogg, A., and Wingham, D.: Increased ice losses from Antarctica detected by CryoSat-2, Geophysical Research Letters, 41, 3899-3905, 2014.

Milillo, P., Rignot, E., Rizzoli, P., Scheuchl, B., Mouginot, J., Bueso-Bello, J., and Prats-Iraola, P.: Heterogeneous retreat and ice melt of Thwaites Glacier, West Antarctica, Science Advances, 5, eaau3433, 2019.

Millan, R., Rignot, E., Bernier, V., Morlighem, M., and Dutrieux, P.: Bathymetry of the Amundsen Sea Embayment sector of West Antarctica from Operation IceBridge gravity and other data, Geophysical Research Letters, 44, 1360-1368, 2017.

Morlighem, M., Rignot, E., Binder, T., Blankenship, D., Drews, R., Eagles, G., Eisen, O., Ferraccioli, F., Forsberg, R., Fretwell, P., Goel, V., Greenbaum, J. S., Gudmundsson, H., Guo, J., Helm, V., Hofstede, C., Howat, I., Humbert, A., Jokat, W., Karlsson, N. B., Lee, W. S., Matsuoka, K., Millan, R., Mouginot, J., Paden, J., Pattyn, F., Roberts, J., Rosier, S., Ruppel, A., Seroussi, H., Smith, E. C., Steinhage, D., Sun, B., Broeke, M. R. v. d., Ommen, T. D. v., Wessem, M. v., and Young, D. A.: Deep glacial troughs and stabilizing ridges unveiled beneath the margins of the Antarctic ice sheet, Nature Geoscience, doi: 10.1038/s41561-019-0510-8, 2019. 2019.

Mouginot, J., Rignot, E., and Scheuchl, B.: Continent-Wide, Interferometric SAR Phase, Mapping of Antarctic Ice Velocity, Geophysical Research Letters, 46, 9710-9718, 2019.

Mouginot, J., Rignot, E., and Scheuchl, B.: Sustained increase in ice discharge from the Amundsen Sea Embayment, West Antarctica, from 1973 to 2013, Geophysical Research Letters, 41, 1576-1584, 2014.

Muto, A., Alley, R. B., Parizek, B. R., and Anandakrishnan, S.: Bed-type variability and till (dis)continuity beneath Thwaites Glacier, West Antarctica, Annals of Glaciology, doi: 10.1017/aog.2019.32. 1-9, 2019a.

Muto, A., Anandakrishnan, S., Alley, R. B., Horgan, H. J., Parizek, B. R., Koellner, S., Christianson, K., and Holschuh, N.: Relating bed character and subglacial morphology using seismic data from Thwaites Glacier, West Antarctica, Earth and Planetary Science Letters, 507, 199-206, 2019b.

Nakayama, Y., Manucharyan, G., Zhang, H., Dutrieux, P., Torres, H. S., Klein, P., Seroussi, H., Schodlok, M., Rignot, E., and Menemenlis, D.: Pathways of ocean heat towards Pine Island and Thwaites grounding lines, Scientific Reports, 9, 16649, 2019.

Nakayama, Y., Schröder, M., and Hellmer, H. H.: From circumpolar deep water to the glacial meltwater plume on the eastern Amundsen Shelf, Deep Sea Research Part I: Oceanographic Research Papers, 77, 50-62, 2013.

Nitsche, F. O., Gohl, K., Larter, R. D., Hillenbrand, C. D., Kuhn, G., Smith, J. A., Jacobs, S., Anderson, J. B., and Jakobsson, M.: Paleo ice flow and subglacial meltwater dynamics in Pine Island Bay, West Antarctica, The Cryosphere, 7, 249-262, 2013.

Nitsche, F. O., Jacobs, S. S., Larter, R. D., and Gohl, K.: Bathymetry of the Amundsen Sea continental shelf: Implications for geology, oceanography, and glaciology, Gechemistry Geophysics Geosystems, 8, Q10009, 2007.

Nitsche, F. O., Larter, R. D., Gohl, K., Graham, A. G. C., and Kuhn, G.: Crag-and-tail features on the Amundsen Sea continental shelf, West Antarctica, Geological Society, London, Memoirs, 46, 199, 2016.

Noormets, R., Dowdeswell, J. A., Larter, R. D., Ó Cofaigh, C., and Evans, J.: Morphology of the upper continental slope in the Bellingshausen and Amundsen Seas - Implications for sedimentary processes at the shelf edge of West Antarctica, Marine Geology, ~~In Press, Corrected Proof,~~258, 100-114, 2009.

Noormets, R., Kirchner, N., Flink, A. E., and Dowdeswell, J. A.: Possible iceberg-produced submarine terraces in Hambergbukta, Spitsbergen, Geological Society, London, Memoirs, 46, 101, 2016.

Nye, J. F.: Glacier sliding without cavitation in a linear viscous approximation, Proceedings of the Royal Society of London, 315, 381-403, 1970.

Ó Cofaigh, C., Dowdeswell, J. A., Allen, C. S., Hiemstra, J. F., Pudsy, C., J., Evans, J., Evans, D. J. A.: Flow dynamics and till genesis associated with a marine-based Antarctic palaeo-ice stream, Quaternary Science Reviews, 24, 709-740, 2005.

Paden, J., Akins, T., Dunson, D., Allen, C., and Gogineni, P.: Ice-sheet bed 3-D tomography, Journal of Glaciology, 56, 3-11, https:// doi .org/10.3189/002214310791190811, 2010.

Parizek, B. R. and Walker, R. T.: Implications of initial conditions and ice–ocean coupling for grounding-line evolution, Earth and Planetary Science Letters, 300, 351-358, 2010.

Pattyn, F. and Van Huele, W.: Power law or power flaw?, Earth Surface Processes and Landforms, 23, 761-767, 1998.

Post, A. L., O'Brien, P. E., Edwards, S., Carroll, A. G., Malakoff, K., and Armand, L. K.: Upper slope processes and seafloor ecosystems on the Sabrina continental slope, East Antarctica, Marine Geology, doi: https://doi.org/10.1016/j.margeo.2019.106091, 2019. 106091, 2019.

Rabus, B. T., Lang, O., and Adolphs, U.: Interannual velocity variations and recent calving of Thwaites Glacier Tongue, West Antarctica, Annals of Glaciology, 36, 215-224, 2003.

Rignot, E.: Evidence for rapid retreat and mass loss of Thwaites Glacier, West Antarctica, Journal of Glaciology, 47, 213-222, 2001.

Rignot, E., Jacobs, S., Mouginot, J., and Scheuchl, B.: Ice-Shelf Melting Around Antarctica, Science, 341, 266-270, 2013.

Rignot, E., Mouginot, J., Morlighem, M., Seroussi, H., and Scheuchl, B.: Widespread, rapid grounding line retreat of Pine Island, Thwaites, Smith, and Kohler glaciers, West Antarctica, from 1992 to 2011, Geophysical Research Letters, 41, 3502-3509, 2014.

Rignot, E., Mouginot, J., and Scheuchl, B.: Antarctic grounding line mapping from differential satellite radar interferometry, Geophysical Research Letters, 38, 2011.

Rignot, E., Mouginot, J., Scheuchl, B., van den Broeke, M., van Wessem, M. J., and Morlighem, M.: Four decades of Antarctic Ice Sheet mass balance from 1979–2017, Proceedings of the National Academy of Sciences, 116, 1095, 2019.

Rippin, D. M., Vaughan, D. G., and Corr, H. F. J.: The basal roughness of Pine Island Glacier, West Antarctica. Journal of Glaciology, 57, 67–76, 2011.

Scambos, T. A., Bell, R. E., Alley, R. B., Anandakrishnan, S., Bromwich, D. H., Brunt, K., Christianson, K., Creyts, T., Das, S. B., DeConto, R., Dutrieux, P., Fricker, H. A., Holland, D., MacGregor, J., Medley, B., Nicolas, J. P., Pollard, D., Siegfried, M. R., Smith, A. M., Steig, E. J., Trusel, L. D., Vaughan, D. G., and Yager, P. L.: How much, how fast?: A science review and outlook for research on the instability of Antarctica's Thwaites Glacier in the 21st century, Global and Planetary Change, 153, 16-34, 2017.

Schoof, C.: Basal perturbations under ice streams: form drag and surface expression, Journal of Glaciology, 48, 407-416, 2002.

Schoof, C.: The effect of cavitation on glacier sliding, Proceedings of the Royal Society A: Mathematical, Physical and Engineering Sciences, 461, 609-627, 2005.

Schoof, C.: Ice sheet grounding line dynamics: Steady states, stability, and hysteresis, Journal of Geophysical Research: Earth Surface, 112, F03S28, doi:10.1029/2006JF000664~~n/a-n/a~~, 2007.

Schroeder, D. M., Blankenship, D. D., and Young, D. A.: Evidence for a water system transition beneath Thwaites Glacier, West Antarctica, Proceedings of the National Academy of Sciences, 110, 12225, 2013.

Schroeder, D. M., Blankenship, D. D., Young, D. A., Witus, A. E., and Anderson, J. B.: Airborne radar sounding evidence for deformable sediments and outcropping bedrock beneath Thwaites Glacier, West Antarctica, Geophysical Research Letters, 41, 7200-7208, 2014.

Shepherd, A., Gilbert, L., Muir, A. S., Konrad, H., McMillan, M., Slater, T., Briggs, K. H., Sundal, A. V., Hogg, A. E., and Engdahl, M. E.: Trends in Antarctic Ice Sheet Elevation and Mass, Geophysical Research Letters, 46, 8174-8183, 2019.

Siegert, M. J., Taylor, J., Payne, A. J., and Hubbard, B.: Macro-scale bed roughness of the Siple Coast ice streams in west Antarctica, Earth Surface Processes and Landforms, 29, 1591–1596, 2004.

Spagnolo, M., Clark, C. D., Ely, J. C., Stokes, C. R., Anderson, J. B., Andreassen, K., Graham, A. G. C., and King, E. C.: Size, shape and spatial arrangement of mega-scale glacial lineations from a large and diverse dataset, Earth Surface Processes and Landforms, 39, 1432-1448, 2014.

Spagnolo, M., Bartholomaus, T. C., Clark, C. D., Stokes, C. R., Atkinson, N., Dowdeswell, J. A., Ely, J. C., Graham, A. G. C., Hogan, K. A., King, E. C., Larter, R. D., Livingstone, S. J., and Pritchard, H. D.: The periodic topography of ice stream beds: Insights from the Fourier spectra of mega-scale glacial lineations, Journal of Geophysical Research: Earth Surface, 122, 1355-1373, 2017.

Spiegel, C., Lindow, J., Kamp, P. J. J., Meisel, O., Mukasa, S., Lisker, F., Kuhn, G., and Gohl, K.: Tectonomorphic evolution of Marie Byrd Land – Implications for Cenozoic rifting activity and onset of West Antarctic glaciation, Global and Planetary Change, 145, 98-115, 2016.

Tinto, K. J. and Bell, R. E.: Progressive unpinning of Thwaites Glacier from newly identified offshore ridge: Constraints from aerogravity, Geophysical Research Letters, 38, 2011.

Vanneste, M., Mienert, J., and Bünz, S.: The Hinlopen Slide: A giant, submarine slope failure on the northern Svalbard margin, Arctic Ocean, Earth and Planetary Science Letters, 245, 373-388, 2006.

Vaughan, D. G. and Arthern, R.: Why Is It Hard to Predict the Future of Ice Sheets?, Science, 315, 1503, 2007.

Vaughan, D. G., Corr, H. F. J., Ferraccioli, F., Frearson, N., O'Hare, A., Mach, D., Holt, J. W., Blankenship, D. D., Morse, D. L., and Young, D. A.: New boundary conditions for the West Antarctic ice sheet: Subglacial topography beneath Pine Island Glacier, Geophys. Res. Lett., 33, L09501, 2006.

Vogt, P. R., Crane, K., and Sundvor, E.: Deep Pleistocene iceberg plowmarks on the Yermak Plateau: sidescan and 3.5 kHz evidence for thick calving ice fronts and a possible marine ice sheet in the Arctic Ocean, Geology, 22, 403-406, 1994.

Walker, D. P., Brandon, M. A., Jenkins, A., Allen, J. T., Dowdeswell, J. A., and Evans, J.: Oceanic heat transport onto the Amundsen Sea shelf through a submarine glacial trough, Geophysical Research Letters, 34, 2007.

Weertman, J.: On the Sliding of Glaciers, Journal of Glaciology, 3, 33-38, 1957.

Weertman, J.: Stability of the junction between an ice sheet and an ice shelf, Journal of Glaciology, 13, 3-11, 1974.

Welch, P. D.: The Use of Fast Fourier Transform for the Estimation of Power Spectra: A Method Based on Time Averaging Over Short, Modified Periodograms, IEEE TRANSACTIONS ON AUDIO AND ELECTROACOUSTICS, 15, 70-73, 1967.

Wellner, J. S., Heroy, D. C., and Anderson, J. B.: The death mask of the Antarctic ice sheet: Comparison of glacial geomorphic features across the continental shelf, Geomorphology, 75, 157-171, 2006.

Whitehouse, P. L., Bentley, M. J., Milne, G. A., King, M. A. and ~~Le Brocq, A. M.~~Thomas, I. D.~~:~~, A new glacial isostatic adjustment model for Antarctica: calibrated and tested using observations of relative sea-level change and present-day uplift rates~~M., A deglacial model for Antarctica: geological constraints and glaciological modelling as a basis for a new model of Antarctic glacial isostatic adjustment, Quaternary Science Reviews~~Geophysical Journal International, ~~32, 1-24~~190, 1464-1482, 2012.

Yu, H., Rignot, E., Seroussi, H., Morlighem, M., and Choi, Y.: Impact of Iceberg Calving on the Retreat of Thwaites Glacier, West Antarctica Over the Next Century With Different Calving Laws and Ocean Thermal Forcing, Geophysical Research Letters, 46, https://doi.org/10.1029/2019GL084066, 2019.

| **Cruise ID** | **Year** | **Multibeam echo sounder (frequency)** | **Source**<br>Data centre and *lead institution* |
|---|---|---|---|
| NBP19-02 | 2019 | Kongsberg EM122 (12 kHz) | IEDA MGDS<br>*BAS/Univ. Houston* |
| NBP19-01 | 2019 | Kongsberg EM122 (12 kHz) | IEDA MGDS<br>*Stanford/Caltech* |
| PS104 | 2017 | Hydrosweep DS-2 (15.5 kHz) | *AWI* |
| JR294 | 2014 | Kongsberg EM122 (12 kHz) | UK PDC<br>*Univ. East Anglia* |
| ANT-XXVI/3 | 2010 | Hydrosweep DS-2 (15.5 kHz) | *AWI* |
| NBP09-01 | 2009 | Kongsberg EM120 (12 kHz) | IEDA MGDS<br>*LDEO* |
| JR179 | 2008 | Kongsberg EM120 (12 kHz) | UK PDC<br>*BAS* |
| NBP07-02 | 2007 | Kongsberg EM120 (12 kHz) | IEDA MGDS<br>*LDEO* |
| JR141 | 2006 | Kongsberg EM120 (12 kHz) | UK PDC<br>*BAS* |
| NBP00-01 | 2000 | SeaBeam 2112 (12 kHz) | IEDA MGDS<br>*Rice University* |
| NBP99-02 | 1999 | SeaBeam 2112 (12 kHz) | IEDA MGDS<br>*Rice University* |
| ANA02C | 2012 | Kongsberg EM122 (12 kHz) | KOPRI |

1890 **Table 1: Research cruises that acquired MBES data used in this compilation. IEDA MGDS is the Interdisciplinary Earth Data Alliance Marine Geoscience Data System (USA; http://www.marine-geo.org/index.php); UK PDC is the United Kingdom Polar Data Centre (UK; https://www.bas.ac.uk/data/uk-pdc/); BAS is British Antarctic Survey; AWI is the Alfred Wegener Institute (Germany); LDEO is Lamont-Doherty Earth Observatory of Columbia University; KOPRI is the Korea Polar Research Institute.**

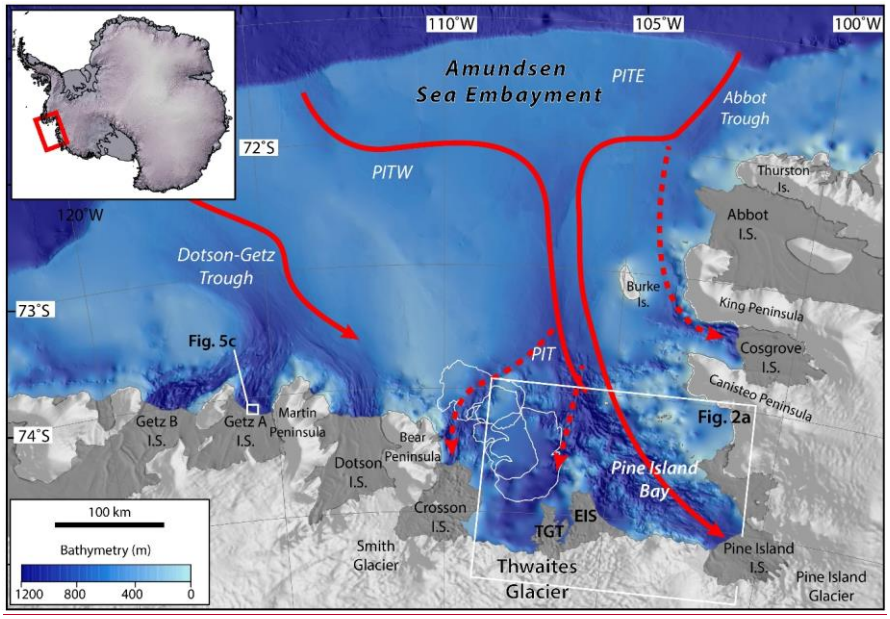


1895

**Formatted:** Centered

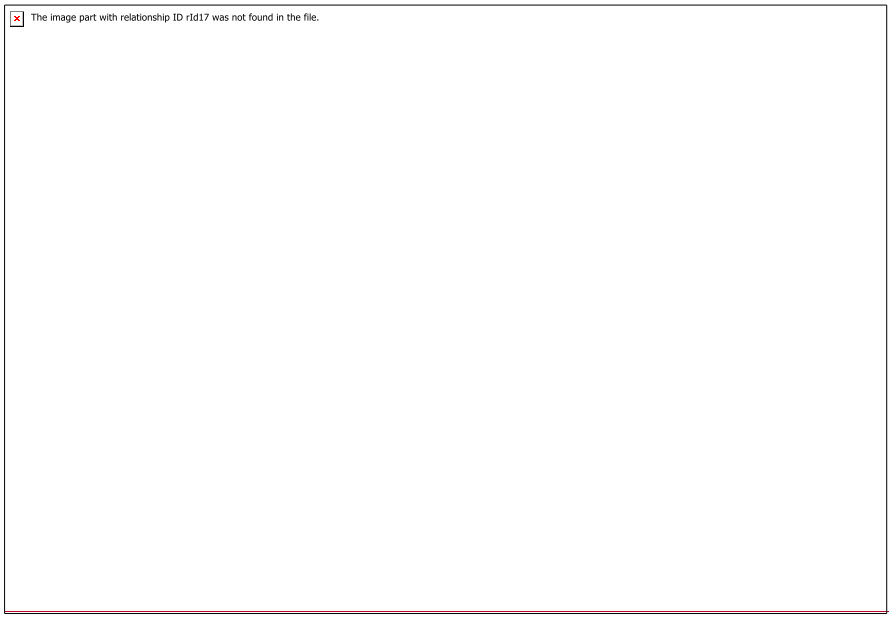


**Figure 1: Regional bathymetry for the Amundsen Sea Embayment and location of Thwaites Glacier (TG), West Antarctica. Bathymetry is from IBCSO (Arndt et al., 2013); arrows show observed (solid) and inferred (dashed) pathways for CDW across the continental shelf towards the grounding lines of Pine Island, Thwaites and Smith glaciers (after Nakayama et al., 2013; Dutrieux et al., 2014; Ha et al., 2014 for Dotson-Getz trough). PIT is Pine Island Trough; PITE is Pine Island Trough East; PITW is Pine Island Trough West; TGT is Thwaites Glacier Tongue; EIS is Eastern Ice Shelf; other ice shelves (I.S.) are also labelled. White outlines north of TG are mapped positions of the B-22A iceberg from 2002, 2010 and 2018, from south to north. Note the more "blurry" look of the bathymetry in front of TG (in IBCSO this bathymetry is based on the Tinto & Bell (2011) gravity-inversion and interpolation), where ship access has been hampered before austral summer 2018/2019 by persistent fast ice and the presence of the B-22A iceberg.**

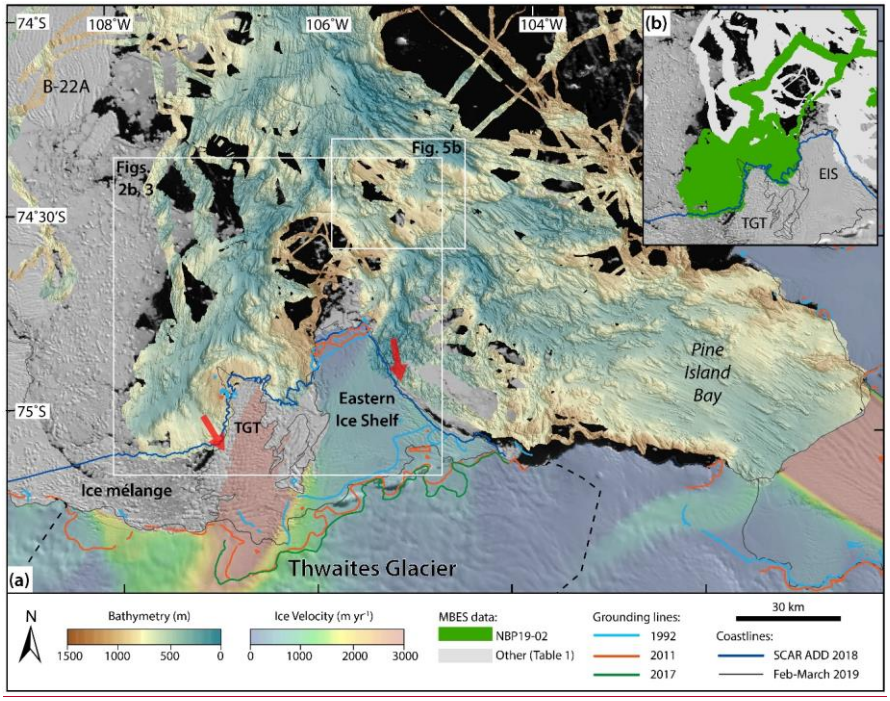


**Formatted:** Centered

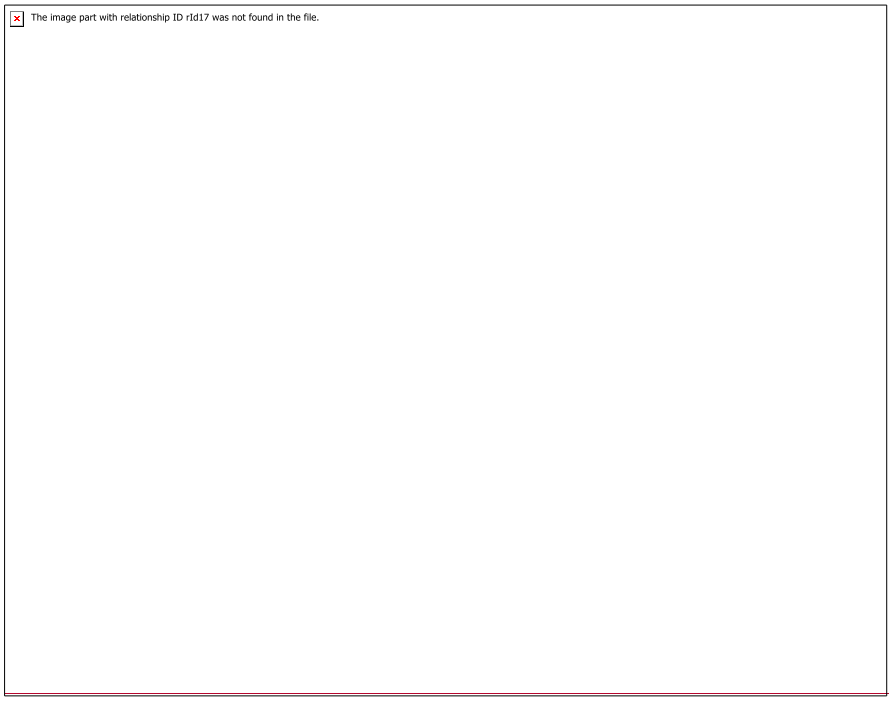


**Figure 2: (a) New MBES grid for the inner Amundsen Sea Embayment. Ice-velocity data from the MEaSUREs V2 dataset (Mouginot et al., 2019); grounding lines for 1992 and 2011 are from Rignot et al. (2011), and that for 2017 from Milillo et al. (2019); red arrows delineate CDW pathways after Dutrieux et al. (2014) and Milillo et al. (2019). The black dashed line marks the boundaries of the drainage basin of Thwaites Glacier (Vaughan et al., 2001). (b) NBP19-02 data coverage versus other MBES datasets (Table 1). The dark blue coastline illustrates the ice-shelf and ice-mélange extent during survey on NBP19-02 and was digitised from Landsat 8 imagery.**

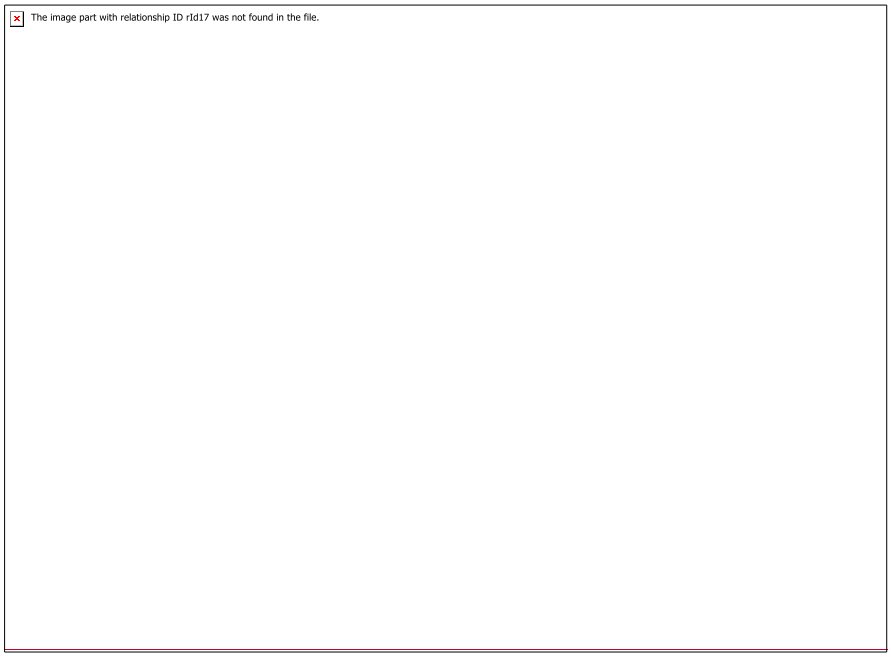
The image part with relationship ID rId17 was not found in the file.

1915

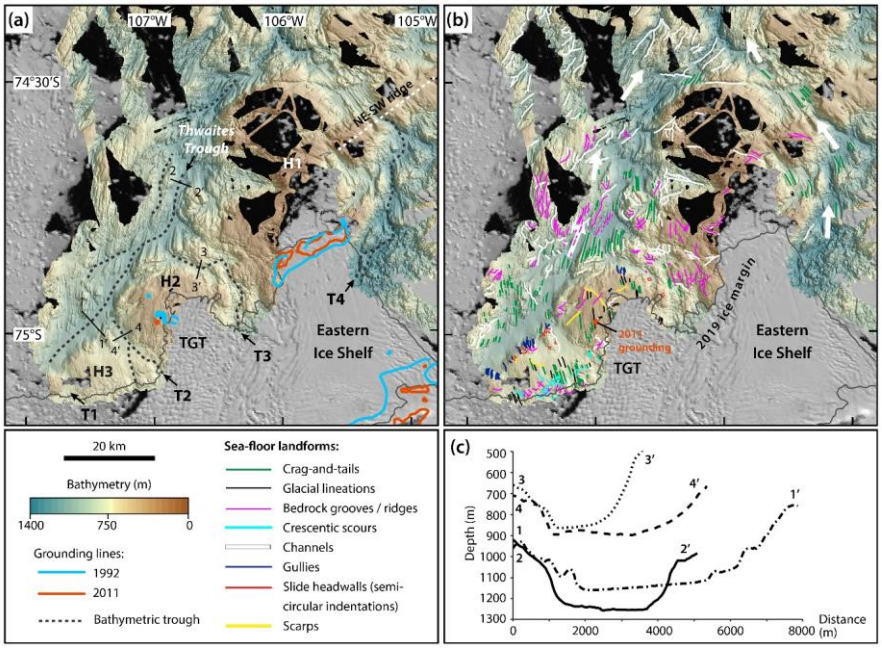
(a)
107°W
106°W
105°W
74°30'S
75°S
Thwaites Trough
NE-SW ridge
H1
H2
H3
T1
T2
T3
T4
TGT
Eastern Ice Shelf
(b)
2019 ice margin
2011 grounding
TGT
Eastern Ice Shelf
20 km
Bathymetry (m)
1400
750
0
Grounding lines:
1992
2011
Bathymetric trough
Sea-floor landforms:
Crag-and-tails
Glacial lineations
Bedrock grooves / ridges
Crescentic scours
Channels
Gullies
Slide headwalls (semi-circular indentations)
Scarps
(c)
Depth (m)
500
600
700
800
900
1000
1100
1200
1300
0
2000
4000
6000
8000
Distance (m)
1′
2′
3′
4′

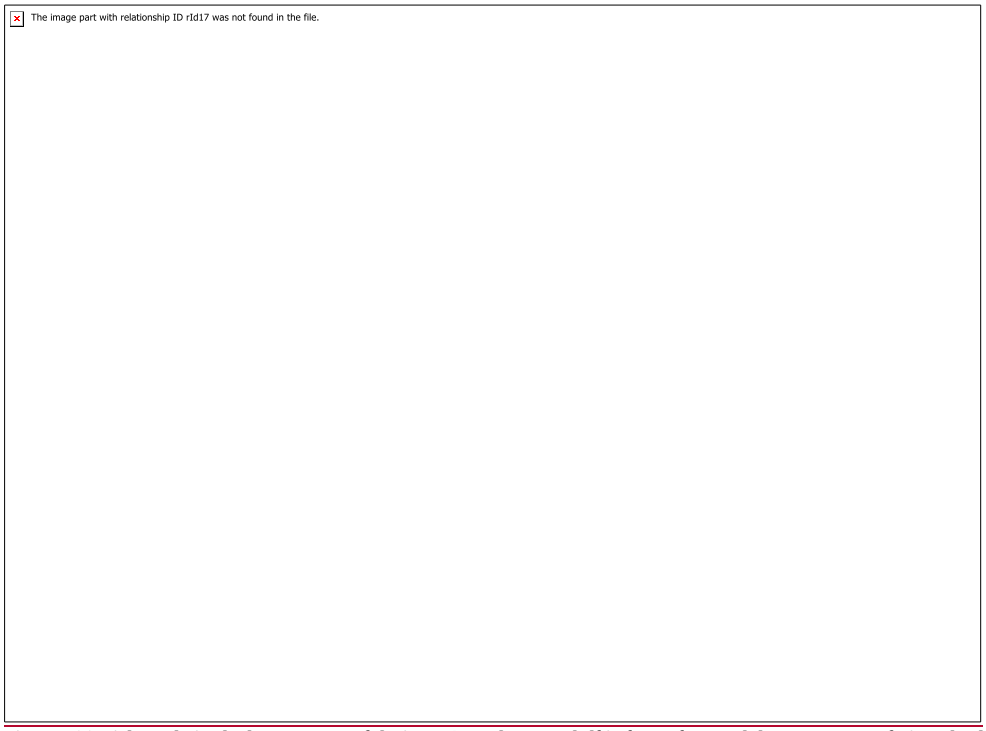


**Figure 3:(a) High-resolution bathymetry map of the inner Amundsen Sea shelf in front of TG and the eastern part of Pine Island Bay showing the large-scale sea-floor morphology including bathymetric troughs (T1-T3; main axes highlighted by black dashed lines) and highs (H1-H3) that form a broad NNE-SSW ridge continuing into a ridge further offshore in Pine Island Bay, northeast of the Eastern Ice Shelf (white dashed line). (b) Mapped sea-floor landforms; streamlined features show the former flow direction of an expanded TG (white arrows). (c) Cross-sectional profiles of the bathymetric troughs; locations of profiles in (a).**


The image part with relationship ID rId17 was not found in the file.

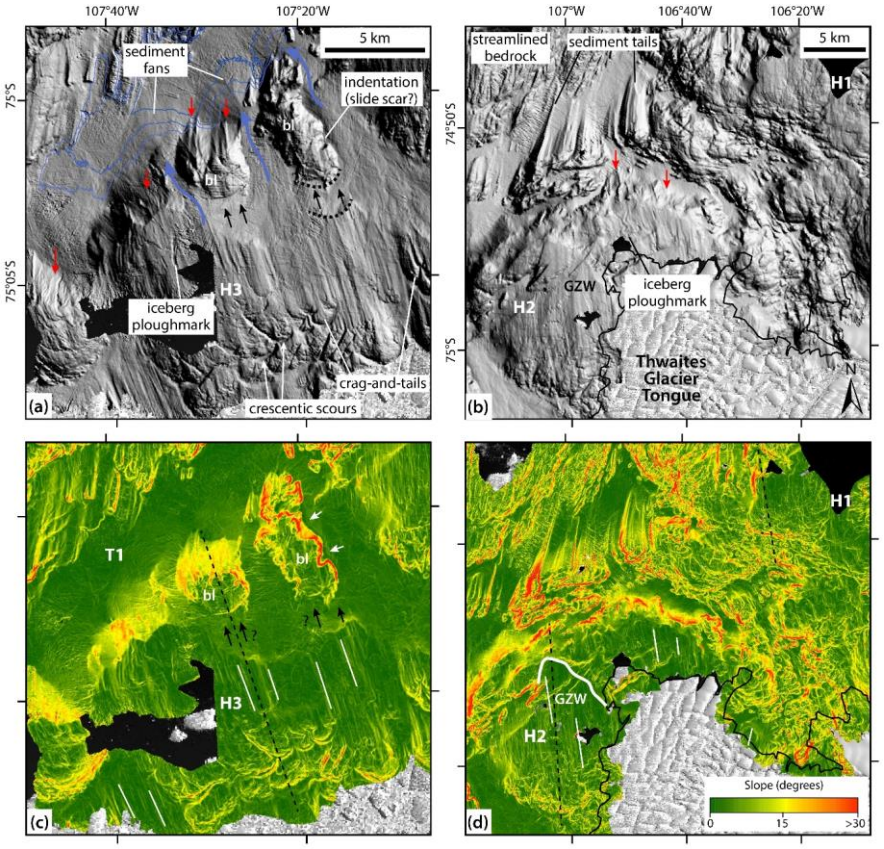


1925

Formatted: Centered


**Figure 4: Detailed maps of the MBES data and its first derivative, slope, over the sea-floor highs in front of Thwaites Glacier. (a) and (c) the H3 high. (b) and (d) the H2 high and western flank of H1. Red arrows in (a) and (b) point to gullies incised into the seaward flanks of the highs; the white lines in (c) and (d) mark glacial lineations; bl are the isolated blocks of H3 and black arrows in (a) and (c) denote their possible transport paths), with the black dotted lines in (a) illustrating semi-circular indentations; white arrows in (c) point to a channel at the base of one of the blocks; blue arrows in (a) indicate the down-slope transport direction of material into sediment fans at the front of H3 highlighted by bulges in the contours (contour levels 1100, 1125 and 1150 m). Black dashed lines in (c) and (d) locate the profiles in Fig. 5a. GZW is grounding-zone wedge.**

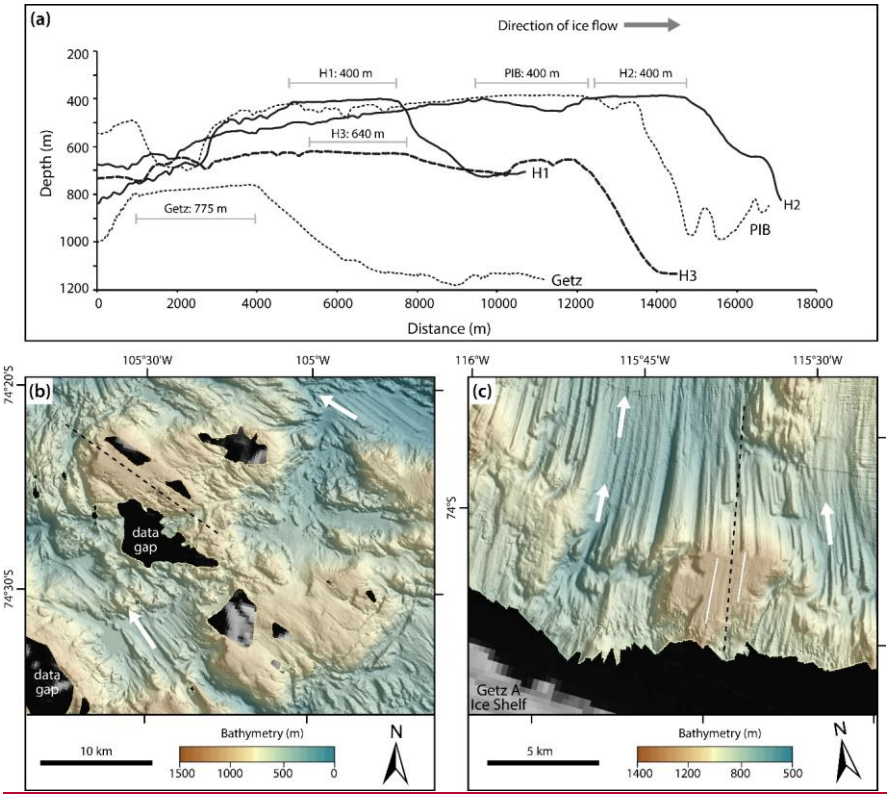
(a)
Direction of ice flow
H1: 400 m
PIB: 400 m
H2: 400 m
H3: 640 m
Getz: 775 m
H1
H2
PIB
H3
Getz
Depth (m)
Distance (m)
(b)
data gap
data gap
105°30'W
105°W
74°20'S
74°30'S
10 km
Bathymetry (m)
1500 1000 500 0
N
(c)
116°W
115°45'W
115°30'W
74°S
Getz A
Ice Shelf
5 km
Bathymetry (m)
1400 1200 800 500
N

1935


The image part with relationship ID rId17 was not found in the file.


**Figure 5: Flat-topped highs in the Amundsen Sea. (a) Cross-sectional profiles over H1-H3 highs at Thwaites Glacier (for location of profiles see Figs. 4c, d), further offshore in Pine Island Bay (PIB; location of high in Fig. 2a, location of profile in Fig. 5b) and offshore from the Getz-A Ice Shelf (location of high in Fig. 1, location of profile in Fig. 5c), showing sea-floor highs planed off at different depth levels. The flat portions of the profiles are marked with grey bars and the depth elevation for that flat-top given above, so "H1:400 m" means the flat part of the profile over H1 high is at 400 m water depth. (b) MBES of flat-topped highs part of the discontinuous sea-floor ridge in PIB. (c) MBES of a flat-topped high with glacial lineations (white lines) just in front of the Getz-A Ice Shelf (after Nitsche et al., 2016). White arrows show direction of past ice flow based on streamlined subglacial landforms.**

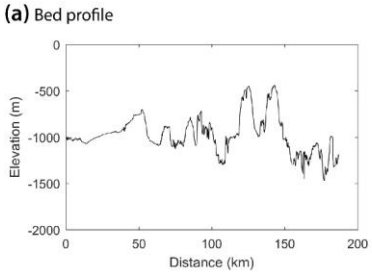


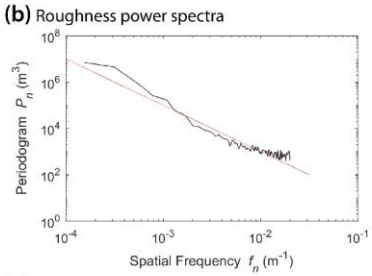


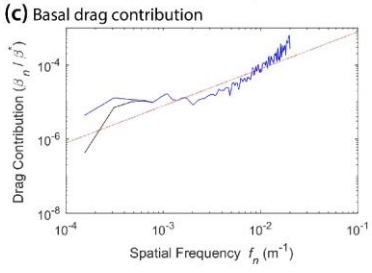


The image part with relationship ID rId17 was not found in the file.

**Figure 6: (a) Bed elevation ( = water depth for sea-floor data) verses distance along flow line. (b) Roughness power spectra $P_n$ verses spatial frequency $f_n$. (c) Scaled basal drag contributions $\beta_n/\beta^*$ verses $f_n$ for along-flow profile (6) offshore from Pine Island and Thwaites glaciers (for location see Fig. S1a). The red lines in (b) and (c) are based on an assumption of Brown-noise power spectrum that falls off as the inverse square of spatial frequency~~, with variance of roughness decaying as the inverse square of spatial frequency~~. At low spatial frequencies, drag contributions depend on the function $F$ (see Section 4.2) with the two limiting cases shown: $F_1$ (blue), $F_2$ (black).**

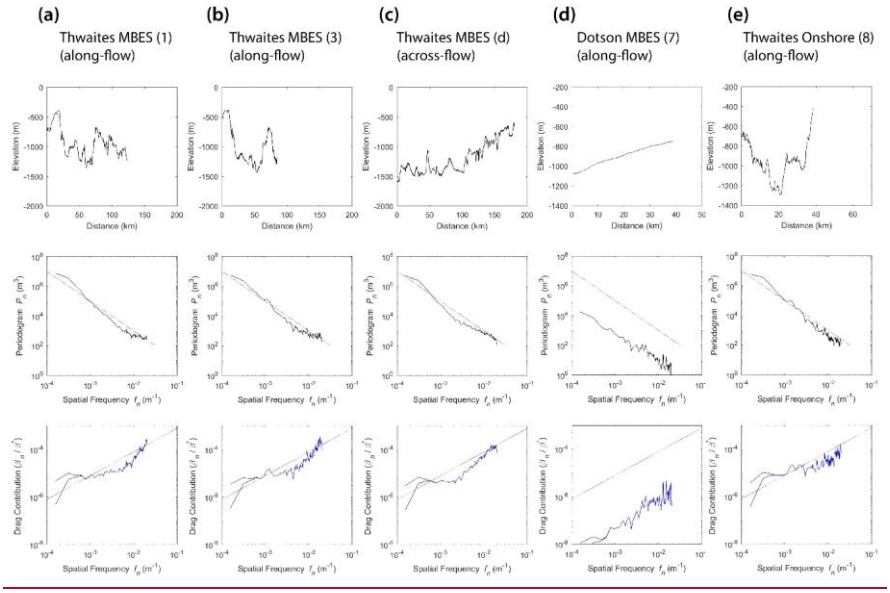


Formatted: Centered


**Figure 7: Selection of bed profiles (top), derived power spectra (middle) and basal drag contributions (bottom) for: (a, b) along-flow profiles (1) and (3) offshore Thwaites Glacier; (c) onshore along-flow bed profile (8) for Thwaites Glacier; (d) across-flow profile "d" for offshore TG; (e) along-flow profile (7) for Dotson-Getz Trough. Profile locations are shown in Figs. S1, S2~~SF1, SF2~~. The red line in power spectra and drag contribution plots are based on an assumption of Brownian motion (i.e. power decays as inverse square of spatial frequency). At low spatial frequency, drag contributions depend on the function *F*. Two limiting cases are shown: $F_1$ (blue), $F_2$ (black).**

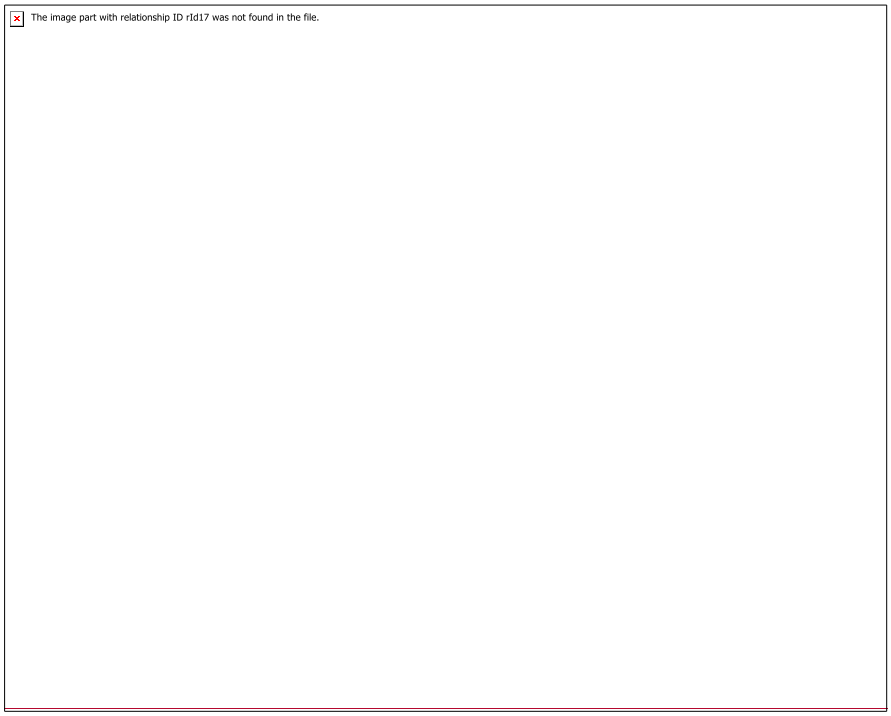
The image part with relationship ID rId17 was not found in the file.

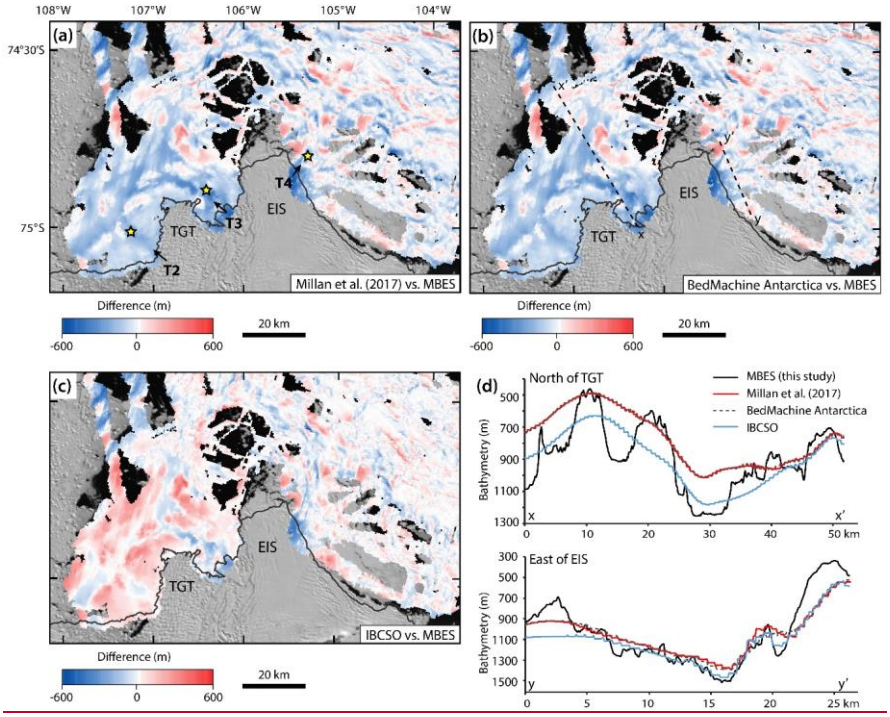


**Figure 8: Difference maps between regional bathymetric datasets and the MBES grid. (a) Millan et al. (2017) minus MBES grid. Yellow asterisks mark the locations of channels discussed in Section 5. (b) BedMachine Antarctica (Morlighem et al., 2019) minus MBES grid. (c) IBCSO (Arndt et al., 2013) minus MBES grid. (d) Profile data for two profiles for each of the regional datasets compared with profiles from the MBES grid; profiles are located in (b). Note that the Millan et al. (2017) and the BedMachine Antarctica bathymetries are very similar and thus return near identical bed profiles in (d)[,]; the BedMachine Antarctica grid is included for completeness as the most recent regional dataset to cover the area and its authors highlight the need for more coastal bathymetric datasets (Morlighem et al., 2019).**

# Supplementary Information for: Revealing the former bed of Thwaites Glacier using sea-floor bathymetry: implications for warm-water routing and bed controls on ice flow and buttressing

Kelly A. Hogan[1], Robert D. Larter[1], Alastair G. C. Graham[2], Robert Arthern[1], James D. Kirkham[1,3], Rebecca Totten Minzoni[4], Tom A. Jordan[1], Rachel Clark[5], Victoria Fitzgerald[4], Anna K. Wåhlin[6], John B. Anderson[7], Claus-Dieter Hillenbrand[1], Frank Nitsche[8], Lauren Simkins[9], James A. Smith[1], Karsten Gohl[10], Jan Erik Arndt[10], Jongkuk Hong[11], Julia Wellner[5]

[1] British Antarctic Survey, Natural Environment Research Council, High Cross, Madingley Road, Cambridge, CB3 0ET, UK
[2] College of Marine Science, University of South Florida, Saint Petersburg, FL 33701, USA
[3] Scott Polar Research Institute, University of Cambridge, Lensfield Road, Cambridge, CB2 1ER, UK
[4] Department of Geological Sciences, University of Alabama, Tuscaloosa, AL 35487, USA
[5] Department of Earth and Atmospheric Sciences, University of Houston, Houston, TX 77204, USA
[6] Department of Marine Sciences, University of Gothenburg, 40530 Göteborg, Sweden
[7] Department of Earth Science, Rice University, Houston, TX 77005, USA
[8] Lamont-Doherty Earth Observatory, Columbia University, Palisades, New York, USA
[9] Department of Environmental Sciences, University of Virginia, Charlottesville, VA 22904, USA
[10] Alfred Wegener Institute for Polar and Marine Research, Postfach 120161, D-27515, D-27515 Bremerhaven, Germany
[11] Korea Polar Research Institute (KOPRI), Incheon 21990, Republic of Korea

*Correspondence to*: Kelly A. Hogan (kelgan@bas.ac.uk)

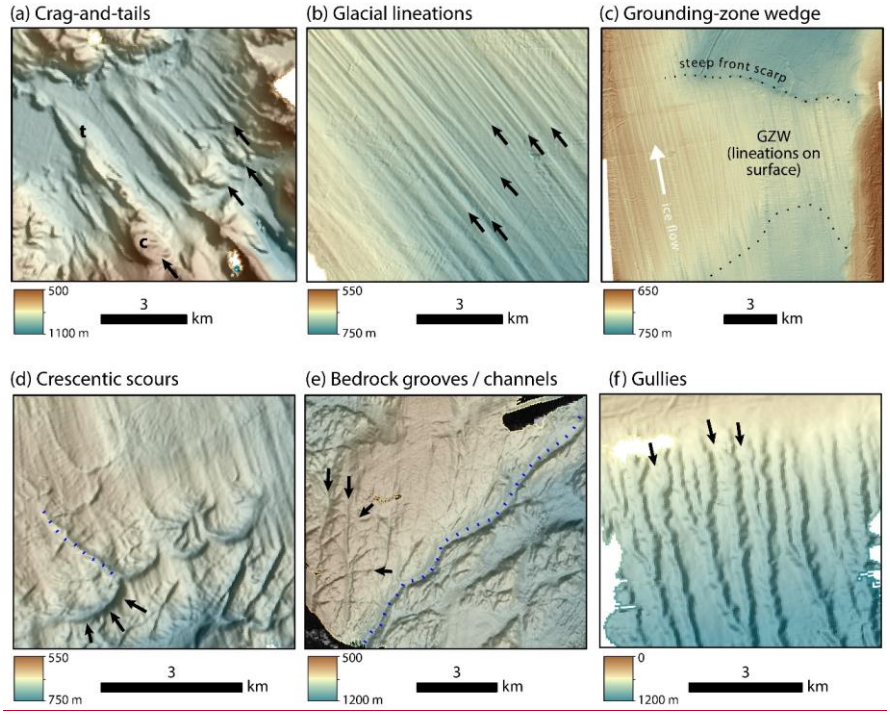


**Supplementary Figure S1: Examples of glacial landforms discussed in the text; all examples are from the Amundsen Sea Embayment. (a) Crag-and-tail landforms (several arrowed) from Pine Island Bay with bedrock crags "c" and sedimentary tails "t" streamlined in the direction of ice flow. (b) Glacial lineations from the Dotzon-Getz palaeo-ice stream trough (several arrowed) and fully described in Graham et al. (2009). (c) A grounding-zone wedge (GZW) from Pine Island Trough on the outer continental shelf. The subtle asymmetric wedge rises only 20 m above the surrounding sea floor and has been overridden by ice as shown by the glacial lineations on its surface. (d) Crescentic scours (curved channels; one arrowed) on the ice-proximal side of the H3 high. Note a bedrock channel is marked by blue dots. (e) Grooves (arrowed) and a channel incised in to bedrock in front of TG. Note the linear or slightly curvilinear form of the grooves which form a crossed patterned of incision versus the sinuous, continuous form of the channel (blue dots). (f) Gullies (arrowed) – relatively straight channels incising a slope - at the shelf edge of the Amundsen Sea.**

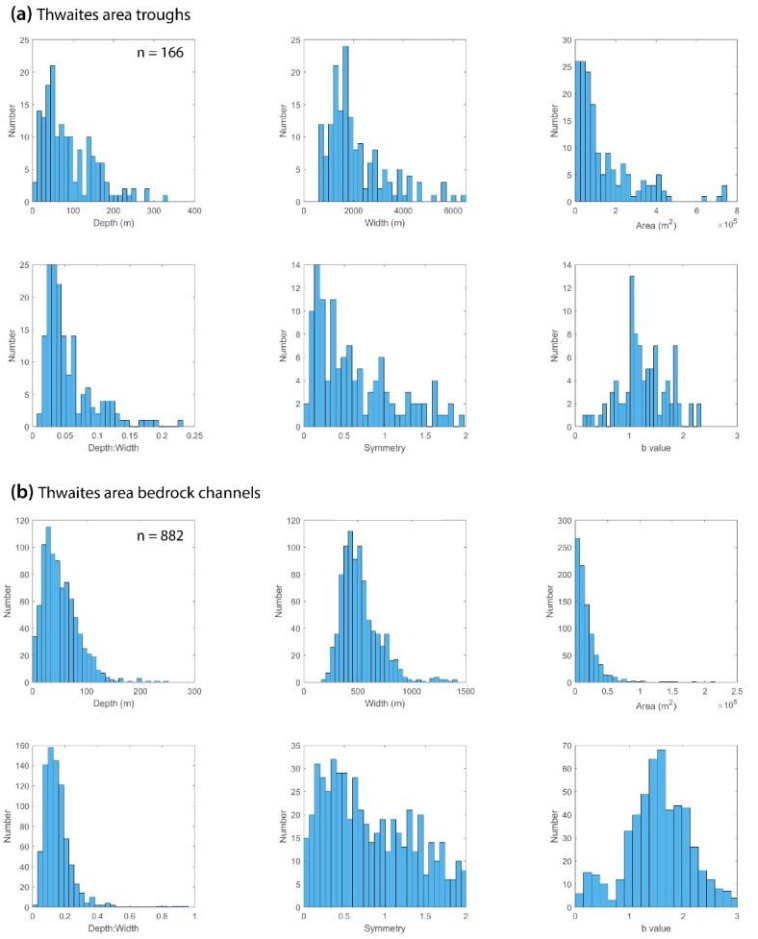


**Supplementary Figure S2: Cross-sectional metrics for (a) bathymetric troughs and (b) bedrock channels identified from the MBES dataset in front of Thwaites Glacier (troughs and channels are mapped in Fig. 3). Note the different scales on some axes. Symmetry values of 1 denote perfectly symmetrical cross sections whilst values >1 and <1 denote left-skewed and right-skewed cross sections, respectively. The b value assesses how V- or U-shaped a cross section is; values of 1 are perfectly V shaped, values of 2 are perfectly U shaped. b values greater than 2 reflect box shaped geometries and values below 1 indicate convex-upward forms.**

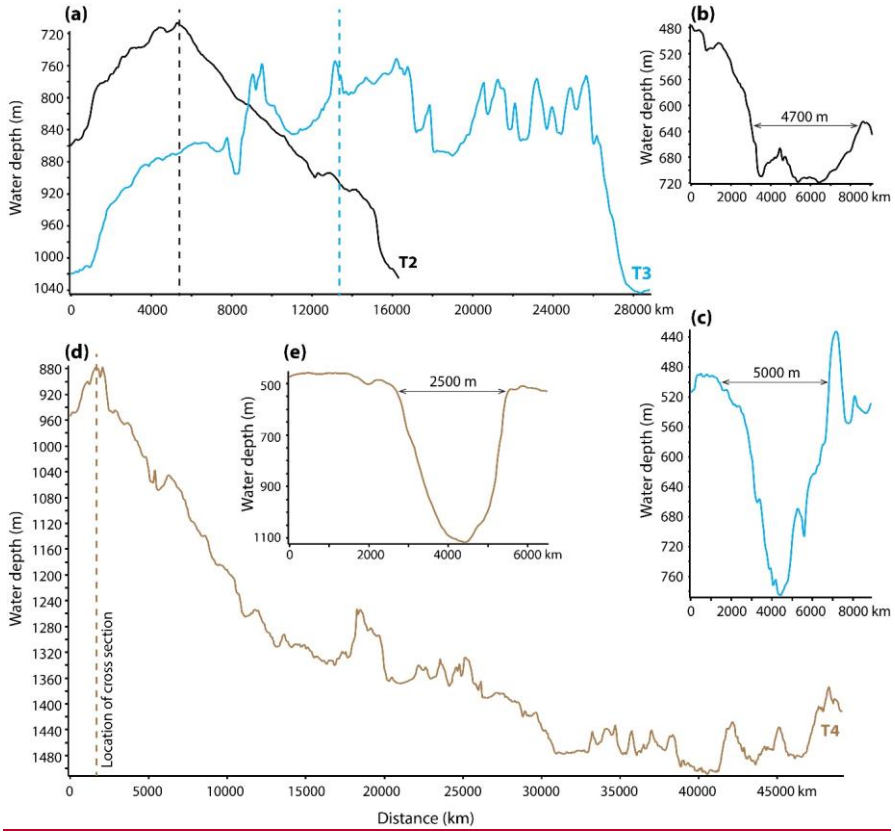


**Supplementary Figure S3: Long profiles and cross-sections for sea-floor troughs in front of Thwaites Glacier. (a) Long profiles for T2 and T3 troughs showing locations of bathymetric sills. (b) Cross section over sill in T2 trough (located in (a)). (c) Cross section over sill in T3 trough (location in (a)). (d) Long profile for T4 trough. (e) Cross section over sill in T4 trough (location in (a)). See Fig. 3a in the main text for locations of long profiles in (a) and (d).**

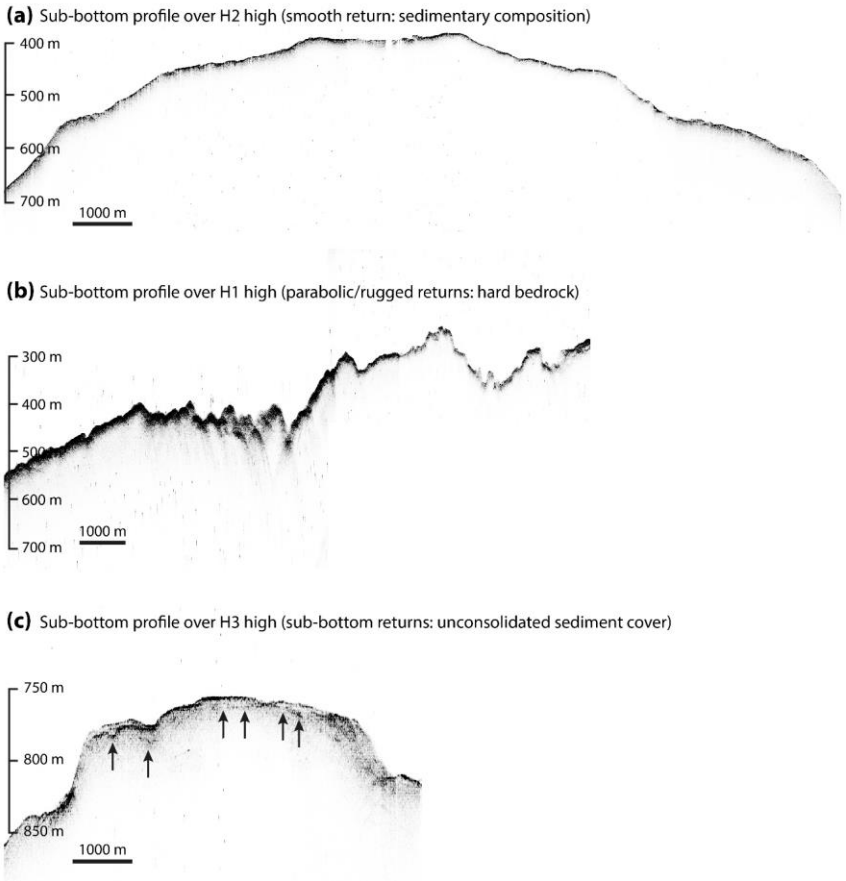


**Figure S4: Example of Knudsen Chirp sub-bottom profiles over the sea-floor highs north of Thwaites Ice Shelf. (a) is a profile over the H2 high showing a very smooth return interpreted as sediment cover that is co-located sedimentary landforms (GZW) observed on MBES data. (b) is a profile from the flank of the H1 high showing diffraction parabola from point reflectors at the sea floor interpreted as hard bedrock lithology. (c) is a profile from the H3 high showing up to 15 m of unconsolidated sediment cover; sub-sea-floor reflections are marked by arrows. All profiles were acquired during cruise NBP19-02 (Larter et al., 2020).**

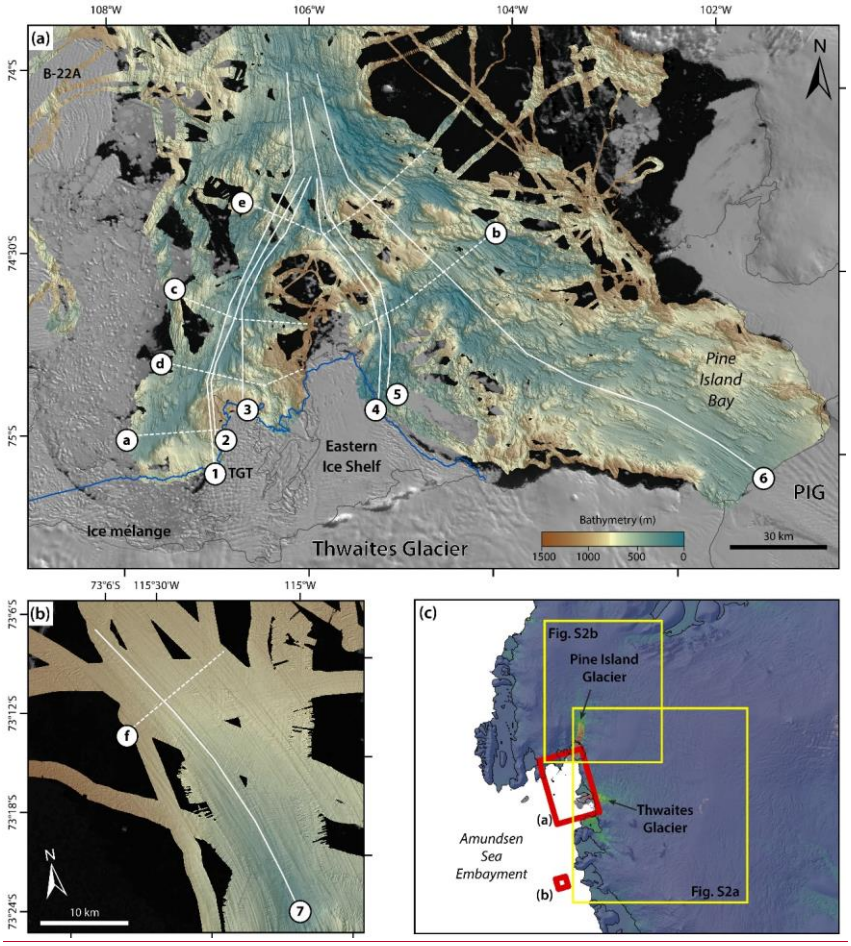


**Supplementary Figure S5: Location maps for bed profiles used in roughness and drag contribution analyses (see Sections 2.2 and 4 in the main text). (a) Palaeo-glacier bed profiles from MBES data offshore Pine Island and Thwaites glaciers. Along-flow profiles are labelled (1)-(6); across-flow profiles are labelled (a)-(e). (b) Palaeo-glacier bed profiles for a "smooth" bed characterised by mega-scale glacial lineations (MSGL) in the mid-shelf section of Dotson-Getz Trough; along-flow profile is labelled (7), across-flow profile is labelled (f). (c) Location map of the Amundsen Sea Embayment and the Amundsen Sea sector of the West Antarctic Ice Sheet showing the locations of Supplementary Figures S1a, b (red outlines) and S2a, b (yellow outlines).**

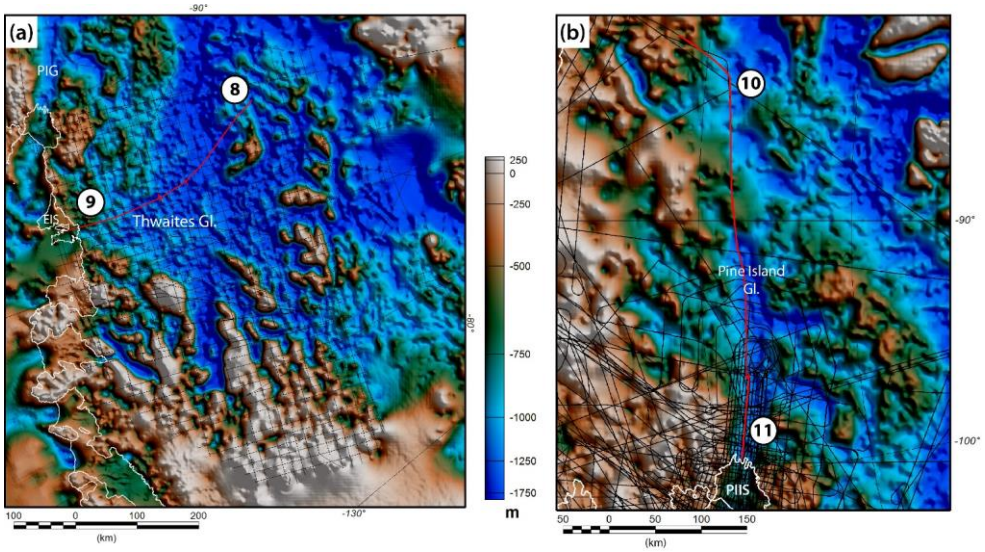


**Supplementary Figure S6: Location maps for airborne radar (onshore) bed profiles used in roughness and drag contribution analyses. (a) AGASEA line used for modern Thwaites Glacier bed profiles; the tick marks denote the ends of the two profiles shown in Fig. S4f and S4g; note the overlap between the profiles. PIG is Pine Island Glacier; EIS is the Eastern Ice Shelf of Thwaites Glacier. (b) OIB profile for modern Pine Island Glacier bed profiles. PIIS is Pine Island Ice Shelf.**

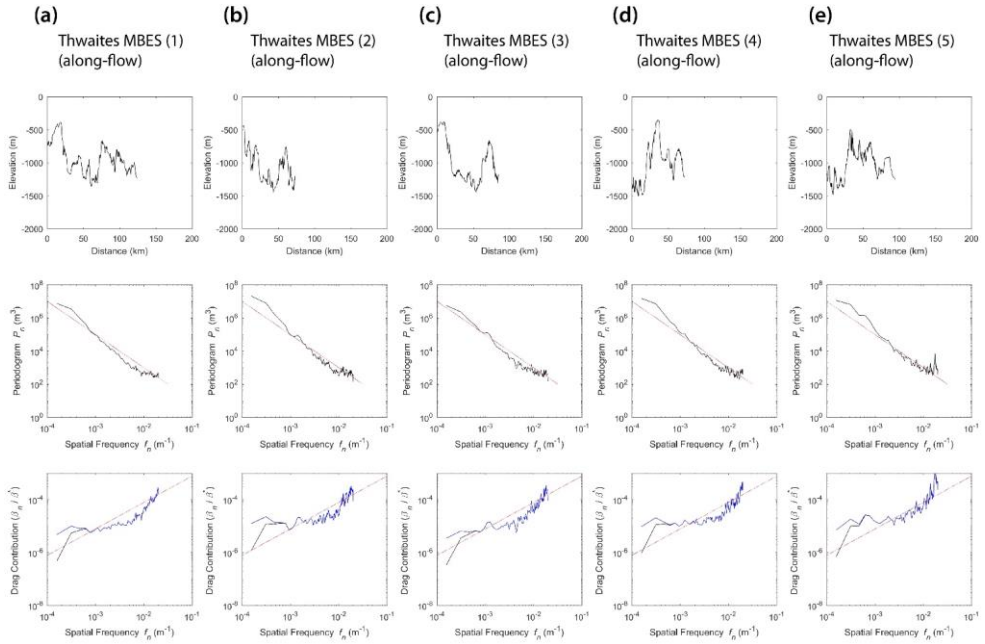


**Supplementary Figure S7: Bed profiles (top), derived power spectra (middle) and basal drag contributions (bottom) for all bed profiles used in this study, for locations see Figs. SF1 and SF2: (a) Thwaites MBES along-flow profile 1; (b) Thwaites MBES along-flow profile 2; (c) Thwaites MBES along-flow profile 3; (d) Thwaites MBES along-flow profile 4; (e) Thwaites MBES along-flow profile 5. As per the main text (Section 4, Figs, 6, 7), the red line in power spectra and drag contribution plots are based on an assumption of Brownian motion (i.e. power decays as inverse square of spatial frequency). At low spatial frequency, drag contributions depend on the function $F$. Two limiting cases are shown: $F_1$ (blue), $F_2$ (black).**

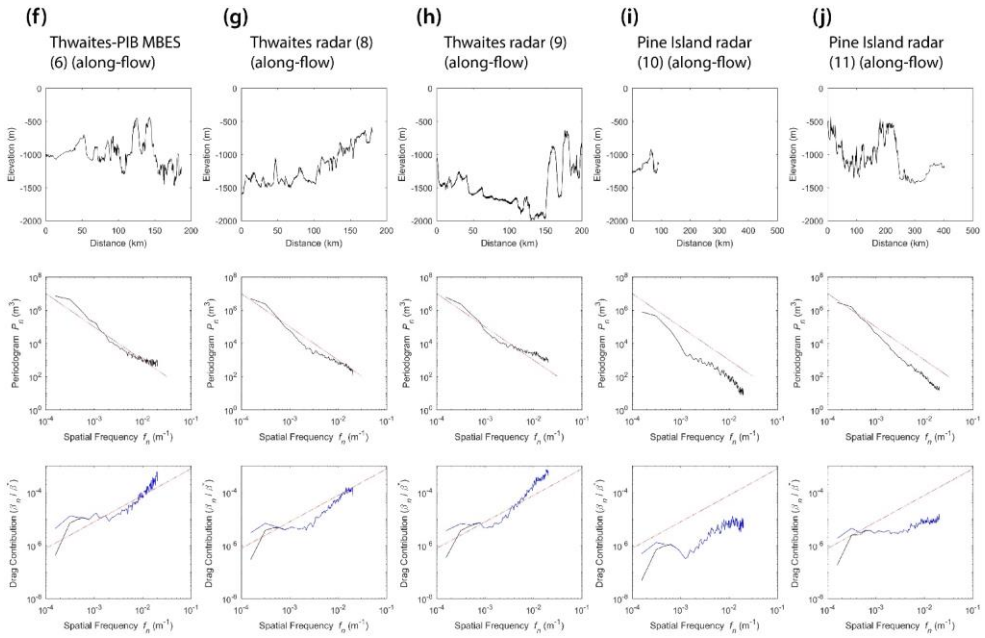


**Supplementary Figure S7 (continued): Bed profiles (top), derived power spectra (middle) and basal drag contributions (bottom) for bed profiles used in this study, for locations see Figs. SF1 and SF2: (f) Thwaites-Pine Island MBES along-flow profile 6; (g) Thwaites radar along-flow profile 8 (upstream area); (h) Thwaites radar along-flow profile 9 (downstream area); (i) Pine Island radar along-flow profile 10 (upstream area); (j) Pine Island radar along-flow profile 11 (downstream area).**

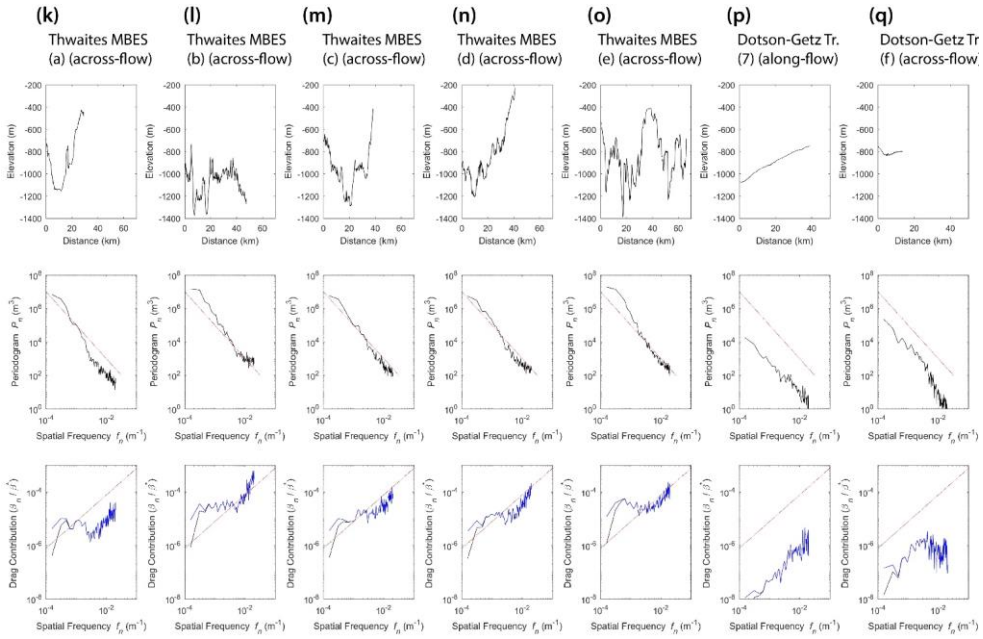


**Supplementary Figure S7 (continued): Bed profiles (top), derived power spectra (middle) and basal drag contributions (bottom) for bed profiles used in this study, for locations see Figs. SF1 and SF2: (k) to (o) are Thwaites MBES across-flow profiles a-e, respectively; (p) is the Dotson-Getz Trough along-flow profile (7); (q) Dotson-Getz Trough across-flow profile f.**

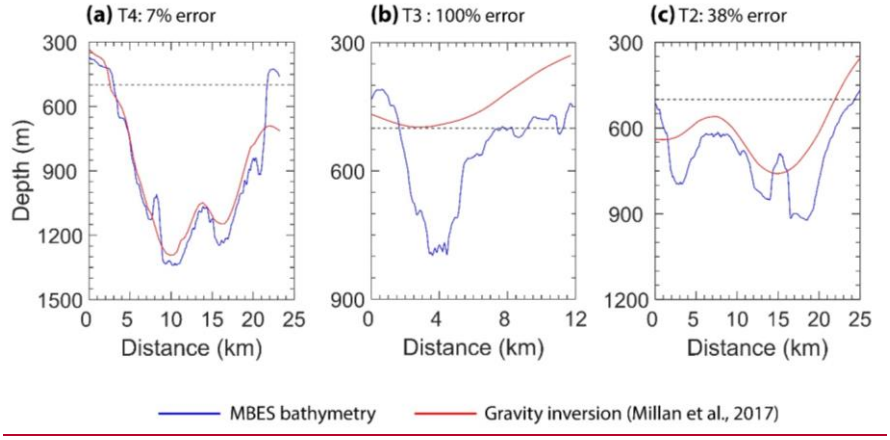


**Supplementary Figure S8: Comparisons of cross-sections over troughs that act as pathways for CDW to the Thwaites grounding zone from our MBES data (blue) and Millan et al. (2017) (red). Locations of the troughs are marked by asterisks in Fig. 8a. For trough T4 east of the EIS (a) the gravity-inversion only gives a 7% error in the trough cross-sectional area compared with the MBES grid below 500 m (dashed line). Trough T3 between the H1 and H2 highs (b) is not resolved by Millan et al. (2017), i.e. the error is 100% below 500 m. The rugged sea floor of trough T2 (c) is poorly-resolved by the Millan et al. (2017) grid resulting in a 38% error in cross-sectional area.**

The table below gives the area of any parts of the cross section that are below 500 m depth.

| Trough | NBP19-02 area ($km^2$) | Millan area ($km^2$) | Area difference (%) | 'Missing water' ($km^2$) |
|---|---|---|---|---|
| T4 | 10.3 | 9.78 | 4.72* | 0.52 |
| T2 | 0.88 | 0 | 100 | 0.88 |
| T3 | 5.17 | 3.20 | 38.1 | 1.97 |

**Supplementary Table 1: Cross-sectional area difference calculations for Millan et al. (2017) and the MBES grid for three troughs (locations are given as asterisks in Fig. 8a). Trough cross-sectional areas are calculated using trapezoidal numerical integration for any part of the trough below 500 m; the depth below which CDW is assumed to be present. *The channel area difference for T4 increases to 7% if we ignore the part of the cross-section from 22 km onwards, which in the Millan et al. (2017) grid underestimates the flank of the channel.**

## Oceanic heat flux calculations

To estimate the heat fluxes through troughs defined by the new MBES grid and the existing regional bathymetric grid of Millan et al. (2017) (Sect. 6.1) we use the equation for heat flux (W/m$^2$) per unit area as given by (Arneborg et al., 2012):

$$F = \rho C_P U(T - T_F) \quad \text{(eqn. 1)}$$

Where ρ (kg m$^{-3}$) is the water density, $C_P$ (J kg$^{-1}$ K$^{-1}$) is the specific heat capacity, U (m s$^{-1}$) is the velocity in the along-trough direction, T (K) is temperature, and $T_F$ (K) is the freezing temperature. The total heat flux $H$ (TW) is then obtained by integrating the flux over a cross-section of the trough. We perform the calculations for trough T2 which showed a 38% increase in cross-sectional area between the regional and MBES bathymetries (see Supp. Table 1). To match these areas we use trough depths as defined by the regional bathymetry (750 m) and our MBES data (900 m), and use a simplified geometry with a constant width below 500 m calculated to match the cross-sectional areas. For example, to obtain an cross-sectional area of 5.2 km2 (below 500 m) we use a trough width of 13 km, that is 5.2 km$^2$ divided by 900 m minus 500 m.

For the calculations, we also need a suitable temperature profile for the water masses in the troughs and the water velocity through the troughs. Recent studies have shown that ocean temperature increases as a function of depth on the inner Amundsen Sea shelf (Christianson et al., 2016; Webber et al., 2019), and that velocity increases with depth approximately proportionally to temperature (Arneborg et al., 2012; Wåhlin et al., 2020). The proportionality occurs because the bottom-intensified component of velocity is driven by the density difference between the deep current and the ambient water, which in these waters is a function of temperature. It has also been shown that the density-driven component, in contrast to the vertically constant (wind-driven) component, is more likely to make it to the grounding zone whereas the wind-driven component can be blocked at the ice shelf front (Wåhlin et al., 2020). Thus, we assume a linear increase in temperature from freezing point at 300 m to pure Circumpolar Deep Water (1.2 °C) at 800 m, similar to observations in Pine Island Bay (Christianson et al., 2016), as well as further west (Arneborg et al., 2012). We perform the calculations for both a constant along-trough velocity (U) and also for a velocity that is proportional to temperature according to (Arneborg et al., 2012):

$$U = 0.02 + 0.01T \quad \text{(eqn. 2)}$$

This takes into account the velocity dependence on density and resembles average velocity profiles in the western Amundsen Sea Embayment (Arneborg et al, 2012).

The table below gives the estimated total heat flux through trough T2 with the different parameters as discussed above.

| T2 trough area ($km^2$) | Bathymetric source | Velocity profile | Total heat flux, *H* (TW) |
|---|---|---|---|
| 750 | Millan et al. (2017) | Constant | 0.5 |
| 900 | MBES (this study) | Constant | 1.11 |
| 750 | Millan et al. (2017) | Proportional to T | 0.45 |
| 900 | MBES (this study) | Proportional to T | 1.27 |

**Supplementary Table 2: Total heat flux estimates through T2 using trough cross-sectional areas as defined by Millan et al. (2017) and the MBES grid (this study).**

## References


Arneborg, L., Wåhlin, A., Björk, G., Liljebladh, B., and Orsi, A.: Persistent inflow of warm water through a submarine trough on the Western Amundsen Shelf. Nature Geoscience, 5, 876-880, 2012.

Christianson, K., Bushuk, M., Dutrieux, P., Parizek, B. R., Joughin, I. R., Alley, R. B., Shean, D. E., Abrahamsen, E. P., Anandakrishnan, S., Heywood, K. J., Kim, T. W., Lee, S. H., Nicholls, K., Stanton, T., Truffer, M., Webber, B. G. M., Jenkins, A., Jacobs, S., Bindschadler, R., and Holland, D. M.: Sensitivity of Pine Island Glacier to observed ocean forcing, Geophysical Research Letters, 43, 10817-10825, doi:10.1002/2016GL070500, 2016.

Graham, A. G. C., Larter, R. D., Gohl, K., Hillenbrand, C.-D., Smith, J. A., and Kuhn, G.: Bedform signature of a West Antarctic palaeo-ice stream reveals a multi-temporal record of flow and substrate control, Quaternary Science Reviews, 28, 2774-2793, 2009.

Wåhlin, A. K., Steiger, N., Darelius, E., Assmann, K. M., Glessmer, M. S., Ha, H. K., Herraiz-Borreguero, L., Heuzé, C., Jenkins, A., Kim, T. W., Mazur, A. K., Sommeria, J., and Viboud, S.: Ice front blocking of ocean heat transport to an Antarctic ice shelf, Nature, 578, 568-571, 2020.

Webber, B. G. M., Heywood, K. J., Stevens, D. P., and Assmann, K. M.: The Impact of Overturning and Horizontal Circulation in Pine Island Trough on Ice Shelf Melt in the Eastern Amundsen Sea, Journal of Physical Oceanography, 49, 63-83, 2019.